

SYNTHESIS AND CHARACTERIZATION OF PLATINUM
FREE, CONDUCTING POLYMER BASED COUNTER
ELECTRODE FOR DYE SENSITIZED SOLAR CELL
(DSSC)

USMAN AHMED

INSTITUTE FOR ADVANCED STUDIES
UNIVERSITY OF MALAYA
KUALA LUMPUR

2019

**SYNTHESIS AND CHARACTERIZATION OF
PLATINUM FREE, CONDUCTING POLYMER BASED
COUNTER ELECTRODE FOR DYE SENSITIZED
SOLAR CELL (DSSC)**

USMAN AHMED

**THESIS SUBMITTED IN FULFILMENT OF THE
REQUIREMENTS FOR THE DEGREE OF MASTER OF
PHILOSOPHY**

**INSTITUTE FOR ADVANCED STUDIES
UNIVERSITY OF MALAYA
KUALA LUMPUR**

2019

UNIVERSITY OF MALAYA
ORIGINAL LITERARY WORK DECLARATION

Name of Candidate: **Usman Ahmed**

Matric No: **HMA170007**

Name of Degree: **Masters of Philosophy**

Title of the Thesis (“this Work”): **Synthesis and Characterization of Platinum Free, Conducting Polymer Based Counter Electrode for Dye Sensitized Solar Cell (DSSC)**

Field of Study: **Renewable Energy**

I do solemnly and sincerely declare that:

- (1) I am the sole author/writer of this Work;
- (2) This Work is original;
- (3) Any use of any work in which copyright exists was done by way of fair dealing and for permitted purposes and any excerpt or extract from, or reference to or reproduction of any copyright work has been disclosed expressly and sufficiently and the title of the Work and its authorship have been acknowledged in this Work;
- (4) I do not have any actual knowledge nor do I ought reasonably to know that the making of this work constitutes an infringement of any copyright work;
- (5) I hereby assign all and every rights in the copyright to this Work to the University of Malaya (“UM”), who henceforth shall be owner of the copyright in this Work and that any reproduction or use in any form or by any means whatsoever is prohibited without the written consent of UM having been first had and obtained;
- (6) I am fully aware that if in the course of making this Work I have infringed any copyright whether intentionally or otherwise, I may be subject to legal action or any other action as may be determined by UM.

Candidate’s Signature

Date:

Subscribed and solemnly declared before,

Witness’s Signature

Date:

Name:

Designation:

SYNTHESIS AND CHARACTERIZATION OF PLATINUM FREE, CONDUCTING POLYMER BASED COUNTER ELECTRODE FOR DYE SENSITIZED SOLAR CELL (DSSC)

ABSTRACT

Among all photovoltaic devices, dye sensitized solar cell (DSSCs) are assumed as one of the most potential renewable energy source (device), due to facile fabrication methods, cost-effectiveness and environmentally friendly behavior. Certain constituents such as photoanode (conventionally titanium dioxide), counter electrode (mostly platinum), sensitizing dye (different kinds including natural and organic dyes) and electrolyte (iodide and tri-iodide) effects the photovoltaic performance of DSSCs. Each component has its own importance but among all, counter electrode also plays a vital role. Counter electrode receives the electron from an external load and transfer them towards the electrolyte for redox reaction. The dye accepts these electrons which helps in the regeneration of dye electron. All these components significantly affect the overall performance of DSSC. Various materials including carbon-based materials, oxides, sulfides, and conducting polymers have been explored as cost effective, stable and highly efficient material for the possible replacement of Pt-based counter electrode (CE) in DSSCs. Recently, researchers are investigating different nanocomposite-based hybrid material as counter electrode for DSSC. It was found that the composite materials possessing high catalytic property of reduction, high surface area toward the flow of electron and low charge transfer resistance showed great potential for the replacement of Pt based CE. In this work, conducting polymer have been studied as counter electrode for DSSC. To examine the structural, chemical composition, optical behavior and photovoltaic performance, Field Emission Scanning Electron Microscopy (FESEM), X-ray powder diffraction (XRD), Fourier-transform infrared spectroscopy (FTIR), Ultraviolet-visible spectroscopy (UV-vis) and electrochemical analysis has been studied. The photovoltaic performance test has been studied to examine the current density vs voltage (J-V), and the power conversion

efficiency (PCE) of DSSC under standard test conditions. It was observed that with the addition of strontium titanite (SrTiO_3) in polypyrrole (PPy) nanocomposite the photovoltaic performance of DSSC has been enhanced. PPy achieved the power conversion efficiency value of 1.29% but with the increment of SrTiO_3 , hybrid polypyrrole nanocomposite PPy- SrTiO_3 -25%, PPy SrTiO_3 -50% and PPy- SrTiO_3 -75% attained the PCE of 1.98 %, 2.52% and 2.08% respectively. Furthermore, in comparison with Pt based CE (2.17%), PPy SrTiO_3 -50% showed enhanced PCE that is 2.17% and 2.52% respectively. In another project, polyaniline (PANI) was used as conducting polymer to fabricate the counter electrode for DSSC. Different concentrations of PANI were taken in order to optimize the concentration of PANI nanoparticles for further studies. PANI due to its unique properties also showed great potential as CE for DSSC. It was noticed that unaided PANI with the concentration of 20mg/ml showed enhance photoelectrochemical response as compare to PANI-1 and PANI-2. The electrocatalytic and photovoltaic performance of PANI-3 can be enhanced with the addition of metal oxide, transition metals and carbonaceous materials and with other materials.

Keywords: Counter electrode; Strontium Titanate (SrTiO_3); Composite materials; Polyaniline (PANI); DSSC.

SINTESIS DAN PENCIRIAN PLATINUM PERCUMA, TINDAK BALUS ELECTRODE BERASASKAN PENGALIR POLIMER UNTAK SEL SOLAR PEKA PENCLUP (DSSC)

ABSTRAK

Di antara semua alat fotovoltan, sel suria peka pewarna (DSSCs) dianggap sebagai salah satu sumber tenaga yang boleh diperbaharui yang paling berpotensi (alat) disebabkan oleh kaedah fabrikasi yang mudah, kos efektif dan mesra alam. Unsur-unsur tertentu seperti fotoanod (kebiasaannya titanium dioksida), elektrod kaunter (kebanyakannya platinum), peka pewarna (pelbagai jenis termasuk pewarna semulajadi dan organik) dan elektrolit (iodida dan tri-iodida) merangsang prestasi fotovoltan DSSCs. Setiap komponen mempunyai kepentingannya tetapi di antara semua, elektrod kaunter memainkan peranan penting. Elektrod kaunter menerima elektron dari beban luaran dan memindahkannya ke elektrolit untuk tindak balas redoks. Pewarna yang menerima elektron ini membantu dalam menganti elektron pewarna. Kesemua komponen ini memberi kesan yang ketara terhadap prestasi keseluruhan DSSCs. Pelbagai bahan termasuk bahan berasaskan karbon, oksida, sulfida, dan polimer yang konduktif telah diterokai sebagai bahan yang kos efektif, stabil dan sangat berkesan untuk penggantian elektrod kaunter berasaskan Pt (CE) dalam DSSCs. Baru-baru ini, banyak penyelidik menyiasat pelbagai bahan hibrid berasaskan komposit nano sebagai elektrod kaunter untuk DSSC. Ia telah ditemui bahawa bahan komposit yang mempunyai sifat pengurangan pemangkin yang tinggi, mempunyai permukaan yang tinggi ke arah aliran elektron dan rintangan pemindahan caj yang rendah menunjukkan potensi besar untuk penggantian CE berasaskan Pt. Di Dalam usaha ini, polimer pengalir telah dikaji sebagai elektrod kaunter untuk DSSC. Untuk mengkaji struktur, komposisi kimia, reaksi optik dan prestasi fotovoltan, Mikroskop Medan Pancaran Pengimbasan Elektron (FESEM), Pembelau Sinar X-ray (XRD), Spektroskopi Inframerah Transformasi Fourier (FTIR), Spektroskopi Ultraungu-Boleh nampak (UV-vis) dan analisa elektrokimia telah dikaji.

Ujian prestasi fotovoltan telah dikaji untuk menyelidik, ketumpatan arus lawan voltan (J-V), dan kecekapan penukaran kuasa (PCE) DSSC di bawah keadaan piawaian. Adalah diperhatikan bahawa dengan penambahan SrTiO₃ dalam komposit nano polypyrrole (PPy), prestasi fotovoltan DSSC telah dipertingkatkan. PPy mencapai nilai kecekapan penukaran kuasa sebanyak 1.29% tetapi dengan peningkatan SrTiO₃, komposit nano polypyrrole hibrid PPy-SrTiO₃-25%, PPySrTiO₃-50% dan PPy-SrTiO₃-75% mencapai PCE 1.98%, 2.52% dan 2.08% masing-masing. Selain itu, berbanding dengan CE berasaskan Pt (2.17%), PPySrTiO₃-50% menunjukkan peningkatan PCE iaitu 2.17% dan 2.52% masing-masing. Dalam projek kedua, polyaniline (PANI) digunakan sebagai polimer pengalir untuk fabrikasi elektrod kaunter untuk DSSC. Kepekatan PANI yang berbeza diambil untuk mengoptimumkan kepekatan untuk kajian lanjut dengan membuat nanocomposite dengan PANI. PANI, kerana sifat uniknya, juga menunjukkan potensi yang besar sebagai CE untuk DSSC. Ia telah dilihat bahawa PANI tanpa bantuan dengan konsentrasi 20 mg/ml menunjukkan peningkatan tindak balas fotoelektrokimia berbanding dengan PANI-1 dan PANI-2. Prestasi elektrokatalitik dan fotovoltan PANI-3 dapat dipertingkatkan dengan penambahan logam oksida, logam peralihan dan bahan-bahan karbonik serta bahan lain.

Kata kunci: Elektrod kaunter; Strontium Titanate (SrTiO₃); Bahan komposit; Polyaniline (PANI); DSSC.

ACKNOWLEDGEMENTS

My utmost gratitude and earnest obligations to the almighty Allah Subh'anahu Wa Ta'ala who has created me and help me to finish all very smoothly and efficiently.

I extremely thankful to my supervisors **Professor Dr. Nasrudin Abd Rahim, Dr. Mahdi Alizadeh** and **Dr. Adarsh Kumar Pandey** for their brilliant supervision, cordial help, enthusiastic encouragement and kind support. Under their kind supervision, I have grown up a student, as a researcher and person. The motivation and moral support helped me to complete my work without facing any difficulty. I am deeply indebted to all the lab and official staff of UM Power Energy Dedicated Advanced Centre (UMPEDAC) for their help and technical support. I would like to mention the name of my mentor **Dr. Shahid Mehmmod** who was always with me in this journey. My deepest regards for him for supporting me and being with me in all my work and in my life. I would also like to thank **Dr. Numan Arshid** and **Dr. Syed Shahabuddin** for their guidance throughout my master's journey.

I like to acknowledge the financial support of Higher Institution Centre of Excellence (HICOE), UM Power Energy Dedicated Advanced Centre (UMPEDAC) for supporting me research work. I am grateful to University Malaya for giving me this opportunity.

I am very thankful to my father (late), my mother, my brother and my sister for their unwavering support and prayers. Specially, to my brothers who always motivate me, and made me who I am today. Finally, I must recognize the strong support of my friends and my lover that kept me steadfast to the goal through all the pains and sufferings throughout this journey. I could not have achieved this much without her assiduous clinch and unremitting love and care.

TABLE OF CONTENTS

| | |
|--|-----------|
| Abstract..... | ii |
| Abstrak..... | iv |
| Acknowledgements..... | vi |
| Table of Contents..... | vii |
| List of Figures..... | x |
| List of Tables..... | xiii |
| List of Symbols and Abbreviations..... | xiv |
| CHAPTER 1: INTRODUCTION..... | 1 |
| 1.1 Background..... | 1 |
| 1.2 First Generation Solar Cell..... | 3 |
| 1.3 2 nd Generation Solar Cell..... | 3 |
| 1.4 3 rd Generation Solar Cell..... | 4 |
| 1.5 Operational Principle..... | 9 |
| 1.6 Measurement..... | 11 |
| 1.7 Problem Statement..... | 12 |
| 1.8 Objective of Research..... | 13 |
| 1.9 Outline of the Methodology..... | 13 |
| 1.10 Significance of Research..... | 14 |
| 1.11 Organization of Thesis..... | 14 |
| Chapter 2: LITERATURE REVIEW..... | 15 |
| 2.1 Counter Electrode in DSSC..... | 15 |
| 2.2 Preparation of Counter Electrode..... | 16 |
| 2.2.1 Thermal Decomposition..... | 16 |
| 2.2.2 Hydrothermal Method..... | 18 |
| 2.2.3 Chemical Vapor Deposition..... | 19 |
| 2.2.4 In Situ Polymerization..... | 21 |
| 2.3 Fabrication of Dye Sensitized Solar Cell (DSSC)..... | 23 |
| 2.3.1 Doctor Blade..... | 23 |

| | |
|---|-----------|
| 2.3.2 Screen Printing..... | 24 |
| 2.3.3 Spin Coating | 25 |
| 2.3.4 Electrodeposition (ED) | 26 |
| 2.4 Carbonaceous Counter Electrode Material..... | 29 |
| 2.5 Conducting Polymers as Counter Electrode..... | 35 |
| 2.6 Metal Oxide Counter Electrode..... | 43 |
| 2.7 Composites Materials Based Counter Electrode | 46 |
| 2.8 Challenges And Limitations | 50 |
| Chapter 3: METHODOLOGY | 52 |
| 3.1 Materials | 52 |
| 3.2 Synthesis of Material..... | 53 |
| 3.2.1 Synthesis of Polypyrrole (PPy)..... | 53 |
| 3.2.2 Synthesis of SrTiO ₃ Nano Cubes..... | 53 |
| 3.2.3 Preparation of Ppy-SrTiO ₃ Nanocomposite..... | 54 |
| 3.2.4 Synthesis of Polyaniline (PANI) | 54 |
| 3.2.5 Electrode Fabrication..... | 55 |
| 3.2.6 Fabrication of DSSC..... | 56 |
| 3.3 Characterizations Techniques..... | 57 |
| 3.3.1 Field Emission Scanning Electron Microscopy (FESEM)..... | 57 |
| 3.3.2 X-Ray Diffraction (XRD)..... | 59 |
| 3.3.3 UV-Vis Spectroscopy | 60 |
| 3.3.4 Fourier Transform-Infrared Spectroscopy (FTIR)..... | 61 |
| 3.3.5 Electrochemical Performance Study..... | 62 |
| Chapter 4: RESULTS AND DISCUSSION..... | 64 |
| 4.1 Strontium Titanate (SRTIO ₃) Nanocubes Interleaved into Conducting Polymer (PPY): A Counter Electrode for Dye Sensitized Solar Cells Applications | 64 |
| 4.1.1 Morphology Analysis | 64 |
| 4.1.2 UV-Vis Analysis..... | 69 |
| 4.1.3 FT-IR Analysis | 70 |
| 4.1.4 XRD Analysis..... | 71 |
| 4.1.5 Cyclic Voltammetry..... | 72 |
| 4.1.6 Electrochemical Impedance Spectroscopy EIS | 74 |
| 4.1.7 Photovoltaic Performance Analysis..... | 76 |

| | |
|--|------------|
| 4.2 Influence of Concentration of Polyaniline (PANI) as Counter Electrode in Dye Sensitized Solar Cell (DSSC)..... | 80 |
| 4.2.1 Morphology Analysis | 80 |
| 4.2.2 XRD Analysis..... | 81 |
| 4.2.3 FTIR Analysis..... | 82 |
| 4.2.4 UV-Vis Analysis..... | 83 |
| 4.2.5 Cyclic Voltammetry..... | 84 |
| 4.2.6 Electrochemical Impedance Spectroscopy EIS | 85 |
| 4.2.7 Photovoltaic Performance Analysis..... | 86 |
| Chapter 5: CONCLUSIONS, RECOMMENDATIONS AND FUTURE WORK.. | 88 |
| 5.1 Conclusions | 88 |
| 5.2 Recommendations | 90 |
| 5.3 Future Work..... | 91 |
| References..... | 92 |
| Appendix..... | 116 |
| List of Publications..... | 121 |

LIST OF FIGURES

| | |
|--|----|
| Figure 1.1: The raise in energy demand from 2006 to 2017 for PV | 2 |
| Figure 1.2: is representing the schematic diagram of DSSC. | 5 |
| Figure 1.3: Operational principle of DSSC..... | 11 |
| Figure 1.4: J-V curve of dye sensitized solar cell (DSSC) | 12 |
| Figure 2.1: SEM images of VO ₂ powder: (a) at low magnification (b) at higher magnification; screen printed VO ₂ thin films: (c) at low magnification (d) at higher magnification..... | 17 |
| Figure 2.2: Formation of cubic PtNi slender tentacles..... | 19 |
| Figure 2.3: (a) Represents attached floated graphene (f-G); (b) f-G coated FTO glass; (c) step-by-step development of CoS NPs onto graphene layer by CVD (d) fabrication of Dye sensitized solar cell via CoS-graphene electrode..... | 20 |
| Figure 2.4: Schematic Representation of the Synthesis of Counter Electrode and Fabrication of DSSC | 22 |
| Figure 2.5: Representing fabrication of DSSC | 22 |
| Figure 2.6: (a) represent the deposition of (HC/TiO ₂) counter electrode by doctor blade approach. (b) Shows complete assembly of dye sensitized solar cell by using HC/TiO ₂ counter electrode | 24 |
| Figure 2.7: Describing process of preparation of Ni _x Sy films | 25 |
| Figure 2.8: Illustrating mechanism for deposition of Pt-Ni/ rGO in electrophoretic deposition cell | 27 |
| Figure 2.9: Complete mechanism for the fabrication of PANI based CE..... | 29 |
| Figure 2.10: SEM image of BCM prepared of different bio wastes: (a) BCM-PW from phoenix wood; (b) BCM-PL from palm leaf; (c) BCM-FP from filter paper; (d) BCM-FT from facial tissue | 32 |
| Figure 2.11: Sketch for preparation of PEDOT-PSS-based mesoporous composite films | 37 |
| Figure 2.12: CV curve of PEDOT at different times | 40 |

| | |
|--|----|
| Figure 2.13: Preparation of poly (3,4-ethylenedioxythiophene) PEDOT counter electrode | 41 |
| Figure 2.14: Challenges and limitation for the commercialization of DSSC | 51 |
| Figure 3.1: Schematic Diagram Representing the Synthesis of Polypyrrole (PPy)..... | 53 |
| Figure 3.2. Schematic Diagram Representing the Synthesis of Polypyrrole (PPy) | 54 |
| Figure 3.3: Schematic Diagram Representing the Synthesis of Polyaniline (PANI)..... | 55 |
| Figure 3.4: Illustrating (a) PPy, (b) PPy-SrTiO ₃ -25 (c) PPy-SrTiO ₃ -50 (d) SrTiO ₃ -75%, and (e) dye dipped TiO ₂ coated photoanode (f) PANI-10 mg (g) PANI-15mg (h) PANI-20 mg counter electrode. | 56 |
| Figure 3.5: Fabrication of Dye Sensitized Solar Cell (DSSC)..... | 57 |
| Figure 3.6: Field Emission Scanning Electron Microscopy (FESEM)..... | 58 |
| Figure 3.7: X-Ray diffraction in crystal lattice. | 59 |
| Figure 3.8: X-ray diffraction (XRD)..... | 60 |
| Figure 3.9: Perkin Elmer LAMBDA 1050 Uv-vis Spectrophotometer. | 61 |
| Figure 3.10. Perkin Elmer FT-IR Spectrophotometer..... | 62 |
| Figure 3.11: Metrohm Autolab PGSTAT-204 used to investigate the electrochemical properties of DSSC | 63 |
| Figure 4.1: FESEM images of (a) PPy nanospheres, (b) SrTiO ₃ Nanocubes (c) PPy-SrTiO ₃ -25%, (d) PPy-SrTiO ₃ -50%, (e) PPy-SrTiO ₃ -75% fabricated as counter electrode in DSSC..... | 66 |
| Figure 4.2: FESEM- EDX Mapping images of (a) PPy-SrTiO ₃ -50%, (b) PPy-SrTiO ₃ -50%, (c) Silicon (d) Oxygen (e) Titanium (f) Strontium (g) Nitrogen (h) Carbon..... | 68 |
| Figure 4.3: UV-visible absorbance spectra of SrTiO ₃ , PPy, (b) PPy-SrTiO ₃ -25%, (c) PPy-SrTiO ₃ -50%, (d) PPy-SrTiO ₃ -75% counter electrodes | 70 |
| Figure 4.4: FT-IR spectrum of Ppy, SrTiO ₃ and PPy-SrTiO ₃ nanocomposites..... | 71 |
| Figure 4.5: XR D patterns of (a) PPy, (b) SrTiO ₃ and (c) PPy-SrTiO ₃ -50% | 72 |
| Figure 4.6: Cyclic voltammetry for PPy, PPy-SrTiO ₃ -25%, PPy-SrTiO ₃ -50%and PPy-SrTiO ₃ -75% CE obtained at a scan rate of 10 mV s ⁻¹ in a 10 mM LiI, 1 mM I ₂ acetonitrile solution containing 0.1 M LiClO ₄ as the supporting electrolyte. | 74 |

| | |
|---|----|
| Figure 4.7: Representing the Nyquist plots of PPy-SrTiO ₃ composite based counter electrodes..... | 75 |
| Figure 4.9: The photocurrent density–voltage curves of DSSC with PPy-SrTiO ₃ composite based counter electrodes. | 77 |
| Figure 4.10: The photocurrent density–voltage curves of DSSC with PPy-SrTiO ₃ -50% and Pt counter electrodes | 79 |
| Figure 4.11: (a) FESEM image of PANI Nanotubes (b) TEM image of PANI Nanotubes | 81 |
| Figure 4.12: XRD pattern of PANI Nanotubes..... | 82 |
| Figure 4.13: The FT-IR spectrum of PANI Nanotubes | 83 |
| Figure 4.14: UV-vis spectrum of PANI Nanotubes..... | 84 |
| Figure 4.15 Cyclic voltammetry of Pt, PANI-3 and bare ITO counter electrode at a scan rate of 50mV/s..... | 85 |
| Figure 4.16: Electrochemical impedance spectroscopy of bear ITO, PANI-3 and Pt counter electrodes..... | 86 |
| Figure 4.17: J-V curve of various concentration of PANI counter electrode Used for DSSC..... | 87 |

LIST OF TABLES

| | |
|--|-----|
| Table 2.1: Photovoltaic properties of DSSCs consisting of BCM counter electrodes derived from various bio-wastes | 32 |
| Table 2.2: Summary of the important results on carbon based counter electrodes..... | 34 |
| Table 2.3: Photovoltaic and electrochemical features of different PANI counter electrodes..... | 38 |
| Table 2.4: Summary of the important results on conducting polymer based counter electrodes..... | 43 |
| Table 2.5: Photovoltaic and electrochemical properties of different metal oxides..... | 46 |
| Table 2.6: Summary of the important results on composite based material as counter electrode in DSSC | 47 |
| Table 4.1: Illustrating the PV performance of PPy-SrTiO ₃ composite based counter electrode in Dye sensitized solar cell | 77 |
| Table 4.2: Summary of previously reported PPy composite based counter electrode for DSSC..... | 78 |
| Table 4.3: Photovoltaic parameters of DSSC based on PPy-SrTiO ₃ -50% and Pt counter electrodes..... | 79 |
| Table 4.4: Illustrating the PV performance of PANI based counter electrode in Dye sensitized solar cell | 87 |
| Table A.1: Copyright permissios | 116 |

LIST OF SYMBOLS AND ABBREVIATIONS

Symbols

| | | |
|-----------|---|---|
| I_{max} | : | Maximum current (A) |
| I_{sc} | : | Short circuit current (A) |
| J_{sc} | : | Short circuit current density (A/m ²) |
| P_{max} | : | Maximum power (W) |
| V_{oc} | : | Open circuit voltage (V) |

Abbreviations

| | | |
|-------|---|---|
| APS | : | Ammonium Peroxydisulfate |
| BCM | : | Bio Wasted Carbon Material |
| CE | : | Counter Electrode |
| CNT | : | Carbon Nano Tubes |
| CNF | : | Carbon Nano Fibers |
| CV | : | Cyclic Voltammetry |
| CVD | : | Chemical Vapour Deposition |
| DSSC | : | Dye Sensitized Solar Cell |
| EDX | : | Energy-Dispersive X-Ray |
| EIS | : | Electrochemical Impedance Spectroscopy |
| FESEM | : | Field Emission Scanning Electron Microscopy |
| FF | : | Fill Factor |
| FT-IR | : | Fourier-Transform Infrared Spectroscopy |
| GW | : | Gigawatt |
| HC | : | Hydrophobic Carbon |

| | | |
|--------|---|---|
| HFCVD | : | Hot Filament Chemical Vapour Deposition |
| ITO | : | Indium Tin Oxide |
| J-V | : | Current Density vs. Voltage Curve |
| LUMO | : | Lower Unoccupied Molecular Orbit |
| MC | : | Mesoporous Carbon |
| NMC | : | Nitrogen-Doped Mesoporous Carbon |
| PANI | : | Polyaniline |
| PCE | : | Power Conversion Efficiency |
| PPy | : | Polypyrrole |
| PV | : | Photovoltaic |
| TEM | : | Transmission Electron Microscopy |
| UV-Vis | : | Ultraviolet–Visible Spectroscopy |
| XRD | : | X-Ray Powder Diffraction |

CHAPTER 1: INTRODUCTION

1.1 Background

Energy is indispensable for human life and safe and accessible supplies of energy are important for the sustainability of modern societies (S. Ahmad et al., 2012). Fossil fuels, in various forms, have been used as the primary source of energy supply and serve the energy needs for thousands of years. Conventionally, oil, coal and gas are the main fossil fuel sources used for energy harvesting (Edmonds & Reilly, 1983; Herzog & Golomb, 2004). Extensive use of fossil fuels, global warming, environmental concerns, and lack of cleanliness and depletion of fossil fuels are the main challenges in the doorway of human being. Currently, the use of energy as an economic weapon for unusual geographical supply of energy resources is also responsible for significant increases in fuel prices (O'Brian et al., 2003). Increase in global energy demand is likely to increase rapidly in the coming years. According to the International Energy Outlook Report (IEA-2018) the demand of energy across the globe is expected to rise / grow by 27% from 2017-2040. Energy is one of the most basic needs of humans. The accomplishments of civilizations were largely based on the use of different forms of energy to extend human capabilities to more efficiently and widely (Martin A Green, 2007). Providing adequate and affordable energy, eliminating poverty worldwide, is essential for improving human welfare and increasing quality of life.

The increase in energy consumption, global warming and depletion of non-renewable sources of energy are the alarming threats for modern industrialization. Therefore, the interest of researchers was diverted from fossil fuels toward the renewable sources of energy in the last few decades (Halme, 2002). The renewable sources of energy are also capable of recovering alternative energy, such as the solar energy, geothermal

energy, wind energy, biomass (bio fuels), and hydropower energy (Johansson, Reddy, Kelly, Williams, & Burnham, 1993; Panwar, Kaushik, & Kothari, 2011). Among the others renewable energy resources, solar power is the future of clean energy is considered as clean and highly potential renewable source of energy. Every day, the sun showering continuously to the earth atmosphere with 1367 W/m^2 that can be used to power everything on earth. The sun provides more energy to encounter the demands of the world (Su'ait, Rahman, & Ahmad, 2015). As a renewable energy source, solar power exhibits great potential to transform electricity into an efficient and cost-effective manner. Among other solar energy harvesting approaches, photovoltaic (PV) cells are the most suitable method for direct conversion of solar power into electrical energy (Barua, Tawney, & Weischer, 2012). Solar PV plays a fundamental role in energy sectors in several countries (PVPS, 2017). In last few years estimated 98 Giga Watt (GW) of photovoltaic power has been fixed world wise. The increase in demand for PV from 2006 to 2017 has been illustrated in Figure 1.1

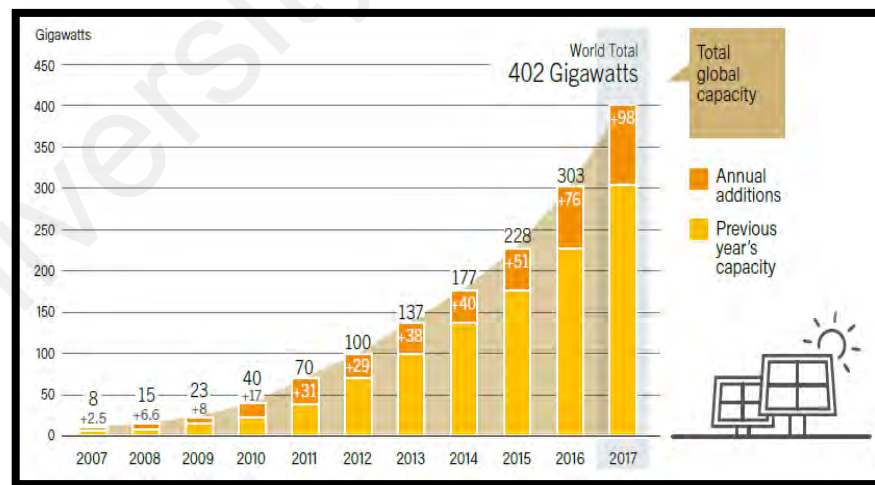


Figure 1.1: The rise in demand for PV from 2006 to 2017

Being a significantly developing technology, different species of solar photovoltaics has been developed in recent few decades. The advancement in PV technology is bases on their efficiency, time payback, durability and technical/ economic feasibility. Few of

them are highly efficient than others but are not economical due to their high cost. Out of many, only a few sorts of PV have been commercialized since many photovoltaic technologies are still not systematically viable (Chopra, Paulson, & Dutta, 2004; Jena et al., 2012). Based on material used, operational principles and commercial maturity, solar cells are parted into three basic generations.

1.2 First Generation Solar Cell

The earliest solar cell technology is the most famous and efficient technology based on thin silicon wafers. These cells are built upon by on single crystal silicon wafers and are very high-priced due to high temperature and highly intricate process of fabrication. Silicon-based photovoltaics were first fabricated in 1954 by Bell's Labs and thus gained significant scientific attention of researchers for nearly more than 50 years in view to their peculiar properties. Currently, 1st generation of solar cell achieved high power conversion value of 22.4 % - 27.6%, revealing high rate of conversion of solar energy to electrical energy (Chu & Majumdar, 2012; Martin A Green, 1990). However, the high cost of silicon, fabrication of large quantity of silicon crystals and state of the art temperature processing for the preparation of Si based solar cell limits the production of 1st generation of solar cell. Furthermore, it was also observed that with the increase of temperature the efficiency of solar panels starts decreasing. Therefore, this technology is expensive and low mechanical flexibility and are rigid.

1.3 2nd Generation Solar Cell

Second-generation solar cells are commonly known as thin-film solar cells. In comparison to first generation solar cell, thin film solar cells are prepared from different layers of semiconductor materials. The combination of using low amount of material and cost effective fabrication technique allows the preparation of solar cell from thin film

solar cell (Yamaguchi, Takamoto, Araki, & Ekins-Daukes, 2005). To fabricate solar panels at low cost, thin film fabrication approach is considered as cost-effective technique. Thin film solar cells are prepared from copper indium gallium diselenide (CIGS), cadmium telluride (CdTe), which are non-silicon materials. Presently, the maximum power conversion efficiency of 2nd generation of solar cell was reported as 23.3% which is nearly comparable with the efficiency of 1st generation of solar cell (Krebs et al., 2009; Yamaguchi, Takamoto, Araki, & cells, 2006). Although thin film and polycrystalline silicon solar cells assured an improvement in solar energy harnessing technology due to low cost, but on the other hand, the materials like CdTe, copper indium gallium diselenide, which are used in 2nd generation of solar cell are less abundant in nature.

1.4 3rd Generation Solar Cell

The high production cost of first generation of solar cell shifted the interest of researchers toward other materials and techniques that led to the 2nd generation solar cells. The fabrication route required a huge amount of energy and manufacture was still high-priced. In 1970's the idea of third generation of solar cells was introduced by "Michal Gratzel" 3rd generation solar cells are considered as potential substitutes which are yet in the scientific research and development stage. There are various photovoltaic (PV) devices includes named as third-generation solar cell including organic/polymer solar cells (max. $\eta \sim 11.5\%$), perovskite solar cells (max. $\eta \sim 22.1\%$) dye-sensitized solar cells (max. $\eta \sim 13.1\%$) and quantum dot solar cells (max. $\eta \sim 11.3\%$) (Martin A. Green et al., 2018). This generation of cells declare a very low environmental effect, easy manufacturing approach and cost effectiveness which produce significant research on this area (Badawy, 2015; Bagnall & Boreland, 2008; Conibeer, 2007; M. Green, 2004; Martin

A Green, 2001; Martin A Green, Emery, Hishikawa, Warta, & Dunlop, 2015; B.-K. Kim & White, 2012; Polman, Knight, Garnett, Ehrlner, & Sinke, 2016).

Among other third generation solar cell approaches, DSSC is one of the most attractive technique owing easy fabrication, flexibility, operational simplicity and utilization of low cost naturally abundant materials. DSSC simply consist of (1) conducting substrate (ITO / FTO / Conducting Flexible sheets), (2) semiconductor active layer (TiO_2 photoanode layer), (3) dye sensitizer (Ruthenizer), (4) electrolyte (Iodide/tri-iodide) and (5) catalyst (Conventionally Py). The photon coming from sunlight hits the dye and it absorbs the photon from the incident light (photon). The excitation of electron occurs, and the excited electron moves towards the conduction band of semiconductor material. Here the excited electron is shifted on the way to external circuit through conducting substrate. The electrolyte present in the cell give its electron to the dye and accepts an electron from the external circuit by the help of counter electrode (Fakharuddin, Jose, Brown, Fabregat-Santiago, & Bisquert, 2014; B. Lee, He, Chang, & Kanatzidis, 2012; M. Wu et al., 2012).

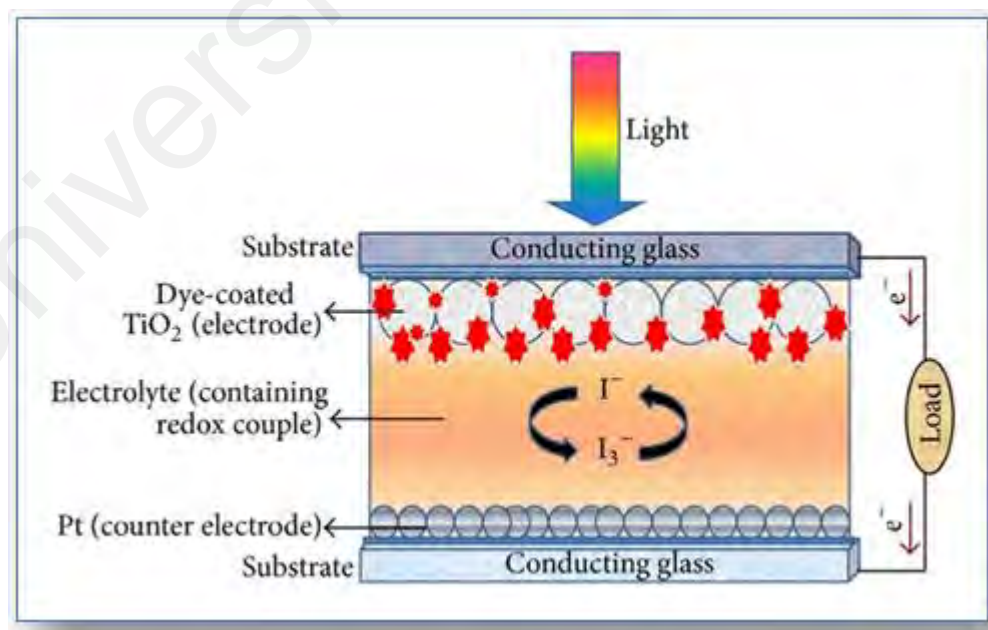


Figure 1.2: Representing the schematic diagram of DSSC
(Copyright permission is attached in Appendix A)

A significant research has been done in past few years for devolving new techniques and methods for the fabrication of efficient and cost-effective dye sensitized solar cell. The power conversion efficiency of DSSC rely on different components including structural morphology, size of the particle, thickness of photoanode layer (TiO_2), electrolyte (Iodide/tri-iodide), and dye (Bockris, 2013; Nazeeruddin et al., 2005). For high performance of DSSC the dye must need to cover the whole infrared and visible spectrum of the available light, and the lower unoccupied molecular orbit (LUMO) of dye must be greater than the LUMO of semiconductor TiO_2 (Baxter, 2012; Hagfeldt, Boschloo, Sun, Kloo, & Pettersson, 2010). Because of the low band gap and excellent area for the transfer of electron TiO_2 nanoparticles are extensively used as Photoanode (Bai, Mora-Sero, De Angelis, Bisquert, & Wang, 2014; K. S. Kim et al., 2012; Mehmood, 2017). With ruthenium dye, TiO_2 based photoanode exhibits the higher PEC value of 12% (lab Scale) (Kakiage et al., 2014). The electrolyte in DSSC helps in the oxidation and reduction of electron and also in the transport of electron from the counter electrode to oxidized dye. However, the liquid electrolyte effect the performance of DSSC due to limitations such as low electrode corrosion, leakage, stability, and limited stability (Theerthagiri, Senthil, Madhavan, & Maiyalagan, 2015). To overcome these limitation the some substitutes such as polymers and ($\bar{\text{I}}/\bar{\text{I}}_3$) composites material (Muthuraaman, Ganesan, Paul, Maruthamuthu, & Suthanthiraraj, 2011) and gelation of solvents (Bandara, Dissanayake, Jayasundara, Albinsson, & Mellander, 2012; M. Huang et al., 2007) have been investigated to enhance the performance of electrolyte (P. Wang, Zakeeruddin, Comte, Exnar, & Grätzel, 2003).

Counter electrode (CE) is an unescapable part of DSSC. Because of exceptional electro catalytic response for oxidation reduction ($\bar{\text{I}}/\bar{\text{I}}_3$), low charge transport resistance, high surface area for the flow of electron, and high stability, Pt coated on transparent conducting oxide (TCO) is widely used as counter electrode in DSSC (Z. Tang, Wu,

Zheng, Huo, & Lan, 2013). The role of CE very essential in catalytic reduction of (\bar{I}/\bar{I}_3) and regenerating electron, Currently, TCO coated Pt based counter electrode is expensive choices which contributes up to 50% in net cost of the device (Fakharuddin et al., 2014; Raj & Prasanth, 2016). Hence the cost of CE contributes up to 50% of the total cost of the device and hence limits the commercialization of DSSC (Mozaffari, Nateghi, & Zarandi, 2017). To overcome the limitation of commercialization and stability it is required to prepare a highly efficient, highly stable and economical counter electrode for DSSC by using naturally available noble metal free materials.

Recently, the efforts of researchers is shifted towards the fabrication of low cost, highly stable and cost effective counter electrode for DSSC. Conducting polymers (Jian He et al., 2014; Jeon, Kim, Ko, & Im, 2011; B.-w. Park et al., 2014; Peng, Tian, Liang, Mhaisalkar, & Ramakrishna, 2011), carbonaceous material (S. Huang et al., 2012; H. Wang, Sun, Tao, Stacchiola, & Hu, 2013; Yeh et al., 2014; Zhai et al., 2014), composite material, alloys (X. Chen, Tang, He, Lin, & Yu, 2014; Liu, Tang, He, & Yu, 2015; Q. Tang, Duan, Duan, He, & Yu, 2015; Wan et al., 2014) and transition metals compound (TMCs) (Banerjee et al., 2014; M. Wu et al., 2013; M. Wu et al., 2012) and have been widely investigated because of their high catalytic response, high surface area lower charge transfer resistance and high stability.

Among all others, nanostructured conducting polymer attained high interest, owing some unique properties of high conductivity, stability, expositional structural morphology which provides high surface area for charge transfer, and flexibility to make composites with other materials. Among other conducting polymers, Polyaniline (PANI), polypyrrole (PPy) and poly(3,4-ethylenedioxythiophene) (PEDOT) are extensively studied conducting polymers. PANI exhibits high catalytic property for redox couple, high conductivity and microporous structure for efficient flow of electron. PANI was

firstly investigated as counter electrode in DSSC by Li et al. (Q. Li et al., 2008b) Furthermore to enhance the catalytic performance and efficiency of PANI, different materials in composition with PANI has been exploited by different researchers previously (Ahmed, Rahim, Shahabuddin, Alizadeh, & Pandey, 2018). Like PANI and PEDOT, Polypyrrole (PPy) also exhibits unique catalytic property, high conductivity, high surface area high stability and mechanical properties. PPy thin film achieved the PCE of 7.66% , and it was found that PPy thin film showed high catalytic response and low charge transfer resistance for the flow of electron (J. Wu et al., 2008b). Demonstrating unique properties PPy can be one of the potential candidates use as counter electrode for DSSC.

On the other hand, the composites of metal and metals oxides is given attention due to their excellent properties, corrosive resistant, stability, high catalytic response and diverse structural morphology. SrTiO_3 exhibits unique structure (Nakashima, Kera, Fujii, & Wada, 2013) , characteristic electrochemical properties and is widely studied for verity of application in the field of photocatalysis (S.-T. Huang et al., 2014), photodegrading [(Shahabuddin, Muhamad Sarih, Mohamad, & Joon Ching, 2016; Shahabuddin, Sarih, Afzal Kamboh, Rashidi Nodeh, & Mohamad, 2016)] and photovoltaics. The high surface area and low charge transfer resistance of SrTiO_3 favors in the efficient transportation of electron from the counter electrode to redox couple electrolyte.

Presently, it is envisaged that polypyrrole in composition with SrTiO_3 conceivably allows a high electrocatalytic response, high conductivity. In Present work, we reported the PPy/ SrTiO_3 composite based counter electrode for dye sensitized solar cell. The structural morphology, optical behavior, composition, conductivity and photovoltaic performance of fabricated counter electrodes were investigated and discussed

1.5 Operational Principle

Photoanode is usually a semiconductor film TiO_2 deposited on the conducting substrate ITO/FTO, which is further sensitized by a single layer of Ru-complex dye (mostly used). The transport of electron from dye molecule to the semiconductor TiO_2 fully depend on the energy level of dye and semiconductor. The power conversion efficiency of DSSC rely on different components including structural morphology (nanorods, nanospheres, nanotubes, nanocubes, nanowires etc), size of the particle, light scattering property, additive materials and fabrication techniques of photoanode layer. Because of the low band gap (3.2 eV) and excellent area for the transfer of electron TiO_2 nanoparticles are extensively used as Photoanode in DSSC [(M. Ahmad, A. Pandey, & N. Rahim, 2018; M. S. Ahmad, A. Pandey, & N. A. Rahim, 2018; Kelly & Meyer, 2001; Pandey, Ahmad, Alizadeh, & Rahim, 2018; Sayama, Sugihara, & Arakawa, 1998)].

The monolayer “Dye” coated on photoanode absorbs sun light (photon) excites the electron in the HOMO of dye. The excited electron jumps from HOMO of the dye to LUMO and then moves to conduction band of photoanode (Hashmi et al., 2011; Pandikumar et al., 2016). For high performance of DSSC the dye must need to cover the whole infrared and visible spectrum of the available light, and the lower unoccupied molecular orbit (LUMO) of dye must be greater than the LUMO of semiconductor TiO_2 (Mozaffari & Nateghi, 2014)

The inserted “electrolyte” between photoanode and counter electrode acts as a bridge for the transport of electrons. (Longo & De Paoli, 2003; Meyer, 1997; J. Wu et al., 2015). Due to high temperature and stability the electrolyte exhibits low viscosity, (Bella, Galliano, Falco, et al., 2016; Bella et al., 2017; S. Zhang et al., 2016) melting point of $-20\text{ }^\circ\text{C}$ and high boiling point ($100\text{ }^\circ\text{C}$) is considered as highly efficient electrolyte.

Furthermore, high chemical stability and low absorption of light are the main parameters which helps in high performance DSSC.

Due to easy penetration of in the nanoporous structure of photoanode, Iodide/tri-iodide electrolyte achieved the attention of researchers from two decades for the high performance of DSSC. However, the liquid electrolyte effect the performance of DSSC due to limitations such as low electrode corrosion, leakage, stability, and limited stability (Theerthagiri et al., 2015). To overcome these limitation the some substitutes such as polymeric electrolytes, (\bar{I}/\bar{I}_3) composites material (Muthuraaman et al., 2011) and gelation of solvents (Bandara et al., 2012; M. Huang et al., 2007) have been investigated to enhance the performance of electrolyte (Bella, Galliano, Gerbaldi, & Viscardi, 2016; P. Wang et al., 2003) . The electrons from external circuit transfers toward counter electrode and then moves to dye via electrolyte (commonly \bar{I}/\bar{I}_3). The excited dye reduces to it normal state by receiving electrons from electrolyte (Theerthagiri et al., 2015).



The RC reduces to the surface of the counter electrode after oxidation.

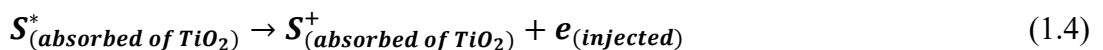


The complete operational principle of DSSC is described in Figure 1.3.

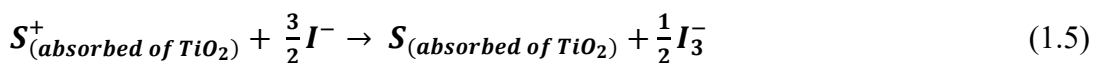
Photoexcitation.



Ejection of the electron.



Regeneration of dye.



Regeneration of iodine.

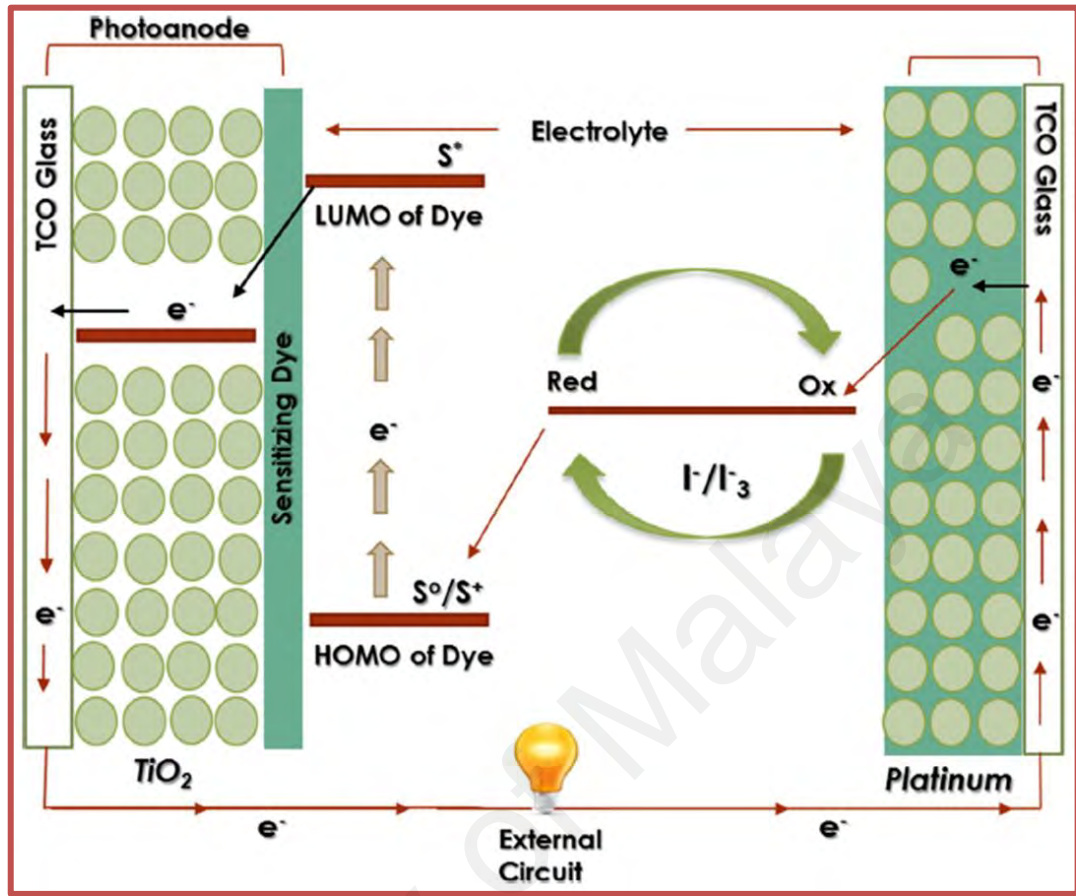


Figure 1.3: Operational principle of DSSC

1.6 Measurement

To evaluate the efficiency (η) of DSSC different parameters including, open-circuit voltage (V_{oc}), short circuit current density (J_{sc}), (between Fermi energy level of TiO₂ and redox mediator potential (\bar{I}/\bar{I}_3) in the electrolyte), fill factor (FF) and incident light power (P_{in}) are set as below:(Grätzel, 2001)

$$\eta(\%) = \frac{V_{oc} \times J_{sc} \times FF}{P_{in}} \times 100 \quad (1.7)$$

where FF is be given as

$$FF = \frac{V_{max} \times J_{max}}{V_{oc} \times J_{sc}} \quad (1.8)$$

Here the maximum voltage (V_{max}) and the maximum current (J_{max}) are the points representing maximum power output in J–V curves (Yu et al., 2016). J_{sc} value is dependent on the absorption of light, intensity of light, and efficient injection of electron. On the other side, the V_{oc} value relies on the Fermi level of the semiconductor and dark current as described in Figure 1.4.

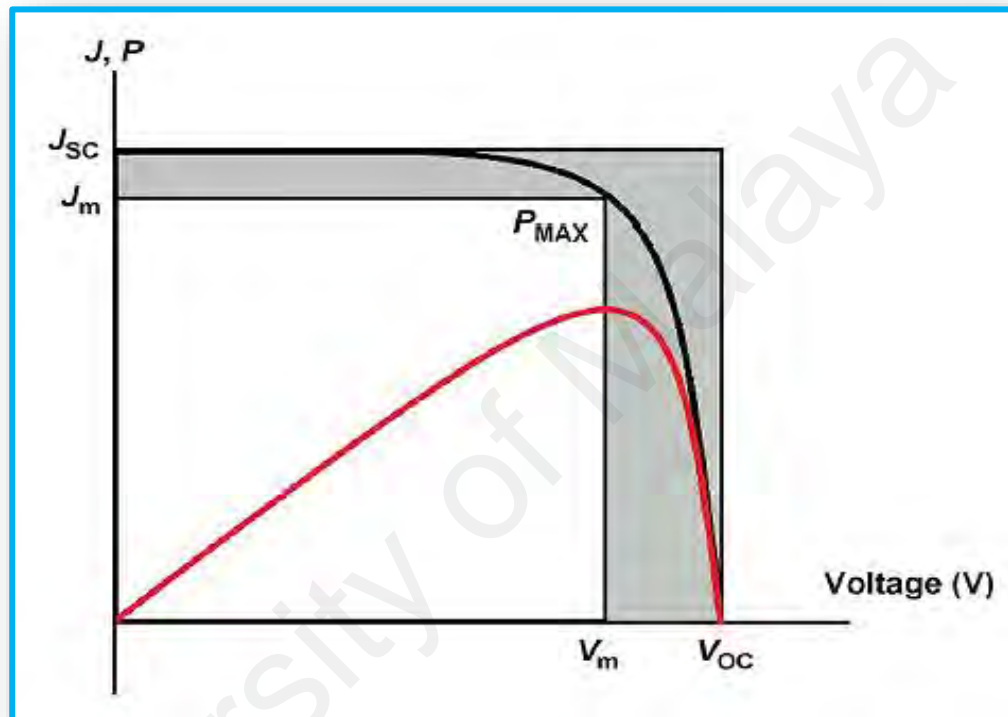


Figure 1.4: J-V curve of dye sensitized solar cell (DSSC) (Kouhnavard, Ludin, Ghaffari, Sopian, & Ikeda, 2015)

1.7 Problem Statement

The estimated cost of dye sensitized solar cell (90-120 USD.m⁻²) based on the highly cost material used for fabrication. In comparison with silicon based solar cell at the efficiency of 13-18% the cost of DSSC module should not be more than 0.65 USD/W. The low efficiency, low stability and high cost of DSSC is the main problem associated with the commercialization of DSSC. CE in DSSC is the main component and contribute about 50% of its cost due to the use of expensive metals. To make DSSC cost effective

and efficient the researchers are focusing toward the use metals free, carbonaceous material and conducting polymer based counter electrode for DSSC. On the other hand, significant amount of research has been done previously for developing low temperature and easy methods for the fabrication of DSSC.

1.8 Objective of Research

Following are the objective which have been set in this work:

1. To synthesize and characterize the conducting polymer based counter electrode for DSSCs.
2. To investigate the performance of conducting polymer based counter electrodes as alternative of Pt based counter electrode for DSSCs.
3. Cost effectiveness and comparative evaluation of conducting polymer based and composites of conducting polymer counter electrodes for DSSCs

1.9 Outline of the Methodology

The experimental methods have been devised to lower the fabrication cost and easy of availability of raw materials. The summery of methodology is as under.

1. Hydrothermal methods, in situ polymerization were used to synthesize conducting polymer-based nanocomposite materials. This method requires no toxic chemicals, eco-friendly and requires less skilled labor.
2. Spin coating, electrophoretic deposition, and Doctor Blade approach was used to fabricate active counter electrode films of nanocomposite materials. These methods are easy to be adopt for mass production and commercialization of the technology.
3. Various nanoparticles will be trailed with different concentrations to investigate their effect on the overall performance of DSSCs.

1.10 Significance of Research

This research has been carried out in the ambiance of nanocomposite-based energy material with unique photo and electro catalytic properties. The aim of this study is to investigate new materials, to improve overall performance and to reduce the cost of DSSC. This enhancement in PCE value and reduction of cost helps in the commercialization of DSSC modules. The use of conducting polymer-based nanocomposites as CE in DSSC will open new paths for the researchers to explore new materials as Platinum free counter electrode in DSSC. Also, easy and simple fabrication method used in our research will help to reduce the manufacturing cost of DSSCs.

1.11 Organization of Thesis

This thesis is consisting of five chapters, the contents of each chapter are organized as: The background of study, working mechanism of DSSC, problem statement, objective and methodology of research is stated in chapter 1.

Chapter 2 contain the comprehensive literature review on development of counter electrode, techniques used for the preparation of counter electrode, fabrication of electrode and problem related with the commercialization of DSSC

Chapter 3 gives the details for synthesis methods used for the preparation of samples, fabrication approach utilized for the fabrication of counter electrode and DSSC. In this chapter an attempt has been made to elaborate the characterization techniques which were involved in this work.

Chapter 4, in this section the obtain results were explaining thoroughly. The chapter presents the detail of the experimental work with the support of theoretical explanation. Then obtain results are then concluded in Chapter 5 with further future recommendations.

CHAPTER 2: LITERATURE REVIEW

2.1 ¹ Counter Electrode in DSSC

Electrode is an electrical conductor from where the electrons transport in an electrolytic or any other path, may be a anode (reduction) or cathode (oxidation), (Faraday, 1834; Weinberg, 2003). In dye-sensitized solar cell, TiO₂ covered electrode is called photoanode and Pt or other material coated electrodes are commonly named as counter electrode. Counter electrode accepts electron and sent them towards electrolyte for further work (Grätzel, 2003). Counter electrode with low value of internal resistance towards transport of electrons exhibits the high electro catalytic activity of reduction towards tri-iodide to iodide and shows high fill factor (FF) value. Despite of the fact that Platinum (Pt) coated (TCO) counter electrode is most expensive and less abundant material, it is still commonly utilized as CE in DSSCs because of high photoelectric property, highly conductivity value, and high stability. The dynamics responsible for high efficiency of the CE are transparency, low value sheet resistance of substrate and low charge transfer resistance of photo anode. The sheet resistance (R_s) should be $\leq 20 \Omega / \text{sq}^1$, charge transfer resistance (R_{CT}) of $2-3 \Omega \text{ cm}^{-2}$ and transparency greater than 80% (Trancik, Barton, & Hone, 2008; J. Wu et al., 2014). To prevail over these issues and to improve the photovoltaic efficiency of CE scientist are exploring new materials to replace Pt CE with highly efficient, cost effective and eco-friendly material for DSSC. Carbon based material, conducting polymers-based CE, metal oxide and sulfides showed great potential towards the replacement of Pt based CE in DSSC. The progression in the several

¹ Chapter 2 has been published (Ahmed, U., Alizadeh, M., Rahim, N. A., Shahabuddin, S., Ahmed, M. S., & Pandey, A. K. (2018). A comprehensive review on counter electrodes for dye sensitized solar cells: A special focus on Pt-TCO free counter electrodes. *Solar energy*, 174, 1097-1125)

types of counter electrode is further discussed thoroughly in this chapter to demonstrate the summary on CEs used in DSSCs.

2.2 Preparation of Counter Electrode

The preparation methods are responsible for the surface and structural morphology of counter electrodes. The preparation method determines the surface area of synthesized material, electro catalytic response towards redox couple reaction and the efficiency of the CE. The material having a high surface exhibits low charge transfer resistance and the nanoparticle sized materials showed high catalytic activity. There are different methods which were previously used by the researchers to synthesize different morphology and compositions of counter electrode for DSSC. Among all others, thermal decomposition method, hydrothermal method, chemical vapour deposition (CVD) approach and in situ polymerization are widely used for the preparation of different types of counter electrodes based on the material used.

2.2.1 Thermal Decomposition

Thermal Decomposition, an endothermic reaction (reaction which absorbs or requires heat/energy) which is exploited for the synthesis of porous structured CE for DSSC. This process helps to provide a uniform layer to coat on conducting substrate materials which enhances the PCE and stability of counter electrode. Lan. et al. (Lan, Wu, Lin, & Huang, 2012) used thermal decomposition technique to the fabrication of Pt counter electrode. They found that with the increment of very low amount of polyvinyl pyrrolidone (PVP) the size of particles, and coating of Pt on FTO can be improved. Furthermore, with the different weight percent of PVP, they reported that Pt CE having 3 to 5 times PVP in $\text{H}_2\text{PtCl}_6 \cdot 6\text{H}_2\text{O}$ showed the efficiency of 8.98%. Mutta, G. R., et al. (Mutta et al., 2016) studied Sphere-like VO_2 (M1) polymorph for CE in DSSC. Sphere-like VO_2 (M1) polymorph was synthesized via thermal decomposition approach. Figure 2.1 displays the

structural morphology (SEM image) of VO₂ (M1) polymorph and different magnifications were used to validate the sphere-like structure of VO₂ (M1) polymorph-based CE in DSSC. They found that Sphere-like VO₂ (M1) polymorph counter electrode exhibits high catalytic activity towards the reduction of electrolyte, found the efficiency of 1.25%. Zheng et al (Zheng et al., 2014) prepared nitrogen doped carbon tubes capturing FeNi nanoparticle (Pod(N)-FeNi) based counter electrode and achieved the photo conversion efficiency of 8.82%. The preparation of (Pod (N)-FeNi) CE was done through thermal decomposition method. Although the method is good for fabrication of highly efficient material but there is some limitation in thermal decomposition method including the size of particle cannot be adequately controlled and which in uniformity in the distribution of material on substrate (TCO).

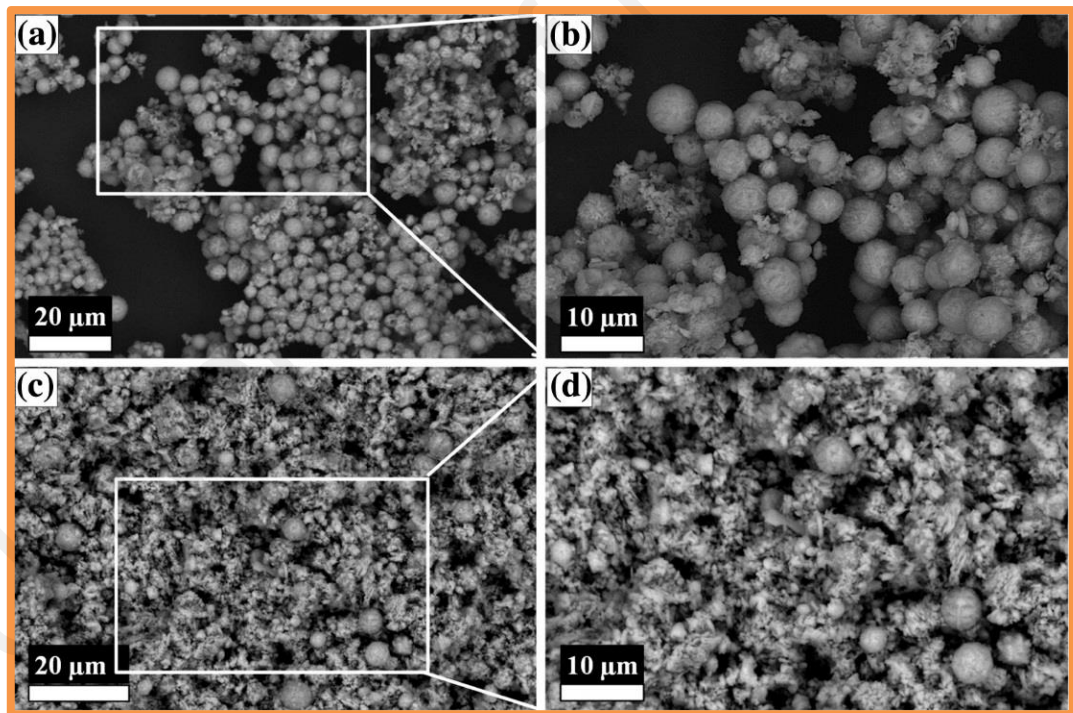


Figure 2.1: SEM images of VO₂ powder: (a) at low magnification (b) at higher magnification; screen printed VO₂ thin films: (c) at low magnification (d) at higher magnification

(Lan et al., 2012)

(Copyright permission is attached in Appendix A)

2.2.2 Hydrothermal Method

Currently, for the synthesis of nanocomposites-based metal oxide and sulfides counter electrodes, the most widely used method is hydrothermal technique. Morey, G. W. and P. Niggli (Morey & Niggli, 1913) give details that in hydrothermal process “the elements are subjected under the influence of solvent (aqueous or non-aqueous) and high temperature above 370 °C at certain pressure”. Li, P., et al. (P. Li, Cai, Tang, He, & Lin, 2014) synthesized binary ruthenium selenide (Ru-Se) CE through hydrothermal approach at normal temperature. The electrocatalytic performance of synthesized material was investigated via CV curves, Tafel polarization curves, Nyquist (EIS plots), and photocurrent density vs. voltage (J–V) curves. They found that Ru-Se alloy-based CE displayed the PCE value of 7.15% which is greater than the power conversion efficiency of Pt counter electrode (5.79%). Xiao, et al (Xiao & Han, 2015) studied nickel (Ni), cubic platinum (Pt) and (PtNi) bimetallic nano-crystal developed by hydrothermal approach (heated = 230 °C, Time (t)= 0.5, 1, 2, and 3 hours). The process for the preparation of cubic PtNi is illustrated in Figure 2.2. They reported that PtNi counter electrode hydrothermally treated for 2 hours shows high catalytic property toward iodides and achieves the power conversion efficiency of 8.95% under standard test condition (STC).

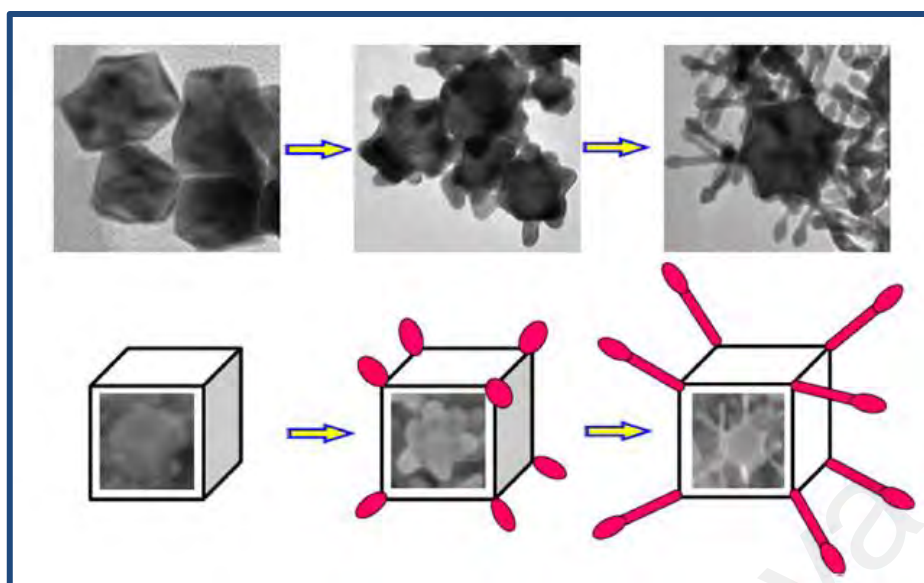


Figure 2.2: Formation of cubic PtNi slender tentacles
(Xiao & Han, 2015)
(Copyright permission is attached in Appendix A)

Luo, Y. et al. (Luo et al., 2014) investigated cobalt selenide ($\text{Co}_{0.85}\text{Se}$) counter electrode on FTO (treated with plasma) by hydrothermal method. They found that ($\text{Co}_{0.85}\text{Se}$) exhibits high surface area and catalytic response for the reduction of electrolyte. In another study, hydrothermal technique was utilized to prepare nanoscale CoS_2/rGO counter electrode by Zhu, L. et al. (2017). They analyzed that the fabricated counter electrode exhibits high catalytic activity reduction towards the tri-iodide to iodide. Comparing with other synthesis methods, hydrothermal approach economical, scalable, and simple method used for the preparation of metals oxide and sulfides with different structural morphologies. Via hydrothermal method, particle of different size, shape, structure and morphologies (nanorods, nanotubes, nanospheres, nano cubes, and nanofibers etc.) can be synthesized easily and effectively.

2.2.3 Chemical Vapor Deposition

A chemical vapour deposition (CVD) method is used for deposition of thin film on conducting or non-conducting substrates having numerous structures (single crystal, polycrystalline, amorphous, epitaxial etc.). This approach is convenient for the deposition

nano powders of different materials, and the thickness layer can be controlled according to desired parameters (Pierson, 1999). This method needs ultra-high temperature (up to 600 °C). Das, et al. (Das et al., 2012) deposited cobalt sulfide (CoS) incorporated with graphene film (G-CoS) by CVD method. The nanoparticles of CoS were distributed uniformly on graphene layers. They reported that G-CoS counter electrode exhibits current density (J_{sc}) value 2.50 mA cm^{-2} , high electrocatalytic activity for redox reaction and low resistance towards the flow of electron i.e $5.05 \Omega \text{ cm}^2$. The mechanism for synthesis and deposition of CoS on the graphene sheets, and fabrication of CE in DSSC is displayed in Figure 2.3. By CVD approach 3-dimensional graphene platform was synthesized by Tang, B. et al. (B. Tang, Hu, Gao, & Shi, 2013) and analyzed that 3-DG-N based CE slightly degrades the power conversion efficiency of DSSC.

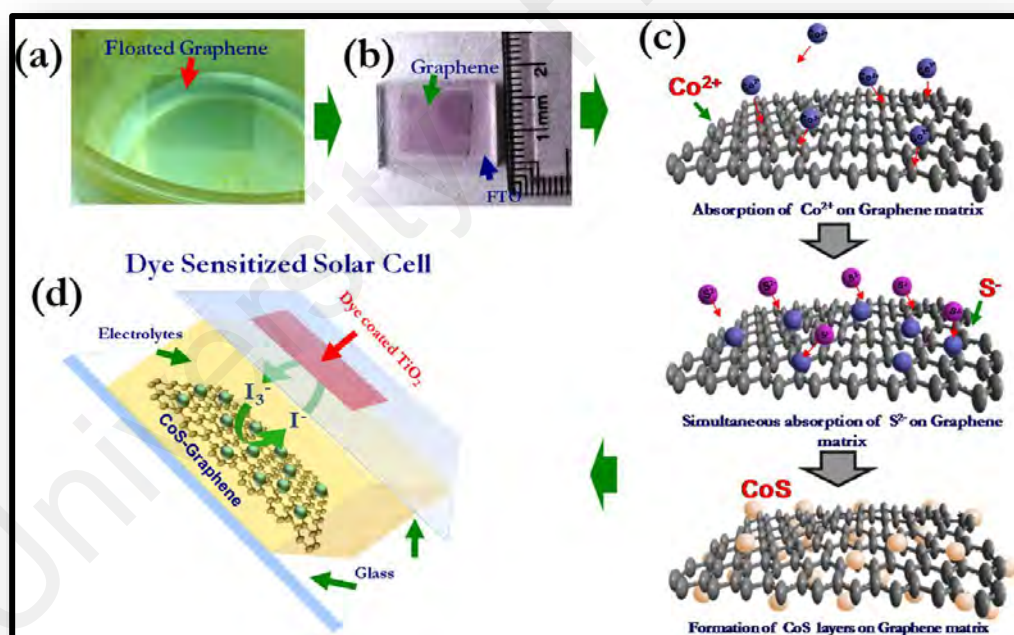


Figure 2.3: (a) Represents attached floated graphene (f-G); (b) f-G coated FTO glass; (c) step-by-step development of CoS NPs onto graphene layer by CVD (d) fabrication of Dye sensitized solar cell via CoS-graphene electrode.

(Das et al., 2012)

(Copyright permission is attached in Appendix A)

Hot filament chemical vapour deposition method (HFCVD), was used by Seo, et al. (Seo, Song, Ameen, Akhtar, & Shin, 2013) to synthesize graphene-like thin film onto

conduction substrate (FTO glass) which was used as a counter electrode in DSSC. They reported that the counter electrode exhibits high photo-current conversion efficiency (PCE) of 4.3%, with open circuit voltage (V_{oc}) of 0.728 V and short-circuit current density (J_{sc}) of 8.65 mA/cm². CVD method is an effective method for the development of thin film counter electrodes for DSSC. Although, having some advantages there are some limitation like, CVD requires high temperature up to 600 °C. Most of the substrates are not stable up to this temperature, hence this is found to be an expensive approach for the preparation of the counter electrodes.

2.2.4 In-situ Polymerization

The covalently bonded connection of monomers to form a large chain polymer is called polymerization. (Ravve, 2013). In situ polymerization approach is used for the development of conducting polymer (PANI, PEDOT, PVP, etc.) counter electrodes on conducting glass substrate. Anothumakkool, et al.(Anothumakkool et al., 2015) fabricated a completely Pt-TCO free counter electrode by synthesizing polyethylenedixythiophene (PEDOT) saturated cellulose paper through in situ polymerization. The mechanism of preparation of counter electrode is illustrated in Figure 2.4. They fabricated counter electrode and reported power conversion efficiency of 6.1 % similar to Pt-base counter electrodes. Further, by applying 40 um thick layer of PEDOT on FTO coated glass they found that PEDOT counter electrode exhibits a sheet resistance of 4 Ω sq⁻¹, and high value of conductivity of 357 S/cm⁻¹.

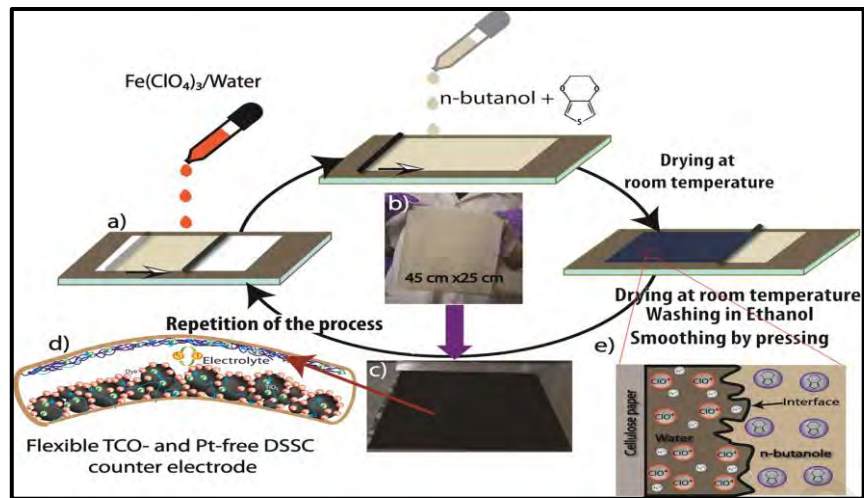


Figure 2.4: Schematic Representation of the Synthesis of Counter Electrode and Fabrication of DSSC (Anothumakkool et al., 2015) (Copyright permission is attached in Appendix A)

Bahramian A, Vashaee D. (Bahramian & Vashaee, 2015) synthesized polyaniline (PANI) based counter electrode by in situ polymerization. The coral-like TiO_2 photoanode was prepared by the sol-gel method at low temperature. The fabrication of DSSC utilizing PANI as counter electrode is illustrated in Figure 2.5. They reported that the PANI based counter electrode shows high catalytic activity and maximum energy conversion efficiency of 7.81% which is higher than the efficiency of Pt counter electrode (7.75%).

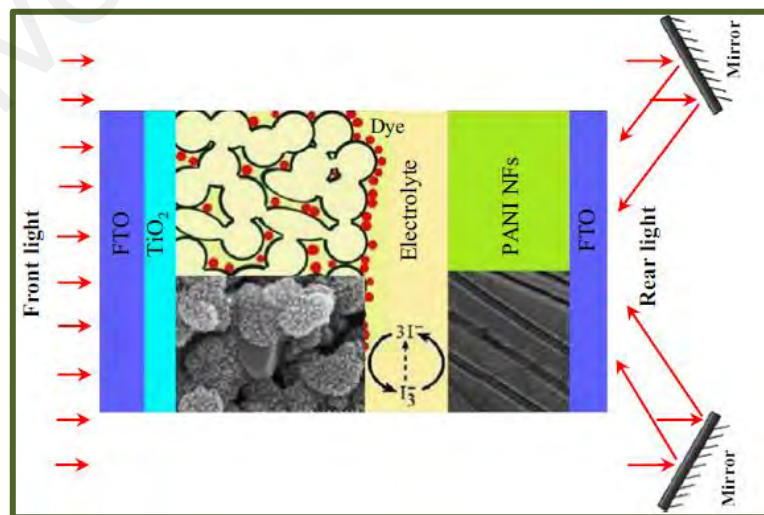


Figure 2.5: Representing fabrication of DSSC (Bahramian & Vashaee, 2015) (Copyright permission is attached in Appendix A)

In-situ polymerization is an attractive approach, which attracts the interest of researchers for the synthesis of conducting polymer-based counter electrodes. This approach helps in the fabrication of low cost and environmentally friendly counter electrodes for DSSC.

2.3 Fabrication of Dye Sensitized Solar Cell (DSSC)

Fabrication techniques of DSSC are also responsible for the efficiency, thickness of deposited layer, and economics. Screen printing, spin coating, electrophoretic coating and doctor blade are well-known approaches which were adopted by the researchers for the fabrication of DSSC.

2.3.1 Doctor Blade

This technique is broadly used for the development of a thin layer of liquid substrate on conducting glass substrate (FTO) having high surface area. Through this technique the thickness of layer varies from 10 μm to 150 μm which can be controlled easily (Aegerter & Mennig, 2013). Reduce graphene oxide/multiwall carbon nanotubes/nickel oxide (rGO/MWCNTs/NiO) counter electrode was synthesized by Al-Bahrani, Ahmad et al. (Al-Bahrani et al., 2015) The synthesized material was deposited on conducting substrate via doctor blade method and was used as counter electrode for DSSC. The photo current conversion efficiency of rGO/MWCNTs/NiO counter electrode was found to be 8.13%. The reported efficiency is greater than the efficiency of nickel oxide (NiO), reduce graphene oxide (rGO), nickel oxide/reduce graphene oxide NiO/rGO and platinum based counter electrodes. Kouhnavard et al (Kouhnavard et al., 2016) prepared hydrophobic carbon (HC) as the counter electrode where fabrication of DSSC was done via deposited coating (HC/TiO₂) on the conducting glass (FTO) by doctor blade method (illustrated in Figure 2.6). The power conversion efficiency was found to be 1.9% under standard test conditions (STC).

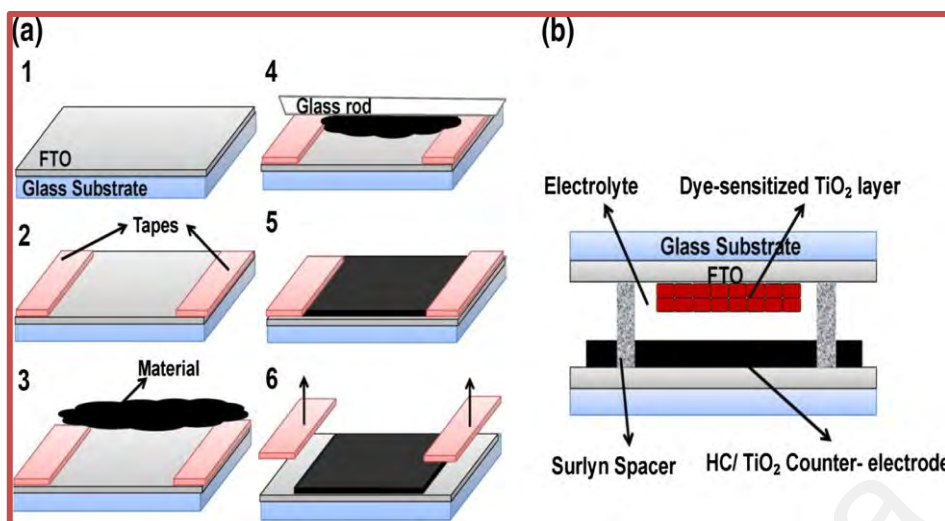


Figure 2.6: (a) represent the deposition of (HC/TiO₂) counter electrode by doctor blade approach. (b) Shows complete assembly of dye sensitized solar cell by using HC/TiO₂ counter electrode (Kouhnavard et al., 2016)

(Copyright permission is attached in Appendix A)

2.3.2 Screen Printing

Screen printing is one of the well-known technique used for the coating of different highly uniform structures and well-defined thin film on conducting substrate (FTO glass) in cost-effective way (Ahmadi et al., 2014). Pt nanoparticles introduced CNTs were synthesized by Gong, H. H. et al. (2014) as a counter electrode for DSSC. Uniform thin film of Pt-CNTs on FTO glass is obtained by screen printing technique. Carbon nanotubes (CNTs) enhance the electrochemical and photovoltaic properties of the counter electrode in DSSC. Pt-CNTs shows electrocatalytic properties reduction toward iodides, and also exhibits stable energy conversion efficiency (Gong, Hong, & Hong, 2014). Luo, Y. et al. (Luo et al., 2015) synthesized cobalt sulfide powder by chemical precipitation approach from cobalt acetate and sodium sulfide solution. Cobalt sulfide film was developed by conducting substrate by screen printing method which achieved the power conversion efficiency of 7.2%.

2.3.3 Spin Coating

Spin coating is a broadly-used quick approach, for the deposition of the thin uniform coating onto the surface of the substrate. The coating solution is dropped onto the substrate surface, uniform layer of solution is spread onto the surface by the high action spinning. The thickness may vary from nanometers to micrometers, which can be adjusted by mean of controlling spinning speed (no of rotation per minutes). Through spin coating fabrication, Kim, et al. (S.-J. Kim et al., 2014) investigated the electrochemical and photovoltaic characteristic of thermally reducing graphene (rGO) as counter electrode for DSSC. They examined variation in efficiency of reduce graphene (rGO) counter electrode under specific temperature and atmospheric conditions. The reported graphene reduces at 450 °C under Ar atmosphere and achieved a photo-current conversion efficiency of 6.02%. Sun, P. et al. (P. Sun et al., 2017) have developed transition metal chalcogenide Ni_xS_y films as a counter electrode through spin coating fabrication method by N,N-dimethyl form amide solution process. The fabrication of Ni_xS_y films is illustrated in Figure 2.7. Ni_xS_y films/FTO showing high electrocatalytic property reduction for iodide, low charge transfer resistance and exhibits high photoconversion efficiency of 6.6% like Pt/FTO counter electrode.

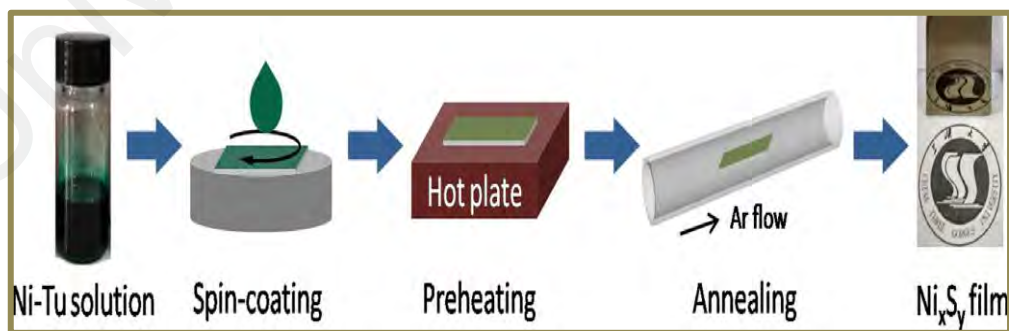


Figure 2.7: Describing process of preparation of Ni_xS_y films
(P. Sun et al., 2017)
(Copyright permission is attached in Appendix A)

2.3.4 Electrodeposition (ED)

Electrophoretic deposition (EPD) is a quick and economical approach for the coating of suitable solvent on the conducting substrate surface. The EPD is obtained by motion of charge particles in an aqueous solution or solvent under the influence of an electric field. (Dickerson & Boccaccini, 2011). Kim, H., et al. (H. Kim, Choi, Hwang, Kim, & Jeon, 2012) developed single wall carbon nanotubes (SWCNTs), multiwall carbon nanotubes (MWCNTs) and graphene coatings as counter electrodes fabricated via EPD. Graphene based counter electrodes exhibited good power conversion efficiency of 5.87% under STC as compared to SWCNTs and MWCNTs. Cobalt sulfide and reduced graphene oxide (CoS/rGO) film was coated onto the surface of SnO₂/FTO glass by EPD approach by Huo, J., et al. (Huo, Wu, Zheng, Tu, & Lan, 2015). They reported that the addition of rGO enhanced the catalytic activity of CoS toward reduction of iodides. Also, they found that CoS/rGO attained higher power conversion efficiency (9.39%) than that of Pt counter electrode (7.34%). Pt-Ni/ rGO as counter electrode for DSSC was investigated by Ghasemi, S., et al. (Ghasemi, Hosseini, & Kazemi, 2017). The fabrication of Pt-Ni/ rGO onto FTO glass surface was done by EPD method as illustrated in Figure 2.8. They reported that Pt-Ni/ rGO exhibits high electrocatalytic reduction of tri-iodide to iodide, low resistance and high surface area for flow of electrons.

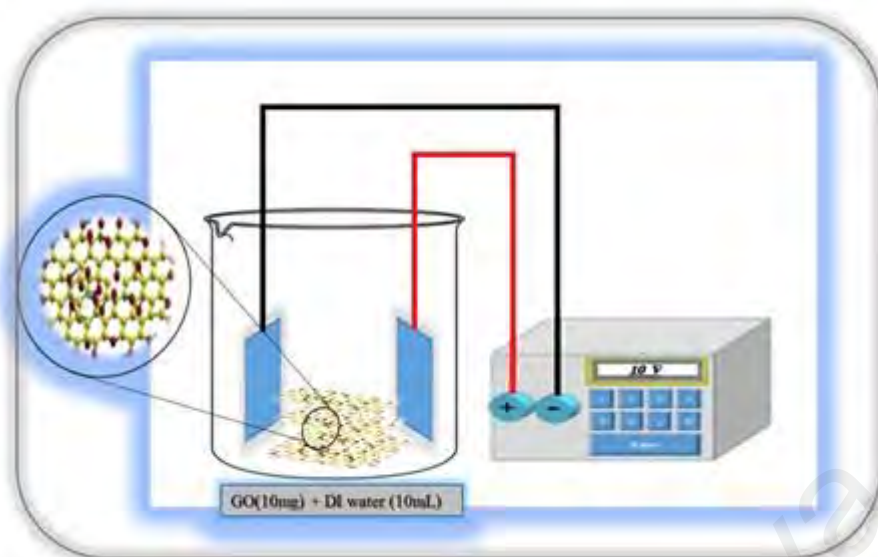


Figure 2.8: Illustrating mechanism for deposition of Pt-Ni/ rGO in electrophoretic deposition cell
(Ghasemi et al., 2017)
(Copyright permission is attached in Appendix A)

Cyclic voltammetry (CV) approach is one of most widely used approach for the electrochemical deposition of counter electrode in DSSCs. For controlled electrochemical deposition of PEDOT onto the surface of titanium mesh, Xiao, Y., et al (Xiao, Wu, Yue, Lin, Huang, Lan, et al., 2012) used cyclic voltammetry method. They investigated the electrochemical behavior of PEDOT/Ti as counter electrode in DSSC. They reported that the PCE of PEDOT/Ti reaches up to 6.3 % which is comparable with Pt. In another work (Xiao, Han, Li, Li, & Chang, 2014) two step cyclic voltammetry (under potential range of 0 V to 1.3 V for 1 cycle and 0 V to 0.8 V for 10 cycle) was used for the fabrication of PANI film on FTO glass. They found that the two steps electrochemically deposited PANI film CE attained the PCE of 6.21%. Carbonaceous materials, conducting polymers and their composites due to their high catalytic properties and high electrocatalytic response, are extensively studied material as CE in DSSCs. Hou, W., et al. (W. Hou, Xiao, Han, & Zhou, 2016) fabricated PPy /MWCNT counter electrode via CV deposition method. Initially, commercially available MWCNTs were functionalized by acid treatment methods (1:3 mixture of HNO₃ and H₂SO₄) and coated on FTO glass by spin coating method. Further, PPy was successfully deposited onto MWCNT coated on FTO.

The electro-polymerization of PPy onto the surface of MWCNTs was conducted for 12 cycles at the potential range of -0.4 V to 0.8 V. They found that the PPy/MWCNTs exhibits the PCE of 7.15 % which is comparable to Pt based counter electrode (7.76%).

Template method is most commonly used method for the synthesis of nanoparticles with different surface and structural morphologies including nanorods, nano wires, nanobelts and nanotubes (Xie, Kocaefe, Chen, & Kocaefe, 2016). This method also involves the deposition of nano sized particles onto the substrate for the preparation of different electrodes (Masuda & Fukuda, 1995; Ren & Tang, 2005; Xiao, Wu, Yue, Lin, Huang, Fan, et al., 2012). Hou, W., et al. (W. Hou, Xiao, Han, Fu, & Wu, 2016) fabricated PANI-NF counter electrode by using V_2O_5 NF as template. Briefly, V_2O_5 NF was prepared by electrospinning approach. For preparation of PANI based counter electrode, electrochemical bath polymerization approach is used for the deposition of PANI on V_2O_5 NF coated FTO. Using HCL as etching solution, PANI nanotube were successfully obtained after the removal of surplus V_2O_5 NF. The complete mechanism for the fabrication of PANI based counter electrode is illustrated in Figure 2.9. They found that PANI-NR counter electrode exhibits high catalytic response, and low charge transfer resistance toward the flow of electron. They reported 7.23% PCE for PANI-NR which was found to be comparable with PCE of Pt (7.42%) based CE. In another work by using poly (methyl methacrylate) (PMMA) as template Hou, W., et al. (H. Li, Xiao, Han, & Hou, 2017) fabricated honeycomb like transparent counter electrode for DSSC. To obtain PMMA film on FTO substrate, PMMA solution with different H_2O concentration were deposited onto FTO substrate via spin coating approach. Then, by CV approach, PEDOT film was deposited onto PMMA substrate. The PEDOT/PMMA film was then washed and dried at room temperature. The finally obtained counter electrodes were immersed in chloroform solution for removal of residual PMMA. They reported the PCE for honey comb like PEDOT counter electrode as 9.12% and 5.75% for front and rear side

respectively. PPy/MWCNT (honey comb structured) film was fabricated by Li, H., et al. (H. Li, Xiao, Han, & Li, 2017) via using PMMA as template. They found that the PPy/MWCNT counter electrode yield front and rear energy conversion efficiency value of 7.07% and 4.11 % respectively. To fabricate a counter electrode with high catalytic activity and larger surface area, Xiao, Y. and G. Han(Xiao & Han, 2016) used electrospun approach for the fabrication of 3D interconnected nanostructured Pt NF counter electrode for DSSC. They reported that by using electrospun technique, the performance of counter electrode in DSSC can be enhanced. The power conversion efficiency of Pt-NF was found to be 9.31%.

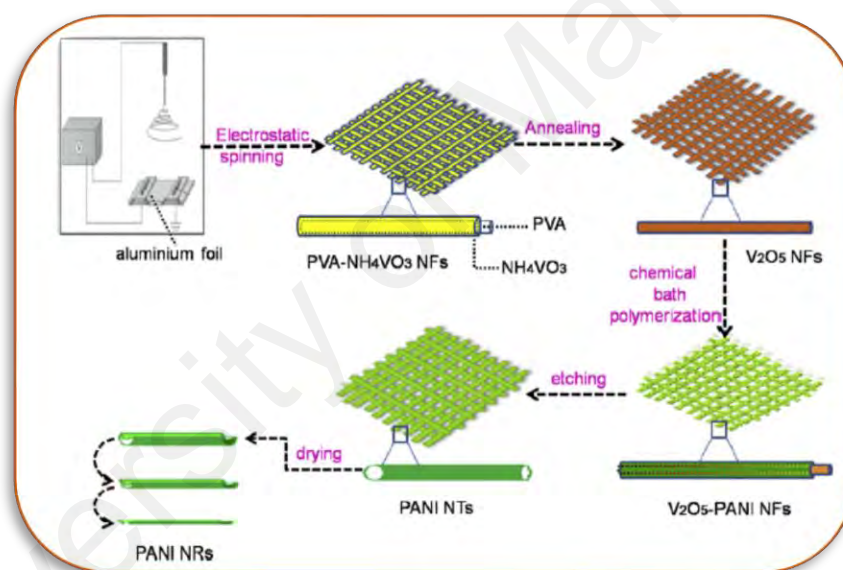


Figure 2.9: Complete mechanism for the fabrication of PANI based CE

2.4 Carbonaceous Counter Electrode Material

Some properties like low cost, large surface area, high conductivity corrosion toward iodine and high reactivity for tri-iodide reduction attracts the researchers to replace platinum electrode with the carbonaceous material (Grätzel, 2003; Numan, Shahid, et al., 2017). Graphene, carbon nanotubes, active carbon, graphite, carbon black, glassy carbon, carbon nanofiber are the suitable candidate to replace Pt as CE (Costa, Lodermeier, Casillas, & Guldi, 2014; Lei Wang, Liu, Konik, Misewich, & Wong, 2013). Graphitic-

carbon black mixture is first carbon-based CE developed by Gratzel in 1996 with power conversion efficiency (PCE) of 6.7% (Kay & Grätzel, 1996). Further the increase in thickness of carbon layer up-to 10 nm resulted in the enhancement of efficiency and fill factor of DSSC (Murakami et al., 2006; S. Xu, Luo, & Zhong, 2011).

Lee et al.(W. J. Lee, Ramasamy, Lee, & Song, 2008) reported power conversion efficiency of 7.56% using Nano-sized carbon as counter electrode. With high mechanical stability, a transparent carbon-based counter electrode was fabricated by in situ carbonization method. It was reported that bifacial counter electrode exhibited the PCE of 6.07% at front-side illumination and 5.04% under rear-side illumination. Further it was founded that, the optical characteristics of carbonaceous material based on composition and electrochemical properties of the carbonaceous material depend on the concentration of precursor (Bu, Liu, et al., 2013). Veerappan et al (Veerappan, Bojan, & Rhee, 2012) investigated spray-coated carbon CE, with the spray timing 420 sec. They have reported that the photoconversion efficiency of spray coated carbon is 6.2%. They also reported that colloidal graphite not only replaces the TCO but can also replace platinum at the same time, it may act dually as substrate as well as an electro-catalyst (Veerappan, Bojan, & Rhee, 2011). Chen et al.(J. Chen et al., 2009) reported PCE of 6.46 % which is higher than that of Pt-FTO based CE (6.37%) by using carbon black coated graphite as CE with the thickness of 0.2mm. Wu et al.(M. Wu, Lin, Wang, Qiu, & Ma, 2011) used different carbonaceous material based CEs including carbon black, discarded toner of a printer, carbon fibre, mesoporous carbon, conductive carbon, carbon dye, carbon nanotube, fullerene, and activated carbon. The mesoporous carbon shows high PCE of 7.5% as compared to others which is in the range of Pt-based CE. The composition of the material, surface area, concentration and crystallinity of the materials play a vital role in the efficiency. The PCE of carbon nano-fibres was studied by varying the temperature between 550-750 °C and found to be higher at 550 °C (Sebastián et al., 2014). Wang et

al. reported PCE of 7.02% using nitrogen-doped mesoporous carbon (NMC) as CE which was found to be comparable with Pt-counter electrode (7.26%). This directs that NMC as one of the best and cheapest replacement for Pt (G. Wang, Kuang, Wang, & Zhuo, 2013). Jian et al.(S.-j. Xu, Luo, Zhong, & Xiao, 2013) used a nonionic surfactant Triton X-100 modified mesoporous carbon (MC) as a carbon-based CE in DSSC and reported maximum PCE of 5.65%.

Xu, Liu et al. (S. Xu, Liu, & Wiezorek, 2018) collected twenty types of bio wasted carbon material (BCM) from a campus in Xinyu University, China. They divided these BCMs into three groups: (i) eleven woods, including weeping willow, Phoenix, camphor, Chinese fir, maple, peach, poplar, cypress, tea-oil camellia, orange, and chinaberry; (ii) seven leaves, including pine needles, camphor, palm, maple, poplar, Chinese fir, and red after-wood; and (iii) two papers, namely filter paper and facial tissue. They found that different carbonaceous material showed different structural morphologies which are illustrated in Figure 2.10. They reported the PCE of eleven kinds of wood ranges in 1.23% to 1.91%, the PCE of seven leaves varies from 1.07% to 1.85%. These efficiencies are higher than that of graphite, i.e. 0.77%. However, filter paper, and facial paper reaches up to the energy conversion efficiency of 4.70% due to better catalytic property and reduction for tri-iodide to iodide. The PV properties of BCMs are illustrated in Table 1.

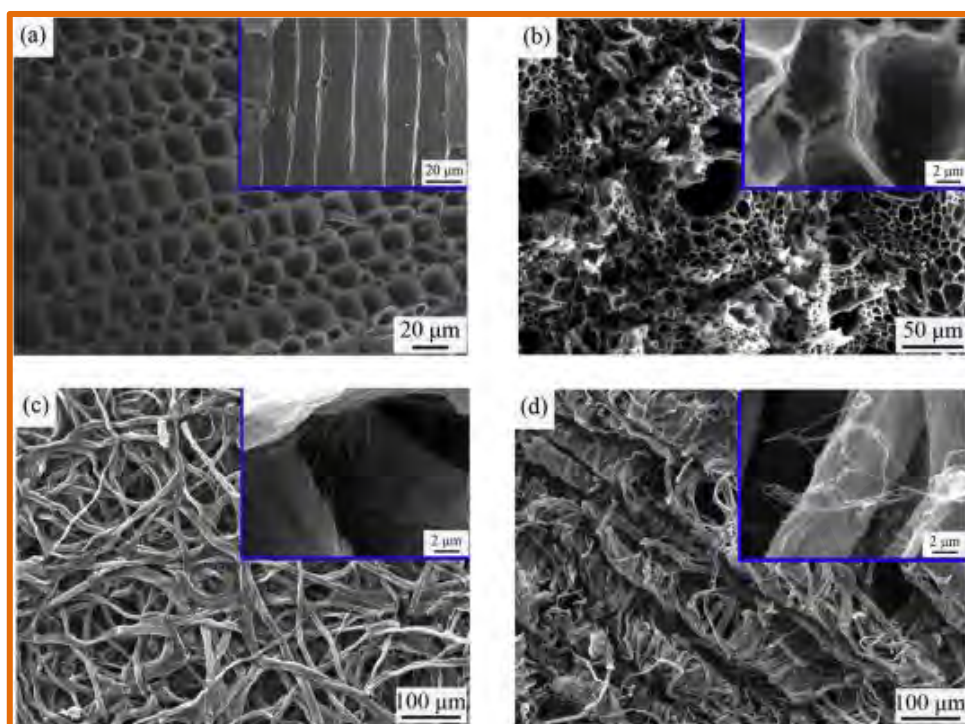


Figure 2.10: SEM image of BCM prepared of different bio wastes: (a) BCM-PW from phoenix wood; (b) BCM-PL from palm leaf; (c) BCM-FP from filter paper; (d) BCM-FT from facial tissue

(S. Xu et al., 2018)

(Copyright permission is attached in Appendix A)

Table 2.1: Photovoltaic properties of DSSCs consisting of BCM counter electrodes derived from various bio-wastes

(S. Xu et al., 2018)

| Group | Bio-waste | BCM yield (%) | Jsc (mA.cm ⁻²) | Voc (V) | FF | η (%) |
|------------------|----------------|---------------|----------------------------|---------|-------|-------|
| Wood | Weeping willow | 26.90 | 11.31 | 0.666 | 0.206 | 1.55 |
| | Phoenix | 28.12 | 12.14 | 0.647 | 0.243 | 1.91 |
| | Camphor | 26.84 | 11.31 | 0.643 | 0.217 | 1.58 |
| | Chinese fir | 29.88 | 10.79 | 0.652 | 0.196 | 1.38 |
| | Maple | 27.71 | 11.58 | 0.668 | 0.217 | 1.68 |
| | Peach | 27.49 | 11.42 | 0.672 | 0.193 | 1.48 |
| | Poplar | 27.69 | 12.15 | 0.621 | 0.243 | 1.83 |
| | | Cypress | 29.15 | 10.94 | 0.672 | 0.167 |
| Tea-oil camellia | | 28.57 | 10.54 | 0.623 | 0.209 | 1.37 |
| Orange | | 27.98 | 12.19 | 0.674 | 0.220 | 1.81 |
| Chinaberry | | 27.62 | 12.58 | 0.641 | 0.206 | 1.66 |

Table 2.1 continue

| | | | | | | |
|--------------|----------------|-------|-------|-------|-------|------|
| Leaf | Pine needles | 28.46 | 10.14 | 0.623 | 0.169 | 1.07 |
| | Camphor | 33.73 | 11.98 | 0.532 | 0.215 | 1.37 |
| | Palm | 30.70 | 11.53 | 0.632 | 0.254 | 1.85 |
| | Maple | 39.33 | 9.64 | 0.508 | 0.245 | 1.20 |
| | Poplar | 34.21 | 10.96 | 0.488 | 0.249 | 1.33 |
| | Chinese fir | 30.72 | 9.07 | 0.529 | 0.227 | 1.09 |
| | Red after-wood | 32.11 | 10.07 | 0.615 | 0.184 | 1.14 |
| Paper | Filter paper | 1.92 | 15.02 | 0.697 | 0.451 | 4.72 |
| | Facial tissue | 4.95 | 14.80 | 0.686 | 0.463 | 4.70 |

Lin, et al. (C.-H. Lin et al., 2017) prepared MoS₂ by simple two-step fabrication at room temperature. They deposit MoS₂ on FTO with 30 scan cycles, which was further annealed at 300 °C in Ar mixture gas to obtain 2-D MoS₂. After hydrophilic treatment, 2-D-MoS₂ nanoparticles were deposited onto the surface of 1D-CNTs to obtain MoS₂/CNTs-3D. They found the maximum power conversion efficiency of 3D vertically aligned MoS₂/CNT hybrid nano-architecture counter electrode was 7.83% which is due to the high catalytic activity of 2D-MoS₂ nanosheets for the reduction of tri-iodide into iodide in an electrolyte, and large surface area provided by 1D-CNTs. Here, the traditional Pt counter electrode shows the photoconversion efficiency of 7.15% which is 9.5% less than the efficiency of the MoS₂/CNTs-3D counter electrode in DSSC. Though, the PCE of MoS₂/CNTs-3D as CE was high as compared to Pt based CE but due to instability issue it has not been commercialized yet. Lukaszewicz, et al. (Lukaszewicz et al., 2017) synthesized graphene flakes by adding PEDOT: PSS or PEDOT: PSS/PVP through CVD method. They reported the energy conversion efficiency of 3.95% nearest to the conversion efficiency of the standard platinum-based counter electrode, i.e. 4.39%. They also reported that after 100 blending, the energy conversion efficiency varies from 2.37 to 3.23% which is higher than that of the Pt-based CE (2.08%).

Mengal, et al. (Mengal, Arbab, Memon, Sahito, & Jeong, 2017) fabricated cationised graphite which is obtained by dipping graphite in cationised lipase enzyme dispersant. They investigated that by nobbling fumed silica into graphite, the catalytic property of reduction from tri-iodide to iodide is enhanced due to the large surface area created by nano-spacer. Using hybrid structure as a counter electrode, they reported that the energy conversion efficiency of graphite is improved from 4.18% to 6.2%.

The important results on carbonaceous based CE are summarized in Table 2. As can be seen from the Table 2, the maximum PCE was found for carbon black (9.1%) as a CE followed by $\text{In}_{2.77}\text{S}_4$ (8.11%). The high PCE of carbon black is due to its high catalytic behavior and the surface area which provides low charge transfer resistance toward the electron flow. The lowest efficiency was found to be for carbon nano fiber CNF-550 °C (2.17%) as CE followed by carbon 300s (5.6%). It was found that CNF-550 °C exhibit high surface area but with the increase in temperature the charge transfer resistance was also increased which decreases the rate of transfer of electron and hence resulted in low PCE of counter electrode.

Table 2.2: Summary of the important results on carbon based counter electrodes

| CE materials | J_{sc} (mA.cm⁻²) | V_{oc} (V) | FF | PCE (%) | PCE (Pt) | Reference |
|----------------------------|--|-------------------------------|-----------|--------------------|---------------------|--------------------------|
| Carbon Black Powder | 11.34 | 0.825 | 0.712 | 6.67 | ---- | (Kay & Grätzel, 1996) |
| Carbon Black | 16.8 | 0.790 | 0.685 | 9.1 | ---- | (Murakami et al., 2006) |
| Glassy Carbon | 19.3 | 0.662 | 0.452 | 5.78 | ---- | (S. Xu et al., 2011) |
| Carbon | 16.50 | .0710 | 0.64 | 7.56 | 7.61 | (W. J. Lee et al., 2008) |
| Transparent carbon | 10.54 | 0.721 | 0.60 | 6.07 | 6.89 | (Bu, Liu, et al., 2013) |

Table 2.2, continue

| | | | | | | |
|---------------------------------------|-------|-------|-------|------|------|--------------------------|
| Carbon-300s | 12.7 | 0.818 | 0.54 | 5.6 | 6.70 | (Veerappan et al., 2012) |
| Carbon-420s | 13.1 | 0.818 | 0.57 | 6.2 | 6.70 | (Veerappan et al., 2012) |
| Graphite- TCO free CE | 12.0 | 0.816 | 0.60 | 5.9 | 6.81 | (Veerappan et al., 2011) |
| Pure Carbon | 13.1 | 0.703 | 0.70 | 6.46 | 6.37 | (J. Chen et al., 2009) |
| Carbon nanofiber (CNF-550 C) | 7.4 | 0.71 | 0.42 | 2.17 | ---- | (Sebastián et al., 2014) |
| NMC-3 | 16.43 | 0.68 | 0.65 | 7.02 | 7.26 | (G. Wang et al., 2013) |
| Graphene/carbon black C25G | 15.07 | 0.70 | 0.57 | 5.99 | 6.09 | (Miao et al., 2013) |
| In_{2.77}S₄ | 17.34 | 0.75 | 0.67 | 8.11 | 8.75 | (Guo et al., 2017) |
| MoS₂/CNTs | 16.65 | 0.74 | 0.66 | 7.83 | 7.15 | (C.-H. Lin et al., 2017) |
| Si@G10% | 16.63 | 0.706 | 0.546 | 6.42 | 7.32 | (Mengal et al., 2017) |
| Graphene | 13.1 | 0.7 | 63.6 | 5.87 | ---- | (H. Kim et al., 2012) |

Due to low cost and abundant availability in nature it has been attractive for the researchers to replace Pt-based counter electrode with carbonaceous material. Some drawback like the lousy connection of carbon film with TCO substrate, the requirement of a large quantity to attain best catalytic activity limits the extended run use of carbonaceous counter electrodes.

2.5 Conducting Polymers as Counter Electrode

The researcher's efforts have led us to the use of conducting polymers from last few years. Polymers exhibit excellent properties such as rapid acceleration of electrons, low cost, high stability, and high-altitude functionality for reducing (Jeon et al., 2011; Rafique, Abdullah, Shahid, Ansari, & Sulaiman, 2017). Polymers like polyaniline (PANI), Polypyrrole (PPy), and PEDOT (3,4-ethylene dioxythiophene) have already been accepted as the counter electrode in the dye-sensitized solar cell also showed

excellent response toward water purification, sensors and supercapacitor applications (Omar, Numan, Duraisamy, Bashir, et al., 2017; Omar, Numan, Duraisamy, Ramly, et al., 2017).

Over the past decade, PANI is one of the most studied polymers due to its natural fabrication, excellent electrical conductivity, environment-friendly, excellent photocatalytic property and good oxidation reduction activity toward iodide (Kang, Neoh, & Tan, 1998; Syed, 2016). Polyaniline (PANI) exhibit high photoelectric characteristics and high electrocatalytic activity for reduction of tri-iodide to iodide in redox reactions. (Q. Li et al., 2008a) Synthesized polyaniline (PANI) which serves as in cost-efficient counter electrode in the dye-sensitized solar cell (DSSC). They reported that polyaniline (PANI) shows the energy conversion efficiency of 7.15% as compared to the traditional Pt counter electrode with PCE of 6.90%. Nano-fiber of PANI also shows high catalytic activity and attain the photocurrent conversion efficiency of 6.21% reported by (Xiao et al., 2014), (J. Wu et al., 2008a) Fabricated nanoparticle polypyrrole (PPy) layered on fluorine tin oxide conducting glass, used as a counter electrode in the dye-sensitized solar cell. PPy electrode shows low charge transfer resistance and high electrocatalytic activity reduction toward tri-iodide to iodide as confirmed through cyclic voltammograms. They reported the power conversion efficiency of PPy counter electrode as 7.66%. Pt as counter electrode shows the efficiency of 6.90%, appearing 11% less than the efficiency of PPy counter electrode.

As a counter electrode, PEDOT conducting polymer exhibits good catalytic properties, notable electrical conductivity and stability. ((Yin et al., 2013)) developed PEDOT counter electrode at low temperature and utilized as a counter electrode in DSSC. They reported PCE of 7.04% for PEDOT counter electrode which is approaching to the Pt-based counter electrode (7.35%). (Sudhagar et al., 2011) reported that by introducing catalytic sulfides, energy conversion efficiency of PEDOT: PSS (PSS=polystyrene

sulfonate) can be enhanced. PEDOT: PSS exhibits PCE of 3.8%, after addition of CoS (copper sulfide) PCE further improves to 5.4%. (Muto, Ikegami, & Miyasaka, 2010) fabricated PEDOT-PSS-based mesoporous composite films which were used as a counter electrode in plastic DSSC. The fabrication process is illustrated in Figure 2.11. PEDOT-PSS mesoporous composite films as counter electrode showed excellent catalytic activity toward reduction of iodide. The reported maximum power efficiency with TiO_2 -ITO/PEDOT-PSS film ITO-PEN counter electrode as 4.38% and without TiO_2 -ITO, PEDOT-PSS film on ITO-PEN as 0.37%. Therefore, from their results they found that TiO_2 nanoparticle exhibited excellent photocurrent enhancement activity with PEDOT-PSS counter electrode as compared to without PEDOT-PSS film.

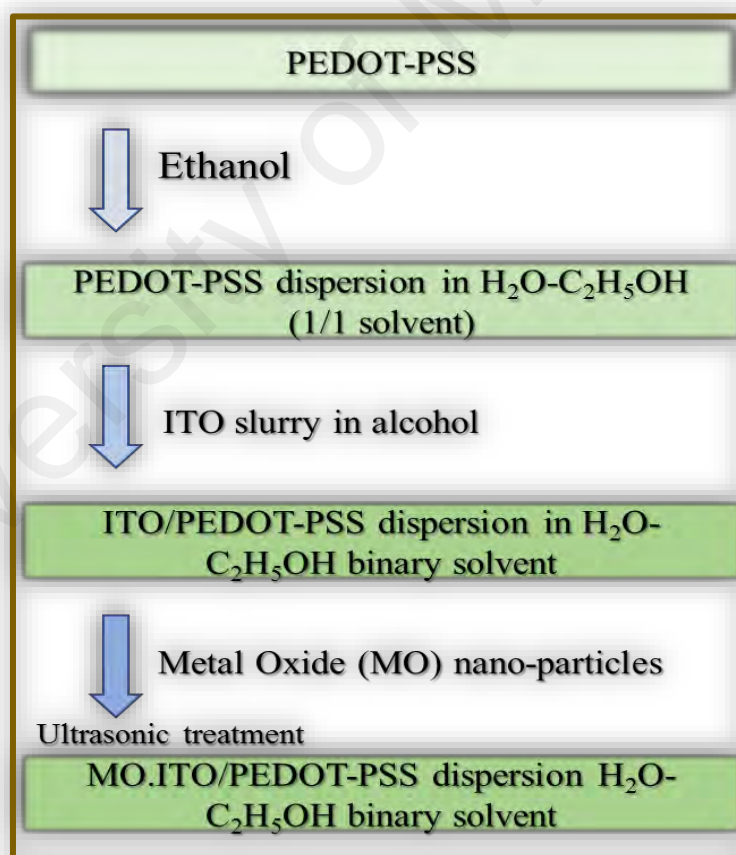


Figure 2.11: Sketch for preparation of PEDOT-PSS-based mesoporous composite films

(Muto et al., 2010)

(Copyright permission is attached in Appendix A)

(Taş, Gülen, Can, & Sönmezoğlu, 2016) fabricated Copper-doped polyaniline based counter electrodes PANI-Cu-X (X stand for the dopants, I⁻ and BF₄⁻) with various solvents such as H₂O, DMF, DO, THF, ACTN and CAN. The different samples were named as PANI (polyaniline), N-PANI (natural polyaniline). PANI-1(H₂O), PANI-2 (DMF), PANI-3 (DO), PANI-4 (THF), PANI-5 (ACTN), PANI-6 (CAN). To analyse the effect of formation of solvents on PANI-Cu-X, various characterisation methods including X-ray diffractions (XRD), Fourier transform infrared spectrometry (FTIR), scanning electron microscopy (SEM), thermal analysis (TGA, DTA), Ultraviolet–visible spectrophotometers (UV–vis) electrical conductivity measurements and energy-dispersive X-ray analysis (EDAX) were carried out. They reported that Polyaniline + Cu (acetonitrile) (NPANI-Cu-X in ACN) solvent reached the maximum photoconversion efficiency of 6.37%. The photovoltaic and electrochemical features of different PANI counter electrodes are illustrated in Table 2. The results give a suitable way for the development of Pt-free counter electrode for DSSC.

Table 2.3: Photovoltaic and electrochemical features of different PANI counter electrodes
(Taş et al., 2016)

| Sample | Code | Conductivity (S cm ⁻¹) | R _s (Ω) | R _{CT} (Ω) | PCE (%) |
|--|--------|---------------------------------------|-----------------------|------------------------|------------|
| Polyaniline | PANI | 1.51 x 10 ⁻⁴ | 14.21 | 20.23 | 2.44 |
| Neutral polyaniline | N-PANI | 14.7 x 10 ⁻⁶ | 14.62 | 31.32 | 1.36 |
| Polyaniline + Cu (water) | PANI-1 | 9.43 x 10 ⁻⁶ | 15.13 | 53.54 | 1.20 |
| Polyaniline + Cu (1,4 dioxane) | PANI-2 | 1.21 x 10 ⁻⁶ | 15.55 | 36.12 | 1.36 |
| Polyaniline+ Cu(dimethylforma mide) | PANI-3 | 8.35 x 10 ⁻⁵ | 14.02 | 28.22 | 1.51 |

Table 2.3, continue

| | | | | | |
|---|--------|-----------------------|-------|-------|------|
| Polyaniline + Cu (tetrahydrofuran) | PANI-4 | 6.54×10^{-3} | 17.15 | 26.88 | 2.07 |
| Polyaniline + Cu (acetonitrile) | PANI-5 | 2.92×10^{-1} | 14.01 | 5.13 | 6.37 |
| Polyaniline + Cu (acetone) | PANI-6 | 5.41×10^{-3} | 21.01 | 19.33 | 2.37 |

Dai, X. et al. (Dai, Li, Wu, & Xie, 2016) fabricated poly (3, 4-ethylene dioxythiophene) (PEDOT) film based CE through solid-state polymerization (SSP) technique. The polymerization was done merely by sintering the monomer, 2, 5-diiodo-3, 4-ethylene dioxythiophene (DIEDOT) at 135 °C. DIEDOTS were heated up to 135°C for different operating hours such as PEDOT-24 (24 hours), PEDOT-36 (36 hours), and PEDOT-48 (48 hours). Under STC (100 mW cm⁻², Temperature, 25 °C, AM 1.5), SSP-PEDOT-36 achieved highest power conversion efficiency of 6.38% with N719-sensitized TiO₂ photo-anode among others studied CEs. The efficiency of PEDOT, PEDOT-24, and PEDOT-48 were found to be 4.40%, 6.05% and 5.57% respectively while, traditional Pt-based CE exhibited the efficiency of 7.35%.

A Pt-free counter electrode by inserting reduce graphene oxide (rGO) into conducting polymers such as polyaniline (PANI), poly pyrole (PPy), and poly(3, 4ethylene dioxythiophene) (PEDOT) were synthesized by Li, et al. (R. Li et al., 2016). The composite of rGO/PPy, rGO/PANI, and rGO/PEDOT were intercalated on flexible polyethylene-terephthalate (PEN) substrate of Ti foil and were used as a counter electrode in the dye-sensitized solar cell. They reported the efficiency of rGO/PPy, rGO/PANI, and rGO/PEDOT for Ti foil substrate as 6.23%, 5.73%, and 4.65% respectively and for PEN substrate as rGO/PPy (4.41%), rGO/PANI (2.93%), and rGO/PEDOT (2.05%) respectively.

By electrochemical deposition method, Ma, J., et al. (Ma, Qingfeng, Fengbao, & Mingxing, 2017) fabricated flexible PEDOT electrode on ITO-PEN (indium-doped tin

oxide coated polyethylenaphthalate) for different deposition time's viz. 40s, 80s, 120s, and 160s. The electrocatalytic activity for reduction toward tri-iodide to iodide was examined by cyclic voltammetry (CV), Tafel polarization curve measurements and electrochemical impedance spectroscopy (EIS). The CV of PEDOT counter electrode with different deposition time 40s, 80s, 120s, and 160s is illustrated in Figure 2.12. They reported that when PEDOT electrode deposited for the 80sis used as a CE in dye-sensitized solar cell, the maximum energy conversion efficiency reaches to 7.18%. To enhance the catalytic activity of PEDOT, Pt/PEDOT composite was also synthesized. The efficiency of conventional platinum (Pt) based counter electrode and Pt/PEDOT was reported to be 7.56 and 7.90% respectively.

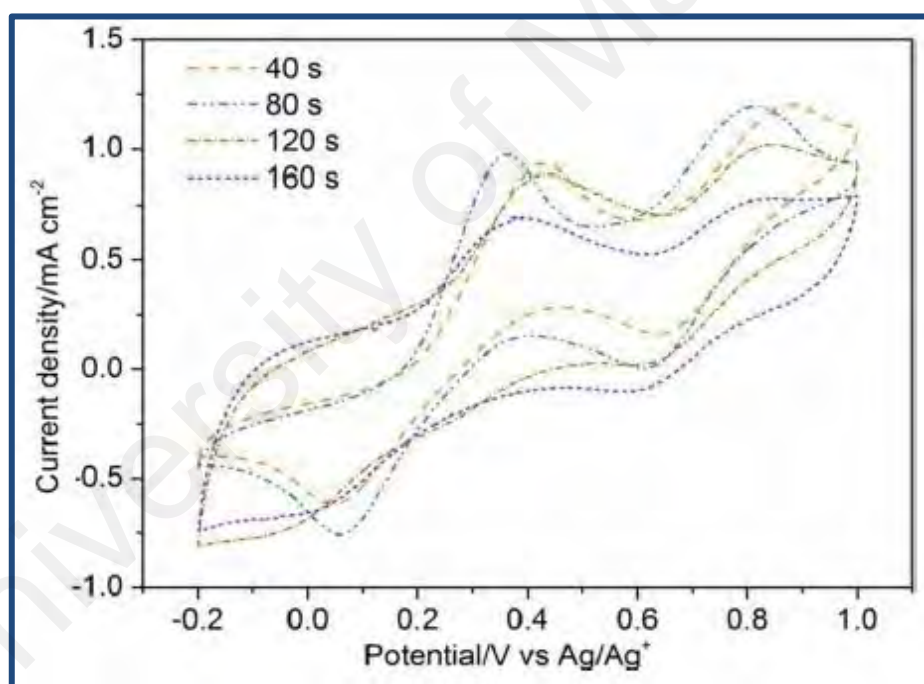


Figure 2.12: CV curve of PEDOT at different times
(Ma et al., 2017)
(Copyright permission is attached in Appendix A)

Li, Z., et al. (Z. Li et al., 2017) investigated the relation between PEDOT sheet resistance and their effect on the DSSC. They reported that the strength of PEDOT sheet resistance is finely adjusted by oxidation and reduction of iodine and hydrazine vapours. The fabrication of PEDOT counter electrode by the oxidation-reduction process is

explained in Figure 2.13. They also reported that V_{oc} is entirely independent of the sheet resistance of PEDOT.

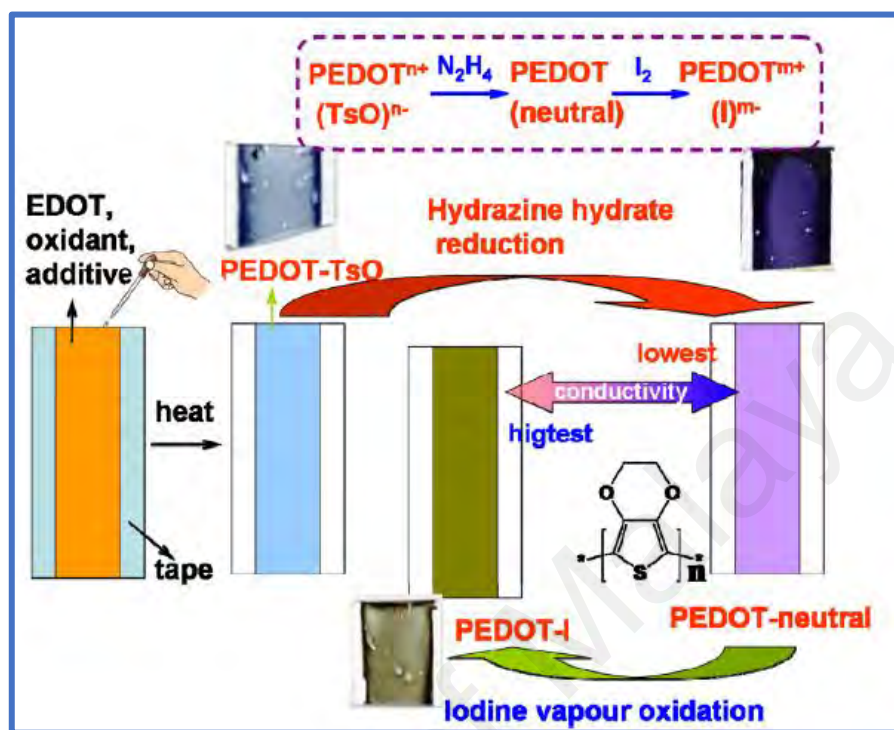


Figure 2.13: Preparation of poly (3,4-ethylenedioxythiophene) PEDOT counter electrode

Aparna, S. et al. (2017) synthesized PANI and PANI-SnO₂ by chemical co-precipitation technique, with a various weight ratio of PANI. The crystallinity, elemental composition, presence of PANI and tin oxide nano-composite and structure of composite are examined by X-ray Diffraction (XRD), Energy Dispersive X-ray Analyses (EDAX), Fourier-transform infrared spectroscopy (FTIR), and Scanning Electron Microscopy (SEM) respectively. On behalf of these results, they reported that PANI-SnO₂ nanocomposite is unexpensive and suitable selection for replacement of Pt-based counter electrode in dye-sensitized solar cell (Aparna, Elakhya, Gopal, Rajesh, & Ramasamy, 2017).

Shih, Y. et al. (Shih, Lin, & Lin, 2017) synthesized Polyaniline /graphene Nanoplatelet/multi-walled carbon nanotube (PANI/GNP/MWCNT) composite by an electrochemical polymerization method. The (PANI/GNP/MWCNT) composite weight

proportion of PANI/GNP/ MWCNT at 1:0.003:0.0045 was used as a cost-effective CE in the DSSC. They reported the highest photocurrent conversion efficiency of $7.67 \pm 0.05\%$ for PANI/GNP/MWCNT counter electrode, which is almost similar to Pt based CE ($7.62 \pm 0.07\%$). They analyzed that V_{OC} is highly related to reduction potential of redox couples but J_{sc} is slightly dependent on reduction current density of I^-/I_3^- . EIS and CV proved that, PANI/GNP/MWCNT composite exhibits low charge transfer resistance and high catalytic activity toward reduction of tri-iodide to iodide.

As can be seen from the Table 4, the maximum PCE was found for 0.3NiS (NP)/PEDOTS-PSS (8.18%) as a CE followed by PANI-G₁C₂ (7.67%). In 0.3NiS (NP)/PEDOTS-PSS based counter electrode the well redox peaks confirm high catalytic activity for redox activity property and the plane surface area provides pathway for the flow of electron which enhances the PCE of polymer based counter electrode. The lowest efficiency was found to be for rGO/PEDOT (2.05%) as CE followed by PEDOT:PSS (3.8%). The low PCE of rGO/PEDOT based counter electrode is due to improper connection of rGO/PEDOT film and conducting substrate (PET). It was analyzed that due to improper connection this CE shows high charge transfer resistance and low transfer rate for flow of electron.

Table 2.4: Summary of the important results on conducting polymer based counter electrodes

| CE materials | J _{sc} (mA.cm ⁻²) | V _{oc} (V) | FF | PCE (%) | PCE (Pt) | Reference |
|--------------------------------------|---|------------------------|-------|------------|-------------|--------------------------|
| PANI | 14.60 | 0.174 | 0.69 | 7.15 | 6.90 | (Q. Li et al., 2008a) |
| Nanofiber PANI (B-3) | 14.70 | 0.72 | 0.59 | 6.21 | 6.39 | (Xiao et al., 2014) |
| PEDOT | 16.26 | 0.710 | 0.61 | 7.04 | 7.35 | (Yin et al., 2013) |
| PEDOT: PSS | 11.6 | 0.66 | 0.49 | 3.8 | 6.1 | (Sudhagar et al., 2011) |
| TiO ₂ :ITO/PEDOT-PSS film | 12.2 | 0.66 | 0.55 | 4.38 | 5.41 | (Muto et al., 2010) |
| rGO/PPy | 14.2 | 0.589 | 0.527 | 4.41 | --- | (R. Li et al., 2016) |
| rGO/PANI | 11.6 | 0.527 | 0.479 | 2.93 | ---- | (R. Li et al., 2016) |
| rGO/PEDOT | 10.6 | 0.495 | 0.383 | 2.05 | ---- | (R. Li et al., 2016) |
| PEDOT-40s | 13.79 | 0.775 | 0.63 | 6.77 | 7.56 | (Ma et al., 2017) |
| PEDOT-80s | 14.17 | 0.788 | 0.64 | 7.18 | 7.56 | (Ma et al., 2017) |
| PEDOT-120s | 13.40 | 0.781 | 0.60 | 6.23 | 7.56 | (Ma et al., 2017) |
| PEDOT-160s | 11.64 | 0.779 | 0.58 | 5.24 | 7.56 | (Ma et al., 2017) |
| 30 _{vol.%} GDS/PEDOT/PSS | 14.70 | 0.718 | 0.70 | 7.36 | 8.46 | (C.-P. Lee et al., 2017) |
| 0.3 NiS(NP)/PEDOTS-PSS | 16.05 | 0.76 | 0.67 | 8.18 | 8.62 | (Maiaugree et al., 2017) |
| PANI-G1C2 | 18.21 | 0.780 | 0.54 | 7.67 | 7.62 | (Shih et al., 2017) |

2.6 Metal Oxide Counter Electrode

In the recent scenario, it was observed that the focus of researchers shifted towards the metal oxides based CEs for many applications (Chong, Numan, Liew, Ramesh, & Ramesh, 2017; Nadiah et al., 2017; Omar et al., 2016), due to their excellent properties such as catalytic activity high conductivity, good stability and are cost-effectiveness (Duraisamy, Numan, Fatin, Ramesh, & Ramesh, 2016; Numan, Duraisamy, et al., 2017; Numan et al., 2016; Shahid, Rameshkumar, Basirun, Juan, & Huang, 2017; Shahid, Rameshkumar, & Huang, 2015). Hence, due to these unique properties and

excellent thermal stability, metal oxide attains the interest of researchers for the fabrication of highly efficient Pt-free counter electrodes.

Wang et al. (H. Wang, Wei, & Hu, 2013) investigated the catalytic activity of zinc oxide as a CE. They reported that by conducting polymer, ZnO shows good photovoltaic performance. The electrochemical properties of ZnO/polymer were enhanced with the increment of ZnO, hence resulting in high surface area, excellent catalytic activity and good electrical response toward conversion of solar light. The achieved maximum power conversion efficiency was 8.17%. Tantalum oxide (TaO) has the high electrocatalytic activity for reduction of tri-iodide like platinum therefore, it can be utilized as a counter electrode in DSSC. TaO counter electrode shows energy efficiency of 6.8% which is better than that of Pt based counter electrode (Yun, Wang, Guo, & Ma, 2012). Feihl et al. (Feihl & Costa, 2012) investigated NiO oxide at different weight ratio. The catalytic activity and electrical response of NiO₂ was investigated with different parameters and at different weight concentration. They reported that 10% of the weight of NiO nanoparticle with ethanol shows good efficiency than others. Hydrogen-treated WO₃ fabricated by Cheng et al. (Cheng et al., 2013) was used as a counter electrode in DSSC and showed the efficiency of 7.25% where the efficiency of commercially available WO₃ is 0.63%. They found that hydrothermal treatment increases the catalytic activity of reduction and low charge transfer resistance due to high surface area.

Pan et al. (Pan, Wang, Jimmy, Liu, & Cheng, 2014) investigated two different phases of SnO₂ as a counter electrode and reported that D-phase SnO₂ shows energy conversion efficiency of 4.81% and the other phase SnO₂ shows the efficiency of 2.88%. D-phase SnO₂ shows high polarization current density and low charge transfer resistance. Due to the abundance of oxygen W₁₈O₄₉ nanofibers show superior electrocatalytic activity for reduction of tri-iodide and show the highest efficiency of 8.58% reported by Zhou et al. (Zhou et al., 2014). The efficiency of the traditional Pt-counter electrode is 8.78%.

Hou et al. (Y. Hou et al., 2013) reported that $\alpha\text{-Fe}_2\text{O}_3$ could be used as counter electrode. The absorption energy of iodine is like Pt counter electrode at acetonitrile/electrode interface. For the electrocatalytic activity of semiconductor, they used first-principles quantum-chemical calculations method.

Du, F. et al. (Du, Yang, Qin, & Li, 2017) investigated ternary oxide with different structural morphologies of NiCo_2O_4 nanosheets (NCO NS), NiCo_2O_4 nanorods (NCO NR), and NiCo_2O_4 nanofibres (NCO NF) as CEs. They fabricated the ternary oxide by the simple hydrothermal method. Among all ternary oxides, NiCo_2O_4 nanofibers (NCO NF) exhibited the highest conversion efficiency of 8.48%, which is higher than the efficiency of the conventional counter electrode. (8.11%). The PCE of other two ternary oxide NiCo_2O_4 (NCO NR), and NiCo_2O_4 (NCO NS) were found to be 6.84 and 3.57% respectively. The CV results revealed that NiCo_2O_4 nanofibers (NCO NF) counter electrode showed excellent catalytic activity toward reduction of tri-iodide to iodide due to 3D spatial structure.

Ahmad, K., et al. (K. Ahmad, Mohammad, & Mobin, 2017) synthesized multiparous nanorod of $\alpha\text{-MnO}_2$ via the hydrothermal process for CE. Multiparous nanorod $\alpha\text{-MnO}_2$ exhibited the power conversion efficiency of 4.1%. Further, they reported that when $\alpha\text{-MnO}_2$ counter electrode was introduced with glassy carbon electrode (GCE), (GCE/ $\alpha\text{-MnO}_2$) it showed excellent catalytic activity and excellent sensitivity for identification of nitroaromatic compounds (PPr) including p-nitrotoluene (p-NT), 2, 4, 6-trinitrophenol (TNP) and 2, 4-dinitrotoluene (DNT). Tsai, et al. (Tsai, Fei, Lin, & Shiu, 2018) investigated the photovoltaic and electrochemical properties of copper oxide (CuO) and graphene nanostructured copper oxide as counter electrode coated on FTO. After analyzing the electrochemical characteristics of CuO and CuO/Graphene nanostructured through CV and, EIS they reported that CuO and CuO/Graphene exhibits the PCE of 2.73% and 3.04% respectively.

As can be seen from the table 5, the maximum PCE was found for NCO-NF (8.48%) as a CE followed by ZnO/Polymer 32:1 as (8.17%). The nano flower like structure in NCO-NF counter electrode provide excellent area for the flow of electron and low charge transfer resistance and show good PCE. The electrochemical properties of ZnO/polymer was enhanced with the increment of ZnO, hence resulting in high surface area, excellent catalytic activity and good electrical response toward conversion of solar light.

Table 2.5: Photovoltaic and electrochemical properties of different metal oxides

| CE materials | J _{sc} (mA cm ⁻²) | V _{oc} (V) | FF | PCE (%) | PCE (Pt) | Reference |
|--------------------------------------|---|------------------------|------|------------|-------------|--|
| ZnO/Polymer (32:1) | 19.71 | 0.862 | 0.48 | 8.17 | ----- | (H. Wang, W. Wei, et al., 2013) |
| TaO | 12.59 | 0.770 | 0.67 | 6.48 | 7.16 | (Yun et al., 2012) |
| H-WO ₃ | 15.46 | 0.745 | 0.47 | 5.43 | 7.14 | (Cheng et al., 2013) |
| SnO ₂ -δ | 17.21 | 0.533 | 0.52 | 4.81 | ----- | (Pan et al., 2014) |
| W ₁₈ O ₄₉ NFs | 17.41 | 0.701 | 0.66 | 7.94 | 9.35 | (Zhou et al., 2014) |
| W ₁₈ O ₄₉ NFBs | 17.08 | 0.711 | 0.63 | 7.66 | 9.35 | (Zhou et al., 2014) |
| α-Fe ₂ O ₃ | 15.92 | 0.784 | 0.56 | 6.96 | 7.32 | (Y. Hou et al., 2013) |
| NiCo ₂ O ₄ -NF | 17.01 | 0.770 | 0.64 | 8.48 | 8.12 | (Du et al., 2017) |
| α-MnO ₂ Nano-rods | 14.70 | 0.655 | 0.38 | 4.10 | ----- | (K. Ahmad et al., 2017) |
| CuO+GNs | 15.62 | 0.690 | 0.31 | 3.40 | 6.36 | (Tsai et al., 2018) |
| WO _{2.72} | 14.90 | 0.770 | 0.70 | 8.03 | 8.08 | (Zhou et al., 2013) |
| NbO ₂ | 13.90 | 0.810 | 0.70 | 7.88 | 7.65 | (X. Lin, Wu, Wang, Hagfeldt, & Ma, 2011) |
| RuO ₂ | 16.51 | 0.813 | 0.54 | 7.22 | 7.17 | (Y. Hou et al., 2014) |
| Fe ₃ O ₄ | 16.67 | 0.693 | 0.63 | 7.65 | 6.88 | (Liang Wang, Shi, Zhang, et al., 2014) |
| CuO-NRs/AB | 15.94 | 0.770 | 0.65 | 8.05 | 6.96 | (W. Ahmad et al., 2015) |

2.7 Composites Materials Based Counter Electrode

To improve the photo catalytic and PV performance of CE electrode researchers are investigating different types of metals and their composite for the development of Pt free

counter electrode in DSSC. Composite is a combination of two or more materials components with different properties. Currently, composite materials had attained the interest for the replacement of Pt free counter electrode. PV performance and stability of CE can be enhanced by taking advantage of proper combination of highly stable and conductive material. Photo electrical properties and PV efficiency of different composite-based counter electrode used in DSSC is summarized in table 7. From PV performance it was found that composite materials showed high PCE and electrochemical stability as compare to binary materials. However, the reason for high PV performance and PCE in DSSC is not elaborated fully, further the contribution of each part in composite based CE needs more clarifications. It is to be consider that in near future the more development of composite material changes the routes for development of economical and highly efficient counter electrode in DSSC.

Table 2.6: Summary of the important results on composite based material as counter electrode in DSSC

| CE materials | J_{sc} (mA.cm⁻²) | V_{oc} (V) | FF | PCE (%) | Reference |
|---|--|-------------------------------|-----------|--------------------|---------------------------------------|
| TiC-SiC-C | 11.13 | 0.78 | 0.65 | 5.7 | (Zhong et al., 2014) |
| MoN nitrogen-doped GO | 14.62 | 0.772 | 0.71 | 7.998 | (X. Zhang et al., 2013) |
| MoN | 14.11 | 0.774 | 0.58 | 6.437 | (X. Zhang et al., 2013) |
| VN peas | 15.06 | 0.73 | 0.66 | 7.29 | (M. Wu et al., 2014) |
| Fe₃C@N-C | 14.97 | 0.74 | 0.74 | 7.36 | (H. Xu et al., 2014) |
| Carbon/Fe₃O₄ | 16.01 | 0.75 | 0.68 | 8.11 | (Liang Wang, Shi, Wang, et al., 2014) |

Table 2.6, continue

| | | | | | |
|--|--------|-------|-------|------|--|
| Pt/TiO₂/WO₂ | 12.54 | 0.830 | 0.7 | 7.23 | (Y. Wang, Zhao, Wu, Liu, & Ma, 2013) |
| Reduce Graphene-TaON | 13.38 | 0.829 | 0.69 | 7.65 | (Y. Li, Wang, Feng, Zhou, & Wang, 2013) |
| CNTs-TiN | 12.74 | 0.750 | 0.57 | 5.41 | (G. r. Li, Wang, Jiang, Gao, & Shen, 2010) |
| Pt/CS flexible, Co electrolyte | 14.24 | 0.859 | 0.74 | 9.05 | (Zhu et al., 2017) |
| Transparent CoS/rGO | 18.9 | 0.767 | 0.677 | 9.82 | (Huo, Wu, Zheng, Tu, & Lan, 2016) |
| CoTe/RGO | 17.41 | 0.770 | 0.69 | 9.18 | (Jia, Wu, Dong, & Lin, 2015) |
| CoTe nanotubes | 21.4 | 0.620 | 0.601 | 8.1 | (Patil et al., 2015) |
| WC-MW 100 °C | 14.11 | 0.731 | 0.61 | 6.51 | (Jang, Ham, Ramasamy, Lee, & Lee, 2010) |
| Tungsten carbide (WC- 800 °C) | 10.54 | ---- | ---- | 4.20 | (Ko, Oh, Lee, Han, & Park, 2011) |
| GNs-350°C | 16.358 | 0.742 | 44.34 | 5.38 | (D. Zhang et al., 2011) |
| GNs-400 °C | 16.988 | 0.747 | 53.62 | 6.81 | (D. Zhang et al., 2011) |
| Ag₈GeS₆ | 16.59 | 0.746 | 0.65 | 8.1 | (Q. He et al., 2015) |
| CuO-NRs/AB | 15.94 | 0.770 | 0.65 | 8.05 | (W. Ahmad et al., 2015) |
| EG + 5BC (expanded graphite + 5B pencil, 1 : 1) | 14.41 | 0.683 | 0.63 | 7.7 | (Wei, Jin, & Ren, 2011) |
| M-AC/CNT-2 PF | 12.4 | 0.72 | 7.19 | 6.26 | (Memon et al., 2017) |
| M-AC/CNT-2 CF | 12.3 | 0.72 | 685 | 6.06 | (Memon et al., 2017) |
| NiS₂/RGO | 16.55 | 0.749 | 0.69 | 8.55 | (Z. Li, Gong, Zhou, & Wang, 2013) |
| Fe₃O₄@RGO-NMCC | 17.01 | 0.760 | 0.71 | 9.04 | (Zhou et al., 2016) |
| CSA/POMA | 18.35 | 0.740 | 0.65 | 8.76 | (Tsai et al., 2016) |

Table 2.6, continue

| | | | | | |
|---|-------|-------|-------|-------|--|
| WC-OMC | 14.59 | 0.804 | 0.701 | 8.18 | (M. Wu, Lin, Hagfeldt, & Ma, 2011a) |
| MoC-OMC | 15.5 | 0.787 | 0.68 | 8.34 | (M. Wu, Lin, et al., 2011a) |
| Nitrited nickel foam | 9.62 | -0.67 | 0.60 | 3.88 | (S. H. Park et al., 2014) |
| Polymer-derived WC (WCPD) | 14.17 | 0.766 | 0.61 | 6.61 | (Jang et al., 2010) |
| Ni_{0.33}Co_{0.67}Se | 17.29 | 0.789 | 0.67 | 9.01 | (Qian, Li, Shao, Jiang, & Hou, 2016) |
| FeN/N-doped graphene | 18.83 | 0.740 | 0.78 | 10.86 | (Balamurugan, Thanh, Kim, & Lee, 2016) |
| Pt/NiO/Ag mirror | 30.1 | 0.810 | 462 | 11.27 | (Lan, Que, Wu, & Wu, 2016) |
| PEDOT:PSS/PPy | 14.27 | 0.75 | 0.71 | 7.60 | (G. Yue et al., 2012) |
| PEDOT/SWCNT Film | 11.04 | 0.58 | 0.64 | 4.01 | (Aitola et al., 2012) |
| PEDOT:MWCNT Film | 17.00 | 0.720 | 0.66 | 8.08 | (K.-M. Lee et al., 2010) |
| TiN/PEDOT:PSS | 14.45 | 0.727 | 0.67 | 7.601 | (H. Xu et al., 2012) |
| Graphene-based MWCNTs | 5.6 | 0.76 | 0.70 | 3.00 | (Choi, Kim, Hwang, Choi, & Jeon, 2011) |
| PANI/ flexible graphite | 15.41 | 0.657 | 0.727 | 7.36 | (H. Sun et al., 2010) |
| PEDOT:PSS/C. | 13.6 | 0.809 | 0.691 | 7.61 | (G. Yue et al., 2013) |
| SiO₂/PEDOT:PSS | 13.5 | 0.72 | 0.58 | 5.66 | (Song et al., 2014) |
| TiS₂/PEDOT:PSS | 13.06 | 0.68 | 0.6 | 5.46 | (C.-T. Li, Lee, Li, Yeh, & Ho, 2013) |
| PEDOT/M-PEDOT:PSS Film | 16.48 | 0.68 | 0.65 | 7.29 | (Chiang & Wu, 2013) |
| (PEDOT)-(PAA)film | 13.52 | 0.758 | 0.62 | 6.35 | (Xiao et al., 2013) |
| SiSe₂/PEDOT: PSS | 16.98 | 0.720 | 0.67 | 8.2 | (C.-T. Li, Tsai, & Ho, 2016) |
| Si₃N₄/PEDOT: PSS | 16.11 | 0.760 | 0.67 | 8.18 | (C.-T. Li et al., 2016) |

Table 2.6, continue

| | | | | | |
|------------------------------|-------|-------|------|------|---------------------------------|
| MWCNTs/PANI | 16.08 | 0.78 | 0.57 | 7.21 | (Niu et al., 2014) |
| MWCNTs/PPy | 14.83 | 0.77 | 0.65 | 7.42 | (G. Yue et al., 2014) |
| TiC-PEDOT | 12.68 | 0.838 | 0.76 | 8.09 | (J. He, Pringle, & Cheng, 2014) |
| TiN-PEDOT | 13.21 | 0.840 | 0.75 | 8.26 | (Jiangjing He et al., 2014) |
| MWCNT/MC nanofibers | 14.9 | 0.76 | 56 | 6.31 | (Park, Jung, Kim, & Lee, 2012) |
| Graphene-based MWCNTs | 5.6 | 0.76 | 0.70 | 3.00 | (Choi et al., 2011) |

2.8 Challenges and limitations

Components such as photoanode, dye, electrolyte and counter electrode plays an important role in the overall performance of DSSC. However, there are some limitations to achieve higher efficiency in DSSC based devices, these limitations include non-optimized dark current, performance of dyes, degradation and low stability of electrolyte, and improper connection of electrodes. Moreover, there are several factors that effects the photo thermal stability of DSSC. These factors are low surface area for the electron flow, structural morphology of photoanode, absorption of photon for dye pickup and architecture of dye.

Furthermore, the flow of electrons and PCE of counter electrode in DSSC are highly affected by the thickness of film and its optimization. Therefore, this optimization is a major challenge because it varies from material to material. Usually several techniques such as spray coating or spin coating are employed for optimization of the films. As a result, the interfacial connection between substrate and film becomes weak due to the longer time of deposition. Additionally, the efficiency of the DSSCs can be varied by the annealing process, which meaningfully effects the electrical conductivity and adhesion of counter electrode. It has been observed that by annealing the carbonaceous materials

and conducting polymers above 400°C, the film starts to leach out from conduction substrate. Also, the flow of electrons, electrical conductivity and PCE of counter electrode in DSSC are affected by further annealing at this temperature,

A major challenge for researchers is development and fabrication of CE material with different morphologies having high surface area. Whereas, PCE of DSSCs are also affected by the connection of electrolyte and counter electrode because the weak connection can result in the low charge transfer and high resistance that may decrease the PCE of DSSCs. The limitation to the commercialization of DSSC is the cost of fabrication of DSSC assembly. The factors that increases the cost of DSSC based devices are typical fabrication techniques such as CVD, spin coatings, electrophoretic deposition and etc. and the use of noble metals (Au, Pt etc.) as counter electrode. Moreover, the common challenges for DSSC are shown in Figure 2.14.

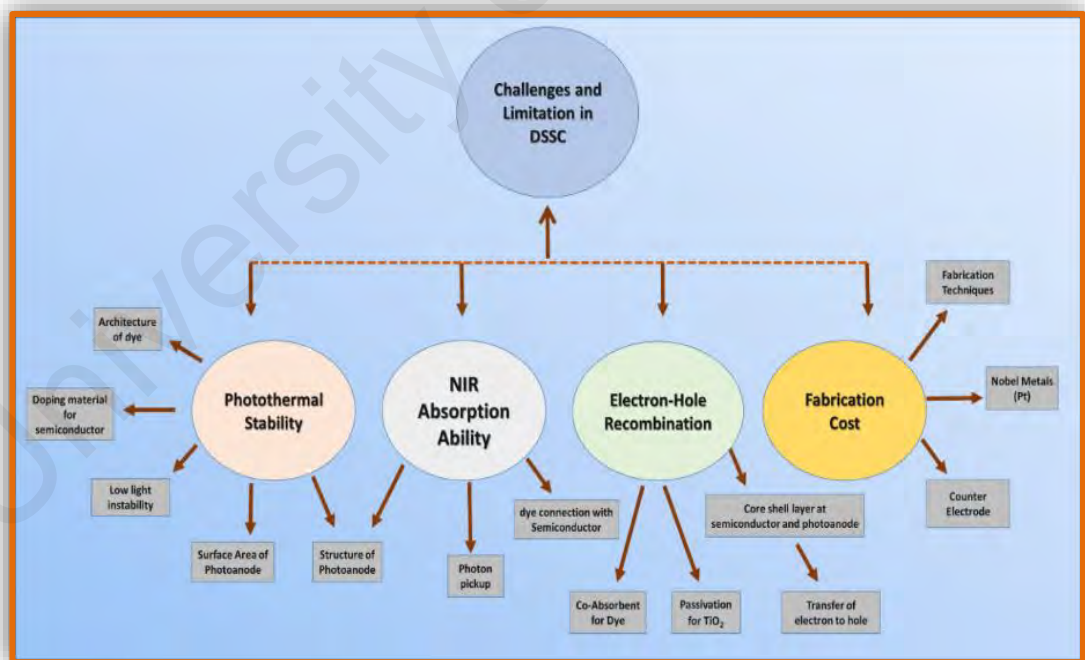


Figure 2.14: Challenges and limitation for the commercialization of DSSC

CHAPTER 3: METHODOLOGY

In this section, the protocols used for the synthesis procedure and parameters exploited for the fabrication are described thoroughly. An effort has been made to elaborate the operational principle of several characterization techniques which has been frequently used to examine the chemical structure, optical properties, purity of synthesized material, and photo electrocatalytic response. In detail, the working principle of characterization such as Field Emission Scanning Electron Microscopy (FESEM), X-ray powder diffraction (XRD), Fourier-transform infrared spectroscopy (FTIR), Ultraviolet–visible spectroscopy (UV-vis) and electrochemical properties has been precisely described in this chapter.

3.1 Materials

Strontium hydroxide octahydrate (Sigma Aldrich, St. Louis, MO, USA, 95%), sulfuric acid, H_2SO_4 (Sigma Aldrich, St. Louis, MO, USA, 98%), acetone (Merck, Kenilworth, NJ, USA, 95%), St. Louis, MO, USA, 98%), titanium(IV) oxide, anatase (Sigma Aldrich, St. Louis, MO, USA, 99.7%), sodium hydroxide, NaOH (Sigma Aldrich), methanol (Merck, Kenilworth, NJ, USA, 99.9%), Ferric Chloride hexa hydrate ($\text{FeCl}_2 \cdot 6\text{H}_2\text{O}$) (Sigma Aldrich, St. Louis, MO, USA), pyrrole (Sigma Aldrich, St. Louis, MO, USA), Ammonium peroxydisulfate (APS, Merck, Kenilworth, NJ, USA, 99%) and Aniline (Fluka, St. Louis, MO, USA, 99%). The deionized water was also used during the study. The reagents involved in this work were of analytical standard

3.2 Synthesis of Material

3.2.1 Synthesis of Polypyrrole (PPy)

Polypyrrole was synthesized by oxidative polymerization. At first 0.1 M distilled pyrrole was dissolved in DI water. Ferric Chloride hexa hydrate ($\text{FeCl}_2 \cdot 6\text{H}_2\text{O}$) taken as an oxidant in the synthesis of Polypyrrole. Briefly, 0.1 M of pyrrole dissolved in 100 ml of DI water and kept on stirring. While stirring the solution, $\text{FeCl}_2 \cdot 6\text{H}_2\text{O}$ oxidant was added in pyrrole solution quickly and was kept for stirring. After 2 hours 400 ml of distilled water was poured in the solution. The reaction mixture was then washed with deionized water to make filtrate neutral. The synthesized polymer was dried overnight by keeping in a vacuum oven under pressure at 60°C . The process for the synthesis of polypyrrole (PPy) is illustrated in Figure 3.1.

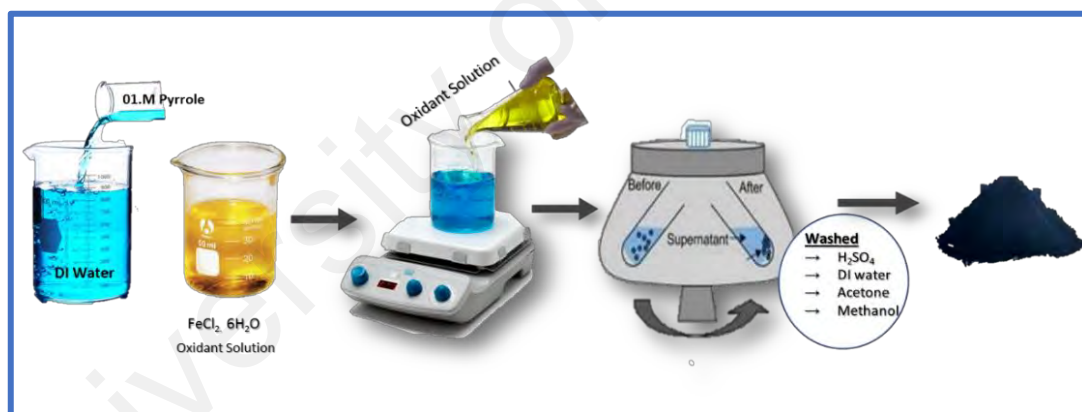


Figure 3.1: Schematic diagram representing the synthesis of polypyrrole (PPy)

3.2.2 Synthesis of SrTiO_3 Nano cubes

The synthesis of SrTiO_3 nanocubes was done by using hydrothermal approach. A 1.4 g of Strontium hydroxide octahydrate was dissolved in 20 ml NaOH (3 M) under constant stirring. Titanium dioxide solution prepared by mixing 0.4 g of TiO_2 in 20 ml NaOH (3 M) was added dropwise at a rate of one drop per second in the above solution, with vigorous stirring. After 30 minutes of stirring, 40 ml of the reaction mixture was transferred to a 100 mL Teflon-lined stainless-steel autoclave and subjected to

hydrothermal treatment at 130°C for 72 hr. The obtained precipitate of SrTiO₃ nanocubes were then washed thoroughly with DI water several times and dried in a vacuum oven at 60°C for 24 hours.

3.2.3 Preparation of PPy-SrTiO₃ Nanocomposite

The SrTiO₃ nanocube-doped nanocomposites of Polypyrrole were prepared with different wt. % of SrTiO₃ (25, 50 and 75% with respect to 0.1 M pyrrole.). The calculated amount of SrTiO₃ nanocubes was dispersed deionized water by sonication and added quickly to pyrrole solution (0.1 M) in DI water with vigorous stirring. The resulting mixture was sonicated for a few minutes until it became uniform. The work-up procedure was the same as described in the previous section. The obtained nanocomposites were labelled as PPy-SrTiO₃-25%, PPy-SrTiO₃-50% and PPy-SrTiO₃-75%, indicating 25%, 50% and 75% wt. ratio of SrTiO₃ nanocubes with respect to 0.1 M pyrrole, respectively.

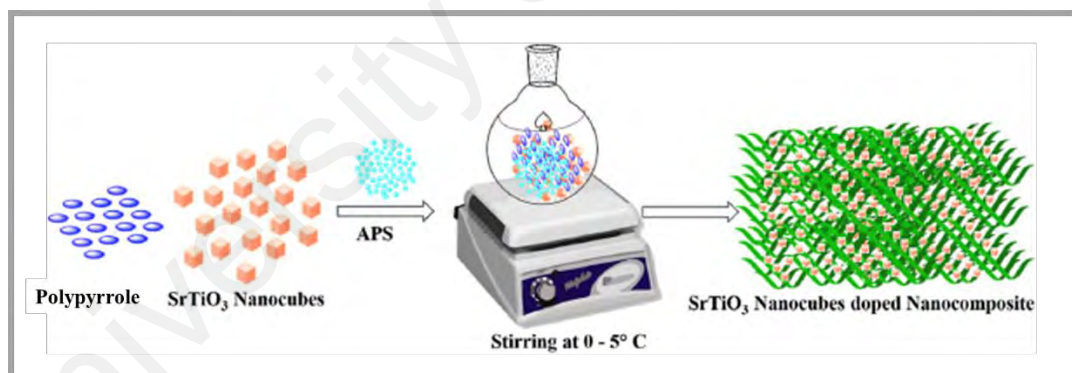


Figure 3.2. Schematic diagram representing the synthesis of polypyrrole (PPy)

3.2.4 Synthesis of Polyaniline (PANI)

Polyaniline (PANI) was synthesized by oxidative polymerization. Initially the aniline was distilled and then was dissolved in aqueous solution of 1M. Hydrochloric acid (HCl). The distilled aniline solution was placed in an ice bath under continuous stirring. In detail, aniline (0.032 mol) was added in 45 ml of HCL solution and was sonicated and placed for stirring. Ammonium persulfate (APS) is used as oxidant for the preparation of

polyaniline nanotubes. APS (0.4026 mol) was added in 45 ml of HCL solution. While stirring the aniline solution, APS solution (oxidant) was slowly added in aniline solution with the drop rate of 1 drop per second at temp (0-5 °C). The solution was then kept on stirring for 3 hours and then was placed in refrigerator for overnight. The solution was then filtered and washed with 0.5 M HCl, for first time and then further was washed DI water. To remove the unreacted oligomers, monomers and impurities, the obtained solution was further washed with 1: 1 solution of methanol and acetone. After removal of impurities the polymers solution was dried in vacuum oven at 60 °C for more than 15 hours. The green colour of the polymer indicates the formation of conducting polyaniline. The process for the synthesis if polyaniline is illustrated in Figure 3.3.

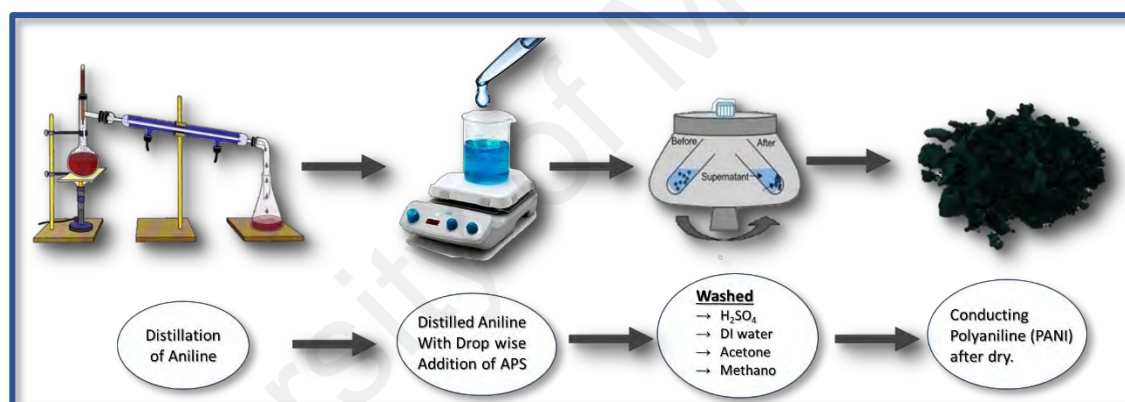


Figure 3.3: Schematic diagram representing the synthesis of polyaniline (PANI)

3.2.5 Electrode Fabrication

The fabrication of electrodes for DSSCs was done by depositing the synthesized material polypyrrole (PPy), nanocomposites of PPy-SrTiO₃ and different concentration of polyaniline (PANI) on FTO coated conducting glass substrate. The FTO coated glass was properly cleaned by washing it with detergent to remove the attached impurities. After this the glass were again with ethanol and were placed for sonication. To removes the unreacted impurities the glass war then washed with acetone, and in last with DI water and then were dried in vacuum oven at the temperature of 50 °C for 30 minutes. The

synthesized material is then coated on clean FTO glass. For the coating of material Doctor Blade technique was used. The coated electrodes were dried at 50 °C for 12 hours and then were used as counter electrode in DSSC. The same coating approach was used for coating TiO₂ thin film. For the annealing TiO₂ photoanode the coated electrodes are placed on hot plate and annealed at 450 °C for 20 minutes. The coated area and thickness of the counter electrodes and TiO₂ photoanode were approximately 10-15 μm and 0.25 cm² respectively. The prepared photoanodes were dipped in an ethanol solution containing 0.3 M N-3 (95%) dye (Sigma Aldrich Chemicals Company) for 24 hours, and then washed with ethanol (purity 95 %) and dried at room temperature. Figure 3.4 is showing the image of coated electrode used as counter and photoanode in DSSC.

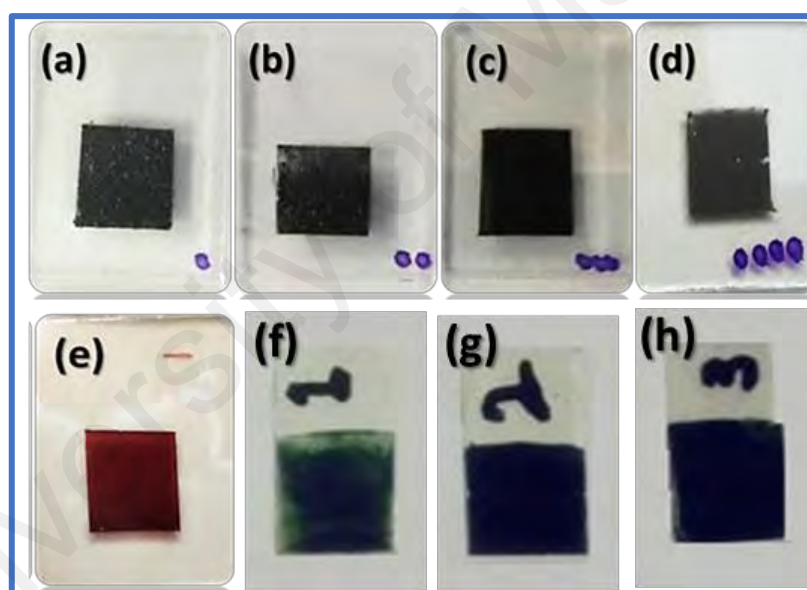


Figure 3.4: Illustrating (a) PPy, (b) PPy-SrTiO₃-25 (c) PPy-SrTiO₃-50 (d) SrTiO₃-75%, and (e) dye dipped TiO₂ coated photoanode (f) PANI-10 mg (g) PANI-15mg (h) PANI-20 mg counter electrode

3.2.6 Fabrication of DSSC

For the fabrication of DSSC (complete device), the dye dipped photoanodes and counter electrodes were dried and then were clamped in such a way that coated area of photoanode and counter electrode faces each other. A thin PVC sheet having width of 50 μm is used as spacer between photoanode and counter electrode. The cell was then sealed

and the redox coupled electrolyte (Iodolyte-100, Solaronix) was injected into the cell through the sides. The assembly of DSSC device is shown in Figure 3.5. To study the electrochemical behaviour of the fabricated device cyclic voltammetry CV, electrochemical impedance (EIS) and current vs voltage relation (J-V) curve was measured under standard test conditions.



Figure 3.5: Fabrication of dye sensitized solar cell (DSSC)

3.3 Characterizations Techniques

3.3.1 Field Emission Scanning Electron Microscopy (FESEM)

The morphology of fabricated electrode plays an important role for device performance. The charge transfer resistance and diffusion coefficient of the electrode depends on the morphology of material. To examine the structural morphology of synthesized counter electrodes, FESEM analysis was performed on FESEM model Quanta FEG 450 shown in Figure 3.6. The synthesized materials were first deposited on silicon wafer (Si substrate) via drop costing and then were fixed inside on sample holder of FESEM instrument. It is important to mention that, for the high quality and clear image the efficient flow of electron is necessary. For this reason, Si-wafer act potentially, which

helps to obtain a good quality image with uniform structural morphology. The FESEM is powerful instrument mostly used to examine the structural morphology, distribution of nanoparticles, and size of nanoparticle and the thickness of deposited layer on the conducting substrate.

The electrons come from the emission source of FESEM and move with high speed in high electrical field in a vacuum chamber. These electrons (primary electrons) are deflected by electronic lenses to generate a contract beam of electrons which are then bombarded on the sample. Hence the electrons (secondary electrons) are emitted out from in the sample and moves with high velocity. The electrons are detected by the detector which generates the electronic signal. These signals are then passed to video scanner and hence we obtain the digital image of structural morphology of the sample. The acceleration and incident angle of secondary electron narrate structural morphology of material



Figure 3.6: Field emission scanning electron microscope (FESEM)

3.3.2 X-Ray Diffraction (XRD)

In X-Ray diffraction, a beam of X-ray is scattered, and diffraction pattern is obtained because of scattering photon having short wavelength (nm). According to Bragg formula;

$$d\sin\theta = n\lambda \quad (3.1)$$

The XRD mechanism is explain Figure 3.7. In the above equation, d is distance from crystal planes, θ is the angle of incident X-Ray, λ is the wavelength of incident beam of X-ray (conventionally it is 1.54 eV) and n is numerical number.

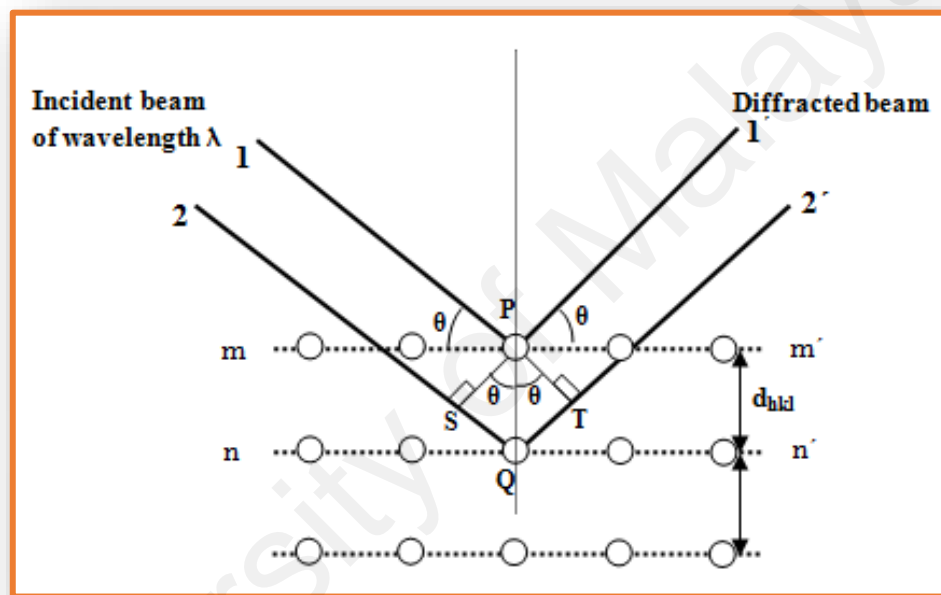


Figure 3.7: X-Ray diffraction in crystal lattice

X-ray powder diffraction (XRD) is standard technique for analysis of crystalline morphology of nanomaterials. It presents intensity vs. 2-theta which is simply an angle of X-Ray. To examine the crystallinity of synthesized counter electrodes, X-ray powder diffraction analysis was performed by Empyrean X-ray diffractometer shown in Figure 3.8. The powder specimen was taken for XRD analysis, and XRD pattern were recorded from $2\theta = 10^\circ - 90$ on the scan rate of 0.02 s^{-1} .

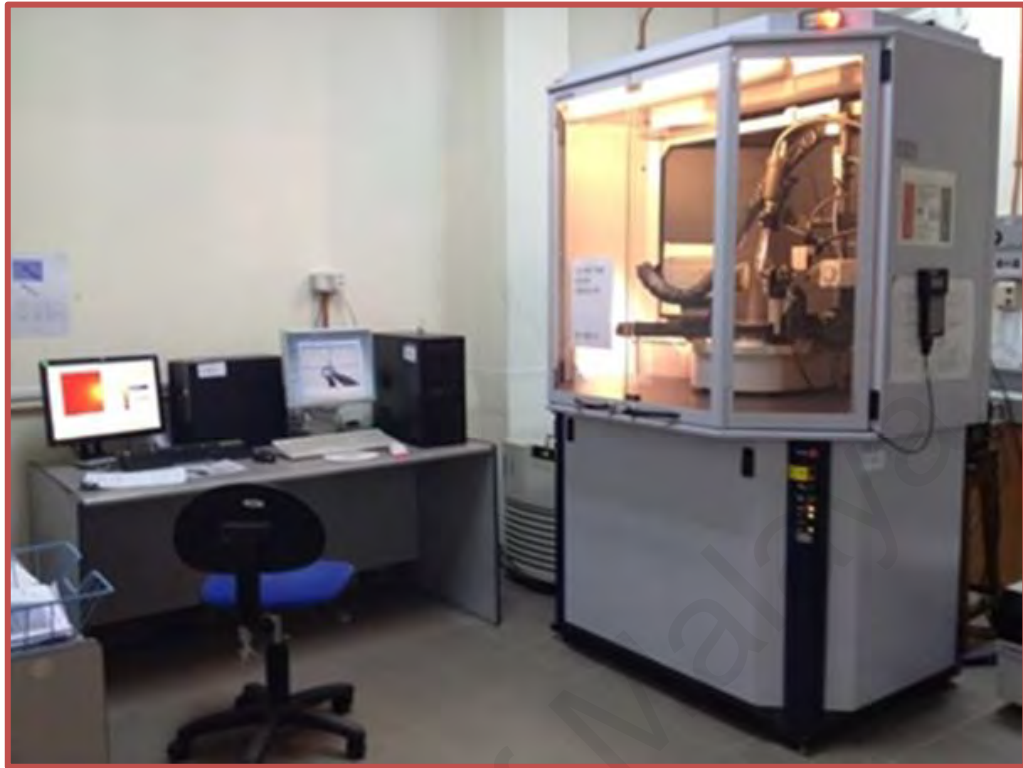


Figure 3.8: X-ray diffraction (XRD)

3.3.3 UV-Vis Spectroscopy

The performance of dye sensitized solar cell depends on the light absorption efficiency of solar energy material. Different materials have different efficiency for absorption of photon from sun light. The materials with lower band gap are considered as most potential candidates for DSSC. The light absorbance of material (sample) is explained by the given equation

$$A(\lambda) = \log_{10} \frac{I^0(\lambda)}{I_t(\lambda)} = -\log_{10} T(\lambda) \quad (3.2)$$

where T is the transmittance of material, which is used to measure the absorbance spectra of materials.

The UV-Vis Spectroscopy has been exploited to investigate the light absorption intensity of synthesized materials. To examine the Uv-Vis spectrum of synthesized material, Perkin Elmer LAMBDA 1050 Uv-vis Spectrophotometer was being used, as

shown in Figure 3.9. To study the absorption spectra the wavelength from 200 (nm) to 1000 (nm) was used.



Figure 3.9: Perkin Elmer LAMBDA 1050 UV-Vis spectrophotometer

3.3.4 Fourier Transform-Infrared Spectroscopy (FTIR)

Fourier Transform-Infrared Spectroscopy (FTIR) is an analytical technique used to identify organic (and in some cases inorganic) materials. This technique measures the absorption of infrared radiation by the sample material versus wavelength. The infrared absorption bands identify molecular components and structure. When a material is irradiated with infrared radiation, absorbed IR radiation usually excites molecules into a higher vibrational state. The wavelength of light absorbed by a molecule is a function of the energy difference between the at-rest and excited vibrational states. The wavelengths that are absorbed by the sample are characteristic of its molecular structure.

The FTIR spectrometer uses an interferometer to modulate the wavelength from a broadband infrared source. A detector measures the intensity of transmitted or reflected

light as a function of its wavelength. The signal obtained from the detector is an interferogram, which must be analysed with a computer using Fourier transforms to obtain a single-beam infrared spectrum. The FTIR spectra are usually presented as plots of intensity versus wavenumber (in cm^{-1}). Wavenumber is the reciprocal of the wavelength. Perkin Elmer FT-IR Spectrophotometer was being used, as shown in Figure 3.910. The intensity can be plotted as the percentage of light transmittance or absorbance at each wavenumber.



Figure 3.10. Perkin Elmer FT-IR spectrophotometer

3.3.5 Electrochemical Performance Study

To investigate the electro catalytic response of materials toward the reduction of Iodide to tri-Iodide cyclic voltammogram (CV) have been exploited individually for all the fabricated electrode. The charge transfer resistance toward the flow of electron from external circuit to electrolyte and then toward the dye is measured by electrochemical impedance (EIS). Furthermore, the overall performance and the power conversion efficiency of DSSC was assayed by current density vs voltage (J-V) curve. The CV, EIS,

and J-V curves were measured by auto-lab (under stander test condition, A.M 1.5, 100 mW.cm^{-2}). Figure 3.11 representing the Metrohm Autolab PGSTAT-204, which was used to investigate phot-electrochemical behaviour of DSSC.



Figure 3.11: Metrohm Autolab PGSTAT-204 used to investigate the electrochemical properties of DSSC

CHAPTER 4: RESULTS AND DISCUSSION

4.1 ² Strontium Titanate (SrTiO₃) Nanocubes Interleaved into Conducting Polymer (PPy); A Counter Electrode for Dye Sensitized Solar Cells Applications

In present work, we successfully synthesized polypyrrole by oxidative polymerization method. PPy is used as counter electrode in DSSC and it exhibit good catalytic property and PV performance. From literature it was found that with the addition of metal oxide the performance of DSSC was enhanced. To enhance the power conversion efficiency of PPy, further we have synthesized SrTiO₃ via hydrothermal approach. SrTiO₃ with different concentration is added in PPy, and then the synthesized nanocomposites were fabricated as counter electrode in DSSC. It was found that the unaided PPy achieved the PCE of 1.29% but with the addition of SrTiO₃, the PCE of PPy-SrTiO₃ nanocomposite was enhanced from 1.29% to 2.52% for PPy-SrTiO₃-50%. The structural morphology, optical behavior, composition, conductivity and photovoltaic performance of fabricated counter electrodes were investigated and discussed

4.1.1 Morphology Analysis

The structural features and morphologies of PPy, PPy-SrTiO₃-25%, PPy-SrTiO₃-50% and PPy-SrTiO₃-75%, nanocomposite was assayed by Field-emission scanning electron microscopy (FESEM), presented in Figure 4.1. The FESEM image (Figure 4.1 (a)) indicates that PPy exhibit highly porous spherical symmetry particles which are randomly assigned onto substrate. The spherical symmetry of PPy nano particles was infrequently reported by few researchers (L. Liang, Chen, & Guo, 2017; Muthusamy, Charles,

² Section 4.1 is submitted (Ahmed, U., Alizadeh, M., Rahim, N. A., Shahabuddin, S., Pandey, A. K. & M.M.Shahid. (2019). Strontium Titanate (SrTiO₃) nanocube interleaved into Conducting Polymer (PPy) as an efficient platform for counter electrode in DSSC. Solar Energy Materials and Solar Cells. (Under Review).

Renganathan, & Sastikumar, 2018; G. Wang, Dong, Yan, Hou, & Zhang, 2018) and spherical symmetric of PPy is due to FeCl_2 , which is used as oxidant during polymerization. The obtained particle sized of PPy nanoparticle was range from 120 nm to 350 nm. The cubical morphology of SrTiO_3 is represented in Fig. 4.1 (b), the size of SrTiO_3 nanocubes vary from 60 nm to 240 nm. Fig. 4.1 (c-d) represent the distribution of SrTiO_3 nanocubes (wt. concentration 25 and 50%) in PPy. The bigger particle size and higher surface to volume ratio of PPy is dominating the SrTiO_3 nanocubes. Also, the SrTiO_3 nanocube are intercolated into the porous structure of PPy. The FESEM microscopy of PPy- SrTiO_3 -75% illustrated in Figure 4.1(e), which confirms the uniform distribution of SrTiO_3 nano cubes in composite with PPy. Furthermore, it was observed that at high concentration (PPy- SrTiO_3 -75%) the nano cube's starts agglomerated with each other in comparison with PPy- SrTiO_3 -50%.

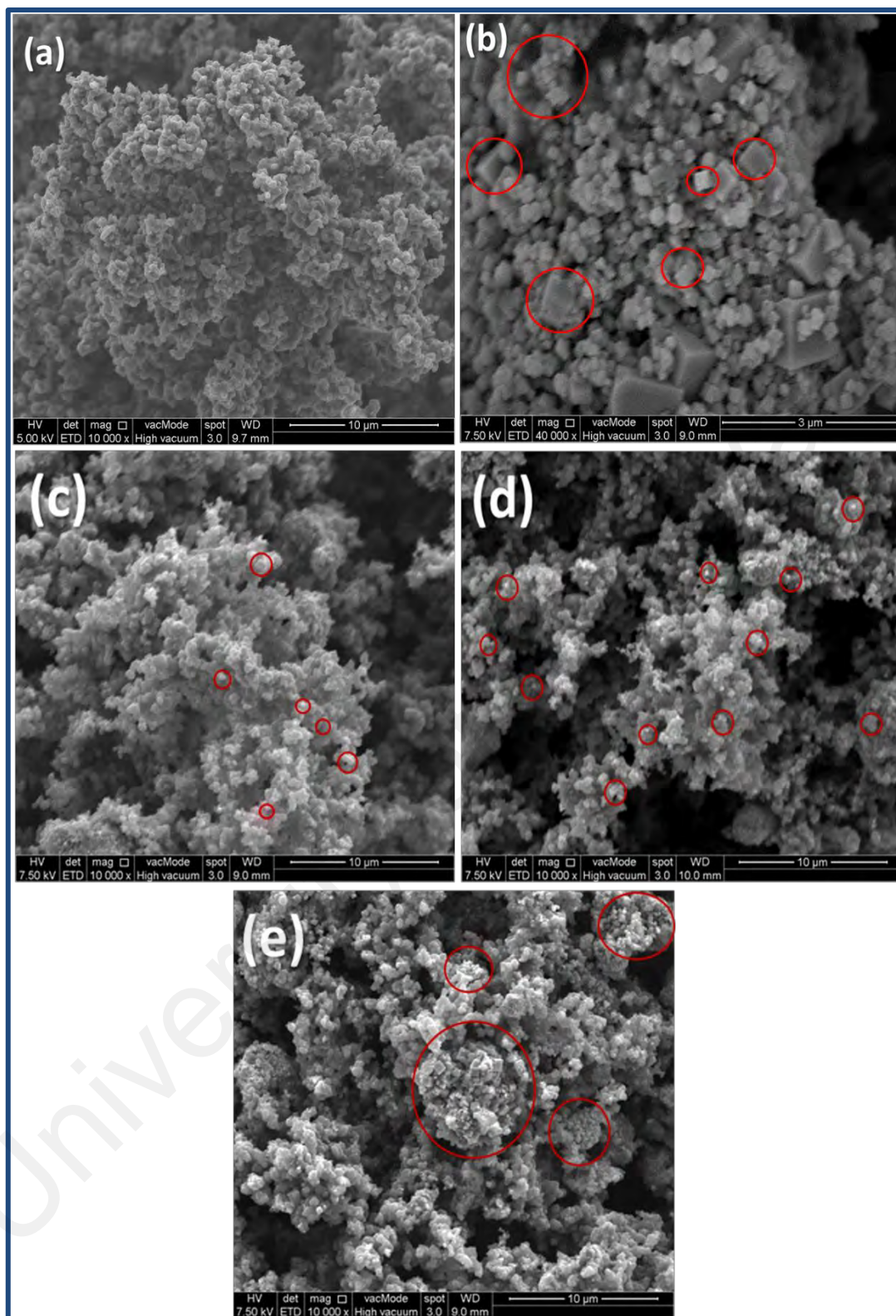


Figure 4.1: FESEM images of (a) PPy nanospheres, (b) SrTiO₃ Nanocubes (c) PPy-SrTiO₃-25%, (d) PPy-SrTiO₃-50%, (e) PPy-SrTiO₃-75% fabricated as counter electrode in DSSC

The distribution of SrTiO₃ nano cubes in composite with PPy (PPy-SrTiO₃-50%) nanocomposite was investigated by EDX elemental mapping analysis (Figure 4.2). The EDX spectrum of PPy-SrTiO₃-50% nanocomposite indicates the presences of elemental Si used as substrate (0.81 wt. %), O (18.16 wt. %), Ti (17.73 wt. %), Sr (24.13 wt. %), N (1.49 wt. %) and C (37.67 wt. %) And hereby validate the signatures of the same in the nanocomposite [Figure 4.2 (a)]. Figure 4.2 (b) shows the FESEM image of the nanocomposite and the elements Si (light blue), O (red), Ti (orange), Sr (magenta), N (blue) and C (green) were scanned as displayed in the EDX mapping morphology of PPy-SrTiO₃-50% nanocomposite (Figure 4.2 (b)). Figure 4.2 (c-h) show the distribution of independent elements Si, O, Ti, Sr, N, and C. The large area coverage of magenta [Fig. 4.2 (f)], orange [Figure 4.2 (e)] and red [Figure 4.2 (d)] colors show the compact bundles SrTiO₃ nanocubes in PPy nanocomposites. An elemental analysis (Figure 4.2) represents the presence of SrTiO₃, which further confirms the formation of SrTiO₃ nanocube-doped polypyrrole nanocomposites.

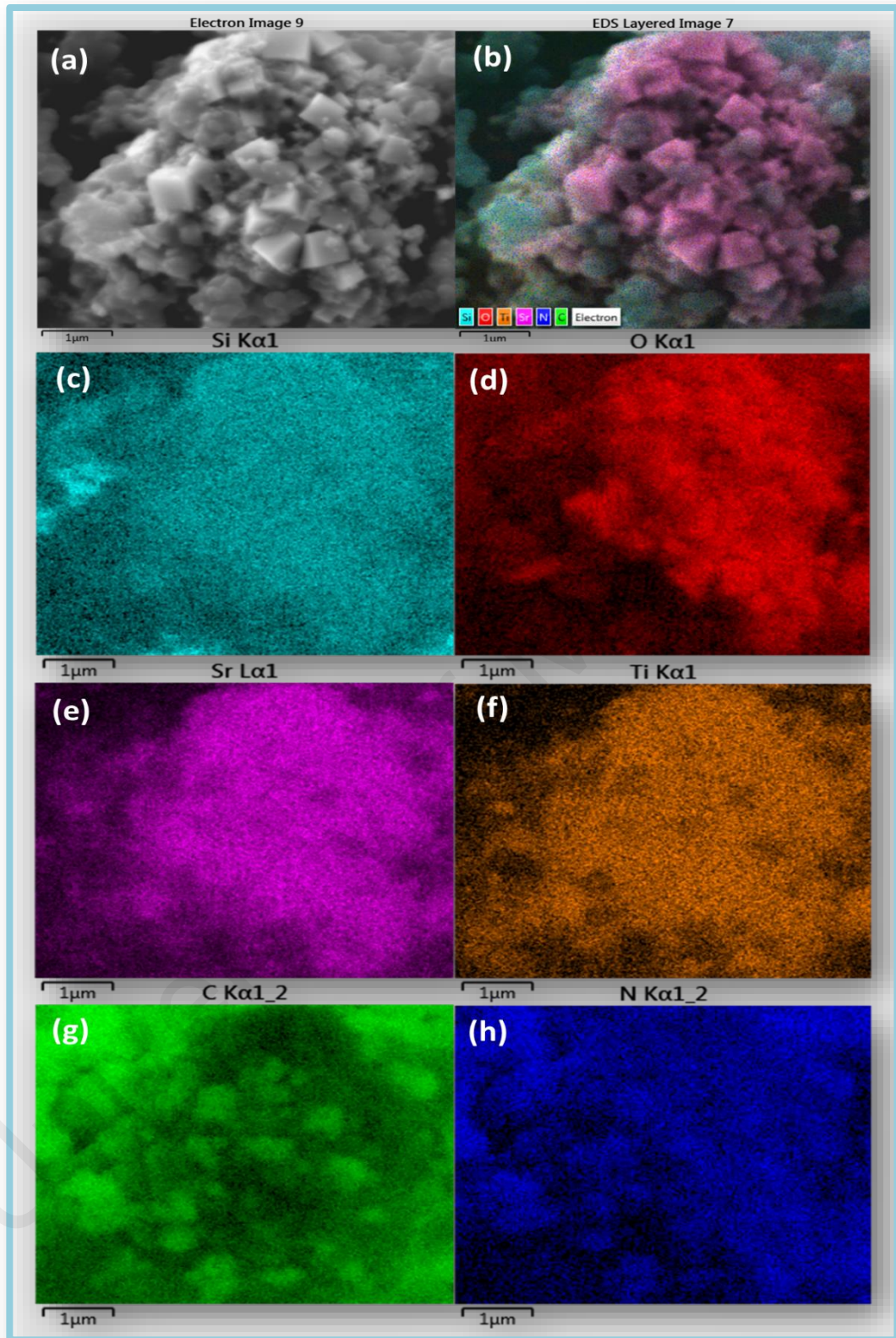


Figure 4.2: FESEM- EDX Mapping images of (a) PPy-SrTiO₃-50%, (b) PPy-SrTiO₃-50%, (c) Silicon (d) Oxygen (e) Titanium (f) Strontium (g) Nitrogen (h) Carbon

4.1.2 UV-Vis Analysis

Figure 4.3 shows the UV-visible spectrum of synthesized SrTiO₃ nanocubes and polypyrrole electrodes composite with different concentrations of SrTiO₃. SrTiO₃ shows specific wide range absorption bands in the range of 200–390 nm. As revealed by Figure 4.3 the sharp absorption 398 nm, this may be assigned to the electronic transition of valence band to the conduction band. SrTiO₃ exhibits the band gap of 3.2 eV. PPy deposited on FTO glass shows great absorption band from the range of 380 nm to 480 nm and the second absorption band range from 520 nm to 720 nm. The absorption band of N-3 Dye range from 450 nm to 650 nm. Hence, the research interest for absorbance of PPy in this range enhances. It is found that with the addition of SrTiO₃, the absorbance of PPy-SrTiO₃ composites is enhanced. With the increment of contents of SrTiO₃ in PPy, the absorption band of PPy- SrTiO₃-75% decreased and ranges from 520 nm to 640 nm. Hence, the UV-VIS results are in good agreement with photovoltaic performance of SrTiO₃-doped polypyrrole nanocomposites

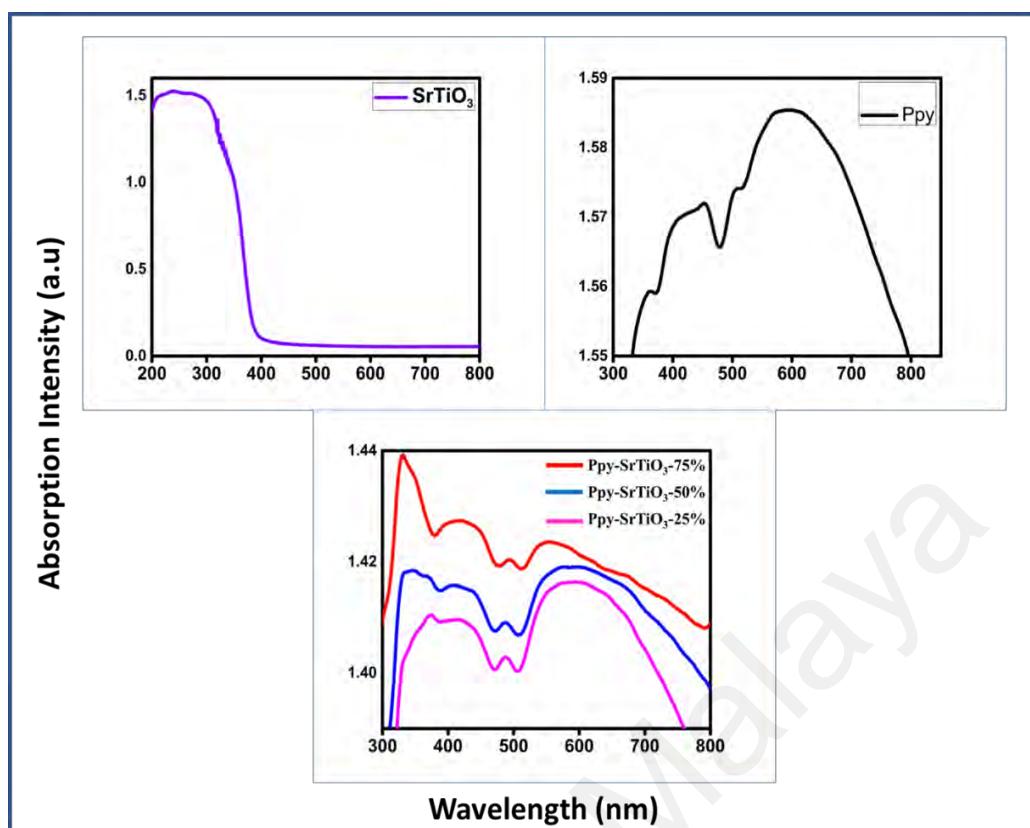


Figure 4.3: UV-visible absorbance spectra of SrTiO₃, PPy, (b) PPy-SrTiO₃-25%, (c) PPy-SrTiO₃-50%, (d) PPy-SrTiO₃-75% counter electrodes

4.1.3 FT-IR Analysis

The FTIR spectrum of PPy, PPy-SrTiO₃-25%, PPy-SrTiO₃-50%, and PPy-SrTiO₃-75% is illustrated in (Figure 4.4). The vibrational modes of polypyrrole are perceived at 1546 cm⁻¹ related to N-H stretching, the other vibrational modes at 1160 cm⁻¹, 1050 cm⁻¹, 950 cm⁻¹ and 789 cm⁻¹ are associated to angular deformation of C-N-C, C-H, and N-H bond in pyrrole. The FT-IR spectra of SrTiO₃ doped PPy nanocomposite represent the bands of polypyrrole. It was observed that with the addition of SrTiO₃, characteristic band of PPy-SrTiO₃ nanocomposite are slightly shifted. Furthermore, the composite exhibits a well-defined, sharp peak at 600 cm⁻¹, owing the presence of SrTiO₃ in composition. Hence, FTIR study indicates the formation of polypyrrole, SrTiO₃ and SrTiO₃-doped polypyrrole nanocomposites and the results are in good contact with previously reported literature (Cheah, Forsyth, & Truong, 1998; X. Liang et al., 2011).

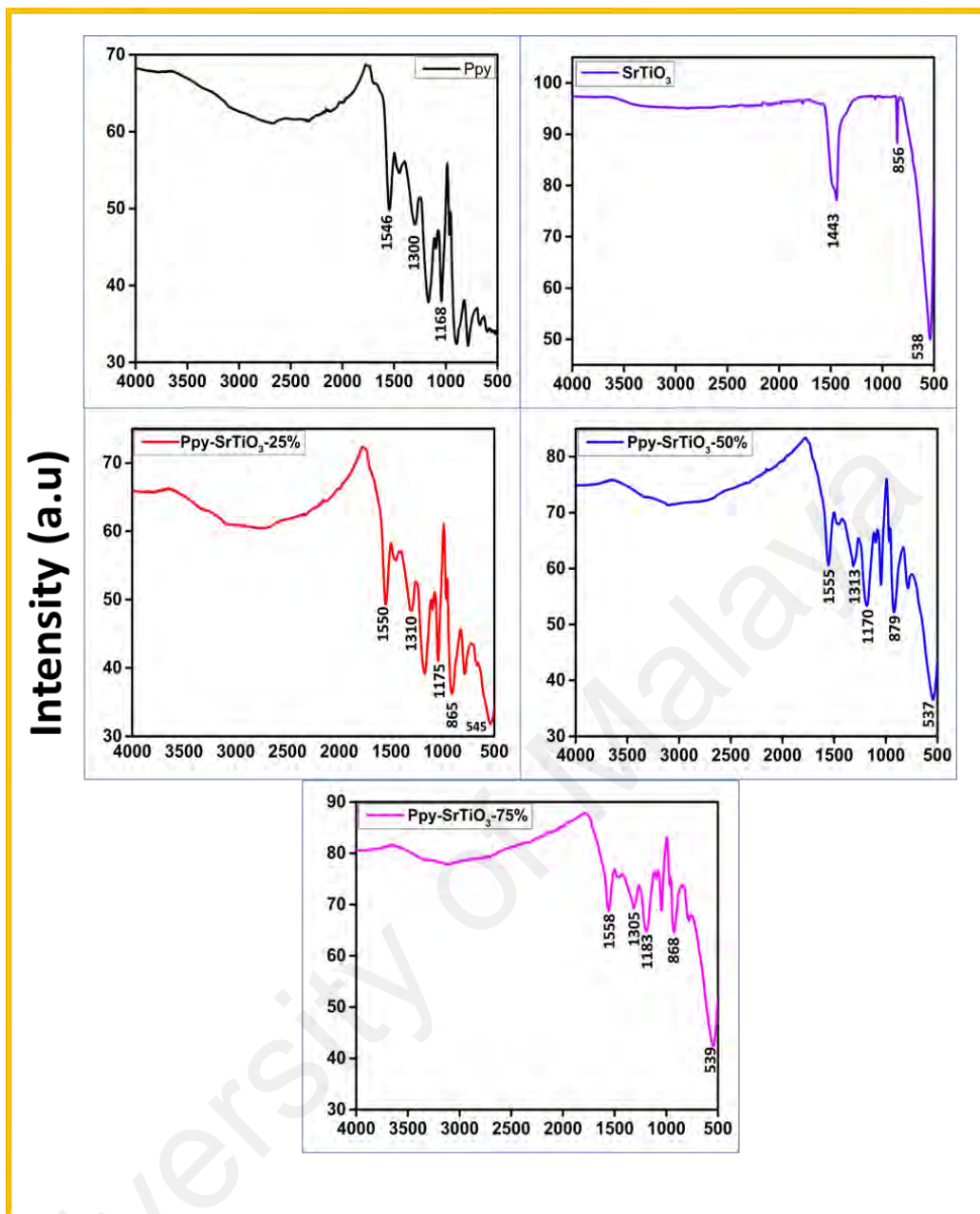


Figure 4.4: FT-IR spectrum of PPy, SrTiO₃ and PPy-SrTiO₃ nanocomposites

4.1.4 XRD Analysis

Figure 4.5 shows the XRD patterns of SrTiO₃, PPy, and PPy-SrTiO₃-50% nano composite. The obtained result shows that the SrTiO₃ exhibits well define crystalline peaks with diffraction peaks that coincide to (100), (111), (200), (220), (222), (211), (311) and (310) planes of nano cubic structure of SrTiO₃ in agreement with JCPDS Card No. 35-07342 (Shahabuddin, Muhamad Sarih, et al., 2016; Shahabuddin, Sarih, et al., 2016). The well define, high intensity sharp peaks of SrTiO₃ confirm formation of highly

crystalline SrTiO₃ nanoparticles. But in case of PPy nanoparticles, low peak intensity can be found. This is due to the amorphous nature and poor crystalline structural morphology of the polypyrrole (Gu et al., 2015). Due to high amorphous nature of PPy it was also observed that in composite of PPy-SrTiO₃-50% the peaks of SrTiO₃ decreased. For PPy-SrTiO₃-50%, the peaks of SrTiO₃, between 20-30 decreased with the addition of PPy nanoparticle. Hence confirming the distribution of PPy and SrTiO₃ nanoparticles.

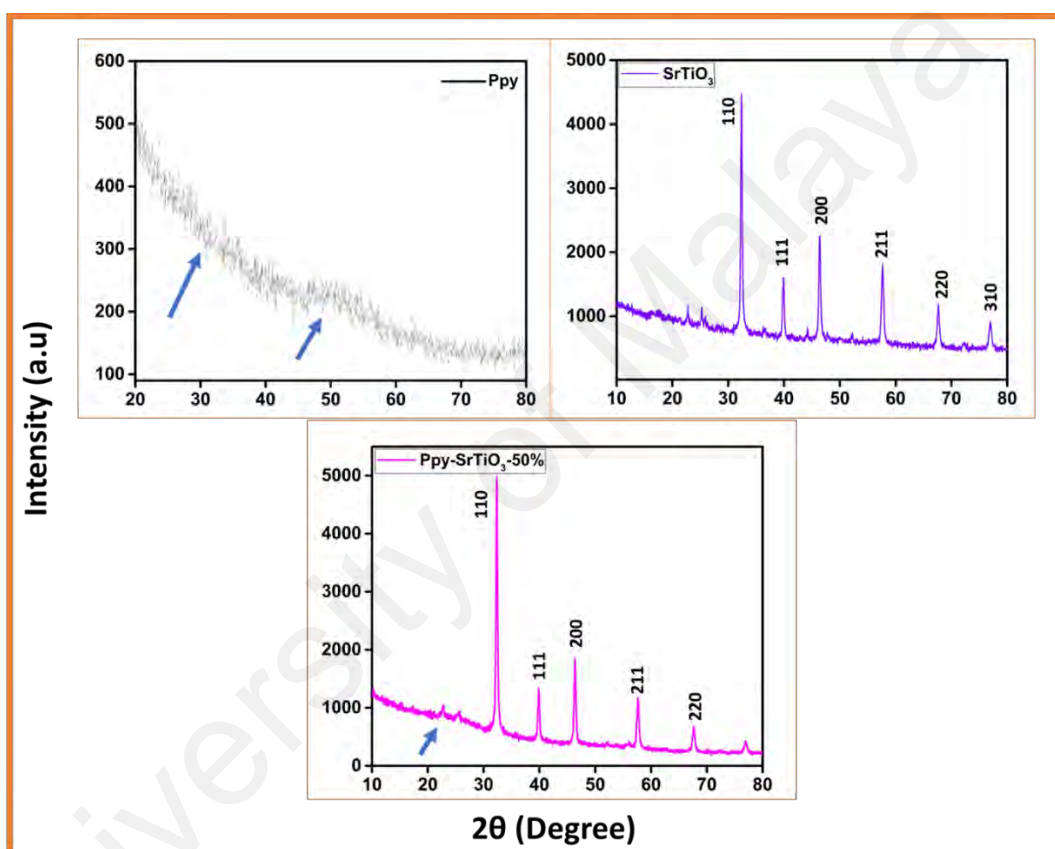


Figure 4.5: XRD patterns of (a) PPy, (b) SrTiO₃ and (c) PPy-SrTiO₃-50%

4.1.5 Cyclic Voltammetry

Cyclic voltammetry technique is widely used to investigate the electrocatalytic performance of counter electrode in DSSC. The electrocatalytic performance of PPy, PPy-SrTiO₃-25%, PPy-SrTiO₃-50% and PPy-SrTiO₃-75%, electrodes as the counter electrodes for DSSC was examined by CV measurements. CV curves of PPy, PPy-SrTiO₃-25%, PPy-SrTiO₃-50% and PPy-SrTiO₃-75%, electrodes were obtained in the

three-electrode system, with 10 mM LiI, 1 mM I₂ acetonitrile solution having 0.1 M LiClO₄ as electrolyte. Ag/AgCl and Pt wire were employed as the reference electrode and counter electrodes, respectively. The catalytic performance of different synthesized counter electrode was investigated in a potential range of -0.2 to 0.6 V (Versus Ag/AgCl as reference counter electrode) using scan rate of 10 mV.s⁻¹. For efficient device performance, reduction of electrolyte is important. Catalytic conversion rate of oxidation/reduction is directly related to peak current density. For evaluating the electro catalytic activity of the electrodes, the peak current density and peak to peak separation (E_{pp}) are the vital parameters. E_{pp} value of PPy-SrTiO₃-50% is smaller as compare to other fabricated counter electrodes. This confirms the PPy-SrTiO₃-50% provides high electrocatalytic response then that of others. The smaller E_{pp} reveal rapid transfer of charges through electrode to electrolyte and the larger electroactive surface area is confirmed by higher current density peak values (G. Q. Wang et al., 2018) . Furthermore, from Figure 4.6, the internal area CV for counter electrode PPy-SrTiO₃-50% is more than other counter electrodes, this also confirm fast ion transportation from electrode to electrolyte.

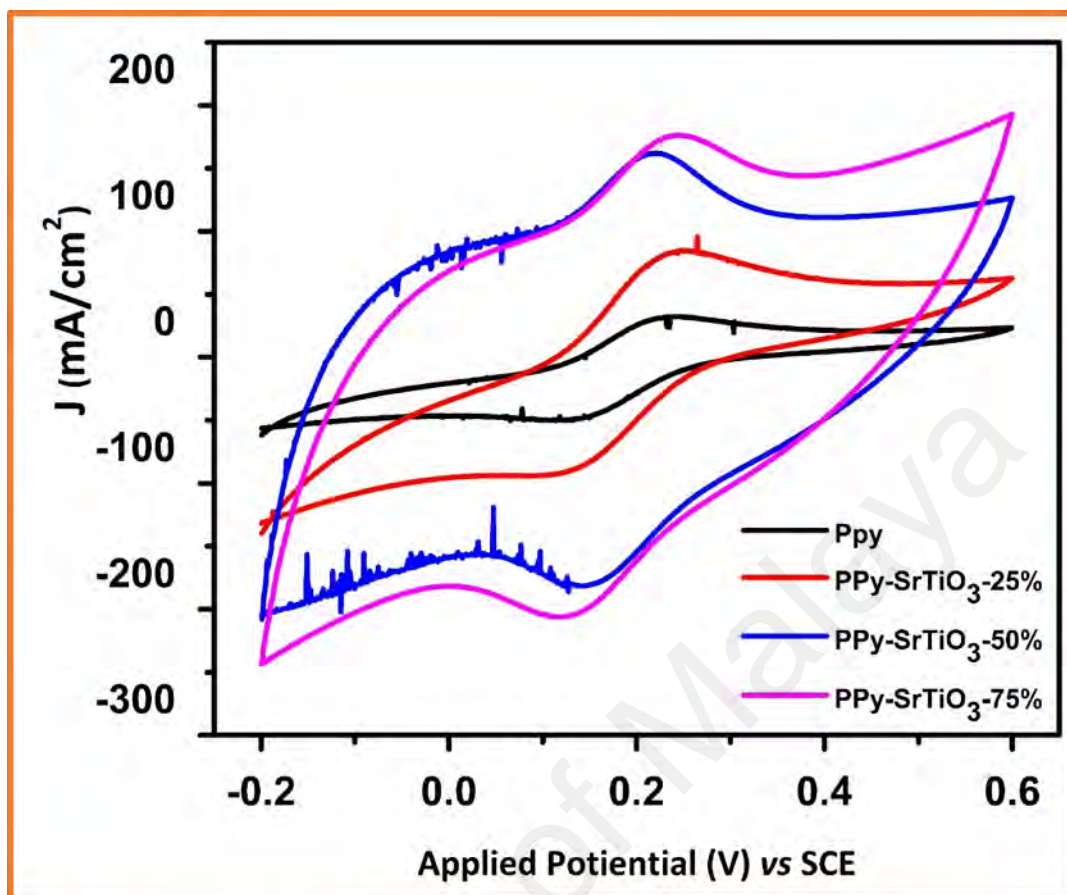


Figure 4.6: Cyclic voltammetry for PPy, PPy-SrTiO₃-25%, PPy-SrTiO₃-50% and PPy-SrTiO₃-75% CE obtained at a scan rate of 10 mV s⁻¹ in a 10 mM LiI, 1 mM I₂ acetonitrile solution containing 0.1 M LiClO₄ as the supporting electrolyte

4.1.6 Electrochemical Impedance Spectroscopy EIS

To investigate the dynamics for transport of electrons, recombination of charges and the interference of electrode and electrolyte, the electrochemical performance of fabricated counter electrodes was examined by Electrochemical Impedance Spectroscopic (EIS) at the frequency range of 0.1 Hz⁻¹ MHz. The semicircle along X-axis in Figure 4.7, represents the charge transfer resistance (R_{CT}) which coincide the transfer of charges occurs at the interference of electrode and electrolyte (G. T. Yue, Li, Li, & Chen, 2016). Initially, PPy showed high EIS spectrum and R_{ct} value of 1014.36 Ω indicating low catalytic behavior. But with the addition of different wt. % concentrations of SrTiO₃ in PPy results in low R_{ct} value and low EIS spectrum, which indicates

improved catalytic performance of PPy-SrTiO₃ counter electrodes. At wt. concentration 50%, PPy-SrTiO₃-50% exhibits lower value of charge transfer resistance 46.40 Ω which reflects accelerated electron transfer at the interface of electrolyte and counter electrode. The EIS results indicate the enhanced photovoltaic performance of polypyrrole with the addition of metal oxides (SrTiO₃). When PPy nanoparticle were entailed with electrolyte, the electrons started to diffuse due to the reduction of I₃⁻ into I⁻ resulting for the reduction of dye electron. In this manner, the addition of SrTiO₃ nanocubes accelerate the redox couple and helps to improve the overall electro catalytic performance of DSSC. Furthermore, the EIS results are consistent with CV results, which confirmed that PPy-SrTiO₃-50% exhibited high electro catalytic response toward the redox couple and exhibits high surface area for the rapid transfer of electron.

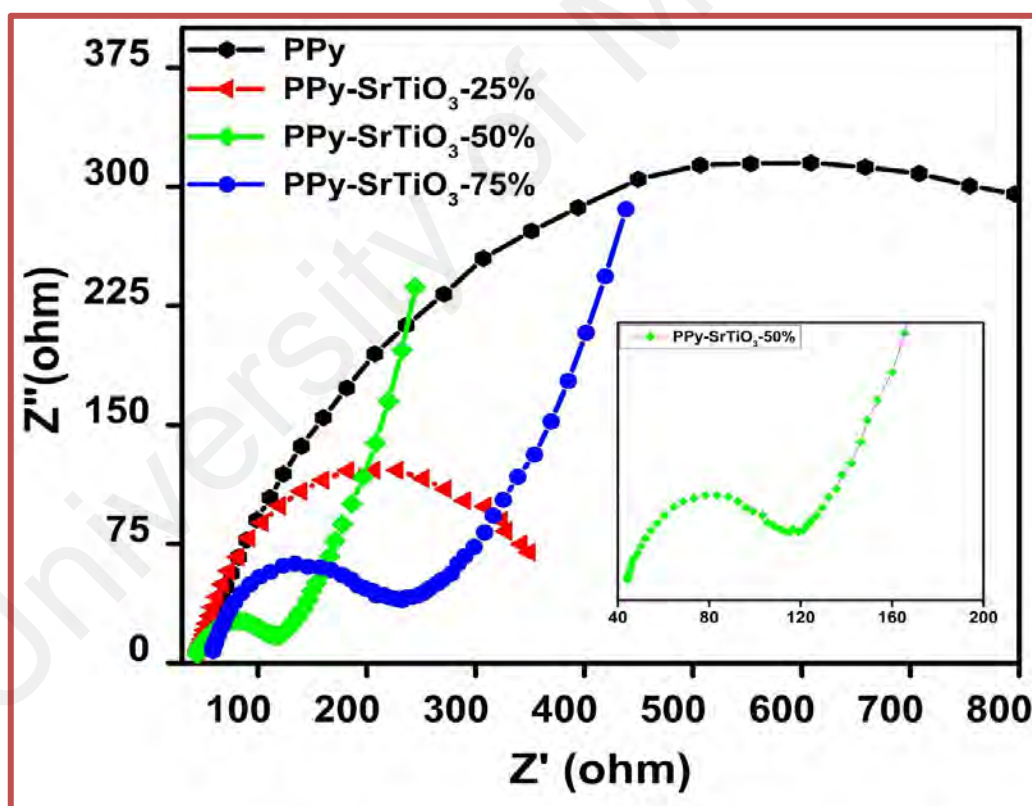


Figure 4.7: Representing the Nyquist plots of PPy-SrTiO₃ composite based counter electrodes

4.1.7 Photovoltaic Performance Analysis

To investigate the photovoltaic characteristic of DSSC, the photo-current density to voltage (J-V) curve was examined for fabricated PPy-SrTiO₃ based counter electrodes. The PV performance of DSSC with PPy, PPy-SrTiO₃-25%, PPy-SrTiO₃-50% and PPy-SrTiO₃-75% counter electrodes are represented in Figure 4.8. The detailed photovoltaic performance parameters including, open circuit voltage (V_{oc}), short circuit current (J_{sc}), maximum current density (J_{max}), maximum voltage across the circuit (V_{max}), fill factor (FF) and photo conversion efficiency (PEC / η) are summarized in Table (1). Due to poor electro catalytic response and high value of charge transfer resistance, PPy counter electrode showed poor PV performance exhibiting short circuit current value 5.867 mA/cm², open circuit voltage value 0.638 V, and power conversion efficiency of 1.13%. The optimization of material plays vital role in order to achieve highly efficient counter electrode for DSSC. In this regard, different wt. concentrations of SrTiO₃ were added in PPy to obtain optimistic counter electrode for DSSC. It has been found that with the addition of SrTiO₃ in PPy, the PCE of DSSC was enhanced until 50% addition of SrTiO₃. The enhancement in the efficiency was on the account of addition of SrTiO₃ in PPy which results to rise the J_{sc} of fabricated DSSC. Moreover, the increase in SrTiO₃ nanocubes directed to decrease in the PEC. This decrease in efficiency can be attributed to dispersion of large number of SrTiO₃, which decreases electro catalytic activity of reduction and increases the value charge transfer resistance. PPy showed low value of J_{sc}, the J_{sc} value raised from 5.867 mA/cm² to 10.451 mA/cm² with the addition of SrTiO₃. PPy- SrTiO₃ composite based counter electrodes achieved the power conversion efficiency of 1.98 %, 2.8% and 2.08% for counter electrodes PPy-SrTiO₃-25%, PPy-SrTiO₃-50% and PPy-SrTiO₃-75% respectively.

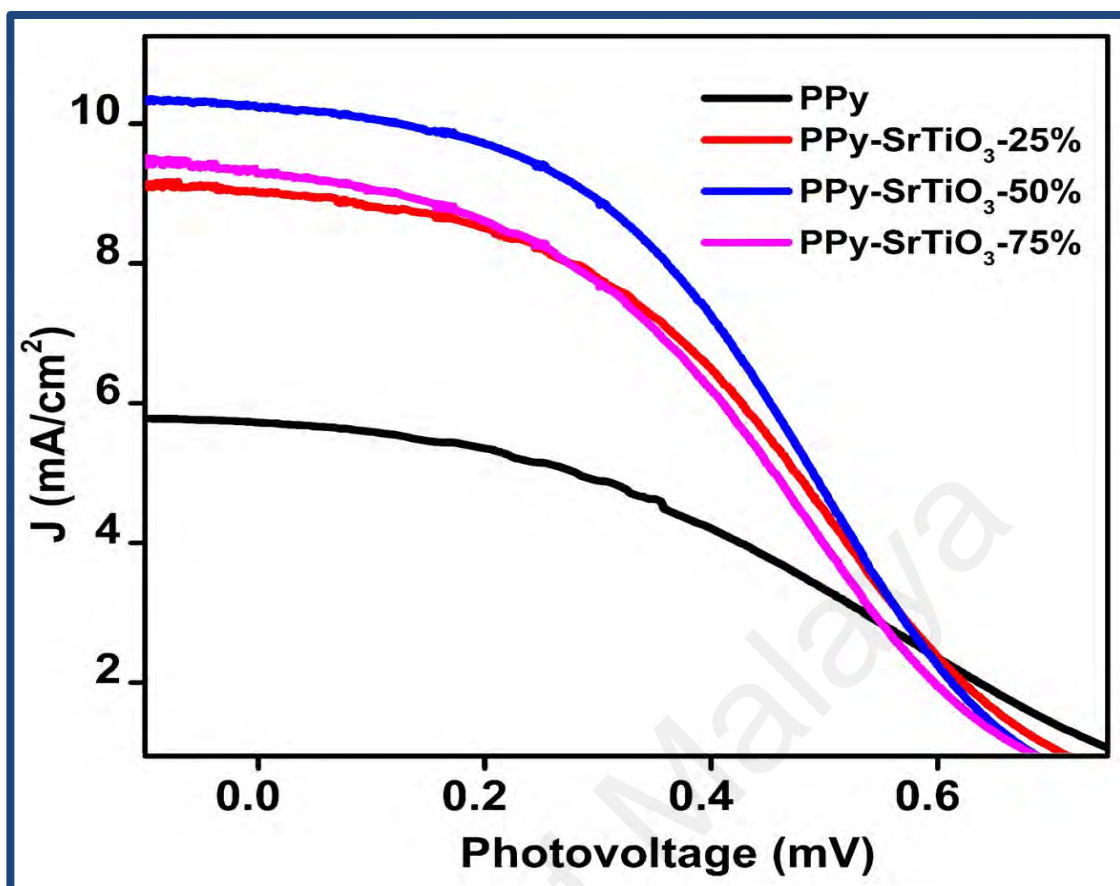


Figure 4.9: The photocurrent density–voltage curves of DSSC with PPy-SrTiO₃ composite based counter electrodes

Table 4.1: Illustrating the PV performance of PPy-SrTiO₃ composite based counter electrode in Dye sensitized solar cell

| Sr. No | Counter Electrodes | J _{sc} (mA/cm ²) | V _{oc} (V) | J _{max} (mA/cm ²) | V _{max} (V) | FF | η (%) | R _{CT} |
|--------|-----------------------------|---------------------------------------|---------------------|--|----------------------|------|-------|-----------------|
| 1. | PPy | 5.867 | 0.761 | 5.211 | 0.227 | 0.29 | 1.29 | 1014.3 |
| 2. | PPy-SrTiO ₃ -25% | 9.239 | 0.671 | 8.351 | 0.219 | 0.32 | 1.98 | 230.39 |
| 3. | PPy-SrTiO ₃ -50% | 10.451 | 0.671 | 9.362 | 0.269 | 0.36 | 2.52 | 46.40 |
| 4. | PPy-SrTiO ₃ -75% | 9.542 | 0.706 | 8.667 | 0.189 | 0.31 | 2.08 | 124.95 |

To enhance the photovoltaic (PV) characteristic of counter electrode significant research has been done previously, different material in composition with PPy were investigated by researchers. The photo catalytic and PV performance of different counter electrode in combination with PPy is summarized in Table 2. From the table it can be

viewed that the binary composite of PPy-SrTiO₃-50% showed enhanced photocatalytic response and electrical conductivity.

Table 4.2: Summary of previously reported PPy composite based counter electrode for DSSC

| Sr. No | Counter Electrodes | J _{sc} (mA/cm ²) | V _{oc} | FF | η (%) | Reference |
|--------|--------------------------------|---------------------------------------|-----------------|------|-------|--|
| 1 | PPy/MWC NT | 4.19 | 0.40 | 0.48 | 0.80 | (Cogal et al., 2018) |
| 2 | PPy/CTAB | 7.36 | 0.65 | 0.36 | 1.73 | (Kuliček, Gemeiner, Omastová, & Mičušík, 2018) |
| 3 | PPy/CTAB/MWCNT | 5.44 | 0.58 | 0.53 | 1.67 | (Kuliček et al., 2018) |
| 4 | PPy/Tween20 | 6.62 | 0.58 | 0.41 | 1.80 | (Kuliček et al., 2018) |
| 5 | PPy/Tween20/MWC NT | 6.08 | 0.56 | 0.55 | 2.11 | (Kuliček et al., 2018) |
| 6 | Polypyrrole free standing film | 4.5 | 0.63 | 0.38 | 1.10 | (Jha et al., 2017) |
| 7 | PPy/ER | 0.90 | 0.52 | 0.45 | 0.22 | (Q. Li et al., 2010) |
| 8 | SS-PPy | 4.98 | 0.70 | 0.67 | 2.36 | (X. Huang et al., 2010) |
| 9 | rGo@PPy | 7.49 | 0.70 | 0.42 | 2.21 | (Lim, Pandikumar, Lim, Huang, & Lim, 2014) |
| 10 | PPy-SrTiO ₃ – 50% | 10.45 | 0.61 | 0.36 | 2.52 | Present research |

Bu, C., et al. (Bu, Tai, Liu, Guo, & Zhao, 2013) Synthesized PPy-IOs via air–water interface polymerization process and reported the power conversion efficiency of 5.73%. The obtained PCE was lower than the power conversion efficiency of used Pt counter electrode i.e.7.24%. Wang, G., et al (G. Wang et al., 2018) Synthesized hierarchical nanostructured polypyrrole (HNPPy), and investigated their electrochemical properties for counter electrode in DSSC. They reported that HNPPy counter electrode exhibit the PCE of 6.78%. Although the reported efficiency is high but is still lower than Pt (7.33%). In another work, PPy prepared by In-situ polymerization, coated on FTO glass was fabricated as transparent PPy counter electrode in DSSC. It was found that transparent PPy counter electrode exhibited the PCE of 5.74% [40]. Previously researchers have used

PPy counter electrode for DSSC and reported the conversion efficiency of up to 7.01%. However, the obtain efficiency is still lower than the power conversion efficiency of Pt counter electrode. In this work we have reported PCE of PPy-SrTiO₃-50% is 2.52% which is higher than the PCE of sputtered Pt counter electrode i.e. 2.17%. Figure 4.10, representing the comparison of J-V curve of Pt and optimize sample of polypyrrole in composite with SrTiO₃ (PPy-SrTiO₃-50%) and the photovoltaic parameters are described in Table 3.

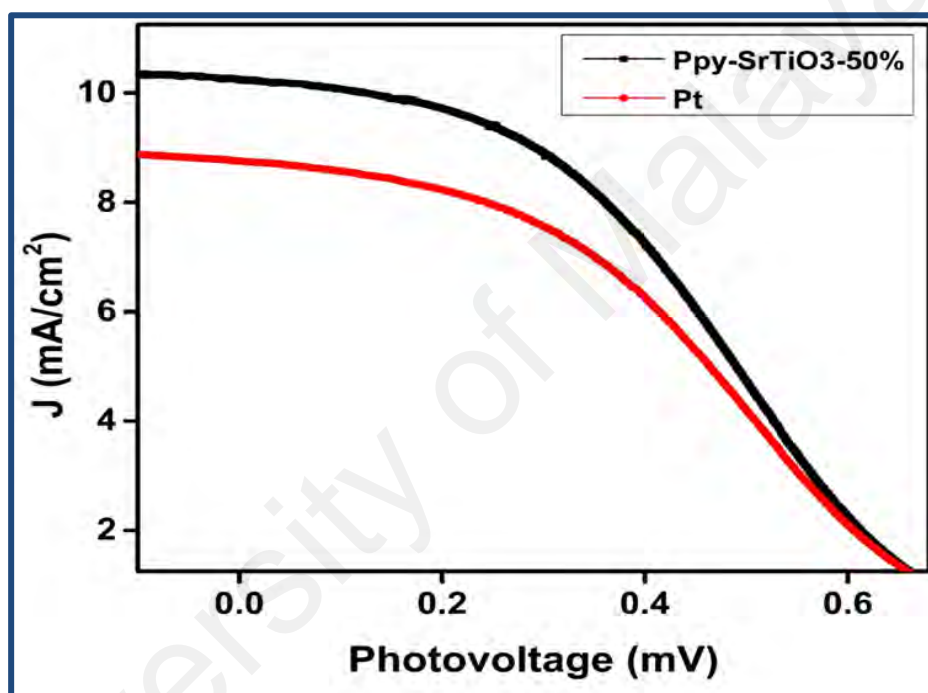


Figure 4.10: The photocurrent density–voltage curves of DSSC with PPy-SrTiO₃-50% and Pt counter electrodes

Table 4.3: Photovoltaic parameters of DSSC based on PPy-SrTiO₃-50% and Pt counter electrodes

| Sr. No | Counter Electrodes | J _{sc} (mA/cm ²) | V _{oc} (V) | J _{max} (mA/cm ²) | V _{max} (V) | FF | η (%) |
|--------|-----------------------------|---------------------------------------|---------------------|--|----------------------|-------|-------|
| 1. | Pt | 9.021 | 0.660 | 7.591 | 0.286 | 0.370 | 2.17 |
| 2. | PPy-SrTiO ₃ -50% | 10.451 | 0.671 | 9.362 | 0.269 | 0.36 | 2.52 |

4.2 ³ Influence of Concentration of Polyaniline (PANI) as Counter Electrode in Dye Sensitized Solar Cell (DSSC)

Conducting polymers are potential candidates for CE in DSSCs, due to exhibiting unique characteristics, such as low cost, excellent conductivity, high mechanical stability, and remarkable electro catalytic response for the reduction of electrolyte. Up to now, several conducting polymers based counter electrode are studied by researchers and I was found that PANI is one of the most extensively examined conducting polymer in last decade, owning its high-conductivity, good environmental stability, simple synthesis method and remarkable redox properties. The structural morphology and low charge transfer resistance of the CEs have a great influence on PV performance of DSSC. Here in this work we have successfully synthesized PANI nanotube by simple oxidative polymerization method. It was found that that concentration of PANI has great influence on the PCE of DSSC. The morphology, chemical composition, conductivity, and the electro catalytic properties of the PANI is discussed in detail.

4.2.1 Morphology Analysis

The structural morphology of polyaniline (PANI) was examined by FESEM. It was found that the synthesized PANI exhibit well define and uniform nanotubes like structure. The average diameter of PANI nanotube was around 80–100 nm (outer diameter) and the 20–30 nm (inner diameter). Due to novel properties PANI nanotubes structures have attained the interest showed great potential for counter electrode in DSSC. Simple polymerization approach was utilized for the synthesis of PANI nanotubes. The nanotubes structure depends on protocols used during the polymerization. Figure 4.11 (a) represents the FE-SEM image of PANI nanotubes. The FE-SEM images show that the

³ Section 4.2 has been published (Ahmed, U., Rahim, N. A., Shahabuddin, S., Alizadeh, M., & Pandey, A. K. (2018). Influence of concentration of polyaniline (PANI) as counter electrode in dye sensitized solar cell.

PANI is of nanotube like structure. The surface area of PANI is also responsible for high conductivity of PANI. The structural morphology and uniformity of PANI nanotube were further confirmed by TEM image. Figure 4.11 (b) represents the structural image of PANI at 20 nm, which further provides the evidence for the morphology of PANI nanotubes that is reliable with the SEM images.

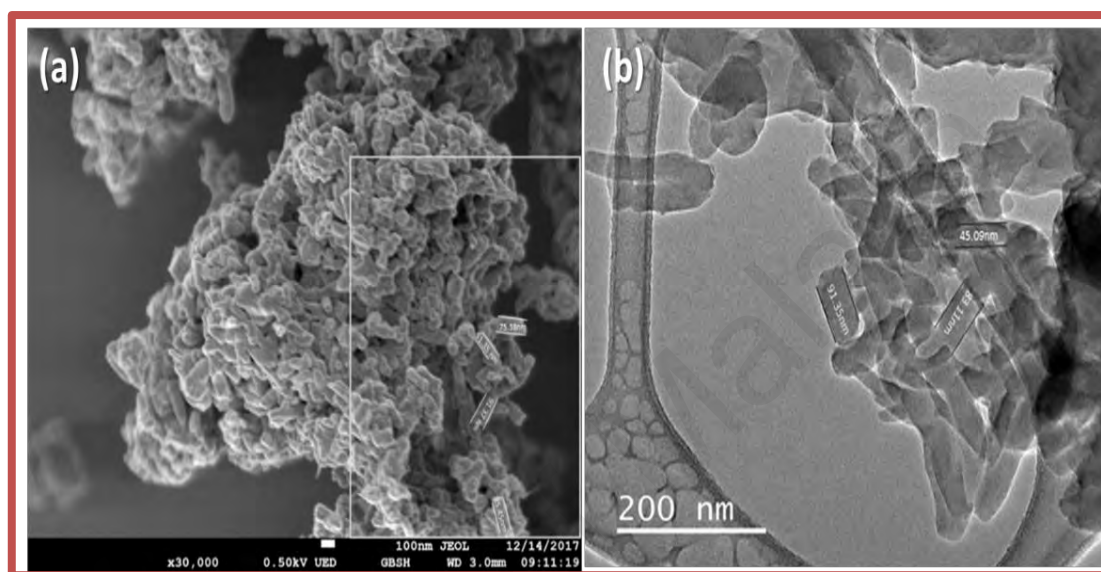


Figure 4.11: (a) FESEM image of PANI Nanotubes (b) TEM image of PANI nanotubes

4.2.2 XRD Analysis

At room temperature, XRD spectra of synthesized PANI nanotubes was studied and is shown in Figure 4.12. The diffraction patterns entailed of wide-ranging crystalline peaks and the well define peak about $2\theta = 15.45^\circ$ may be ascribed to the periodicity corresponding to the polymer matrix, where the well define peak around $2\theta = 25.40^\circ$ is corresponds to the periodicity perpendicular to the order of polymer chain representing the amorphous structure. The peak at angles of $2\theta = 20.30$ and 25.40 matches up with the periodic replication of benzenoid and quinoid rings in PANI chains (Shahabuddin, 2016)

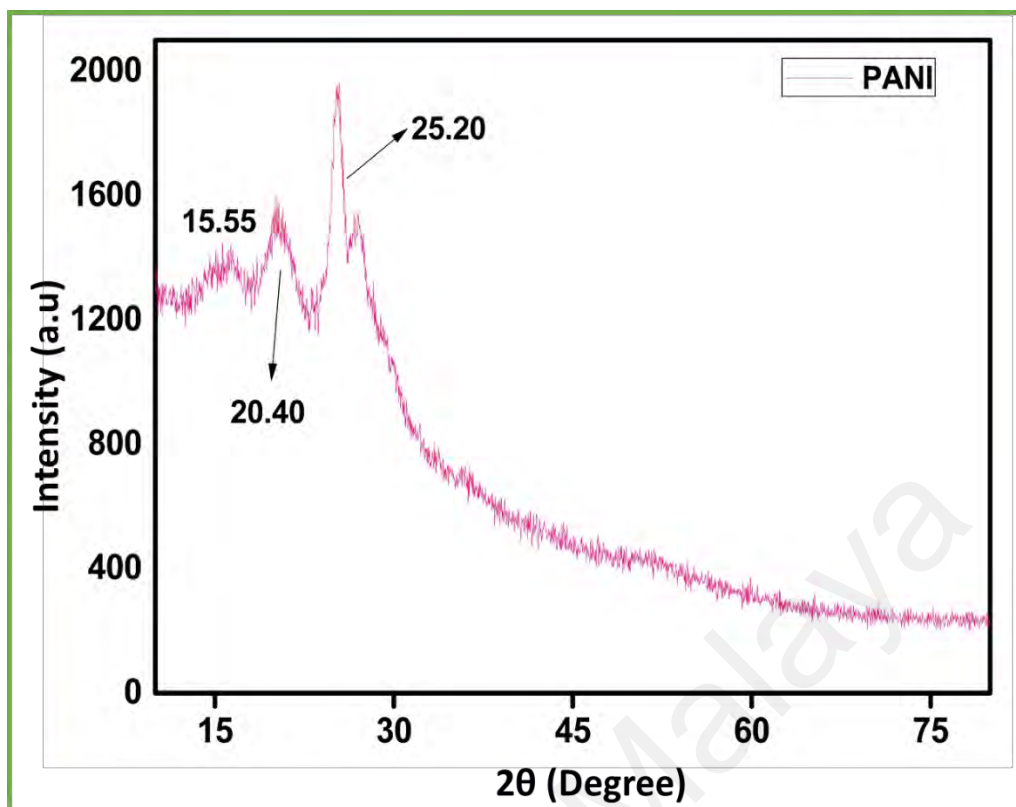


Figure 4.12: XRD pattern of PANI nanotubes

4.2.3 FT-IR Analysis

The FT-IR of the nanotube's structures of PANI is represented in Figure 4.13. The main characteristic bands are allocated as; the bands at 789 and 1285 cm^{-1} are owing to the C–H in-plane and the out-of-plane deformation of C–H. At outer plane the C–H bending vibrations band from a para-permutation pattern at 789 cm^{-1} (Lau et al., 2017). It is found, at 1430 cm^{-1} and 1561 cm^{-1} corresponds to IR absorption band of PANI nanotubes. These are stretching vibration of benzenoid (C=C), and quinoid (C=N=C) rings in PANI. C=C and C=N=C stretching in PANI was attached to a peak have value of 1285 cm^{-1} , and N–H stretching mode in PANI was attached to the peak value of 3425 cm^{-1} . The existence of the quinoid ring and benzenoid ring indicates the high conductivity of PANI.

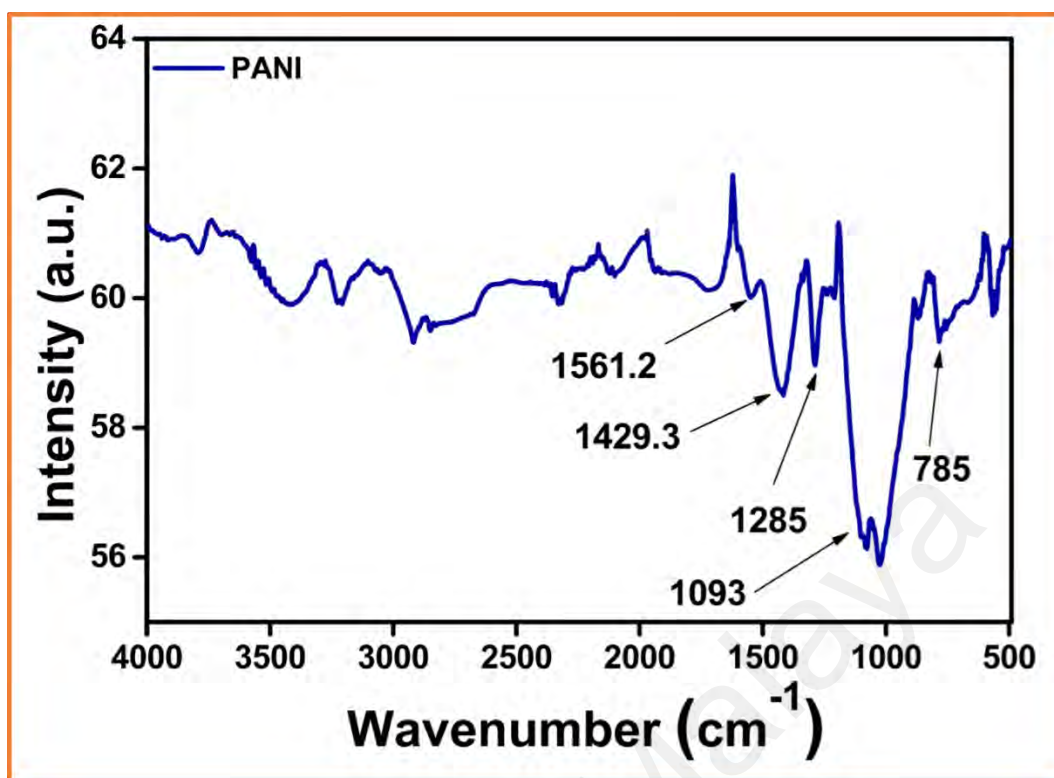


Figure 4.13: The FT-IR spectrum of PANI nanotubes

4.2.4 UV-Vis Analysis

UV-visible spectroscopy of PANI tells that it exhibits unique property for the absorption of light of different wavelength. The protonated form of fabricated PANI having different wavelengths 380–460 nm, 470–500 nm, and 505–780 nm are represented in Figure 4.14. The electron transition (π - π^*) in benzenoid section provides the evidence for first absorption band. The other absorption band were assigned to a quinoid ring of PANI for chain formation.

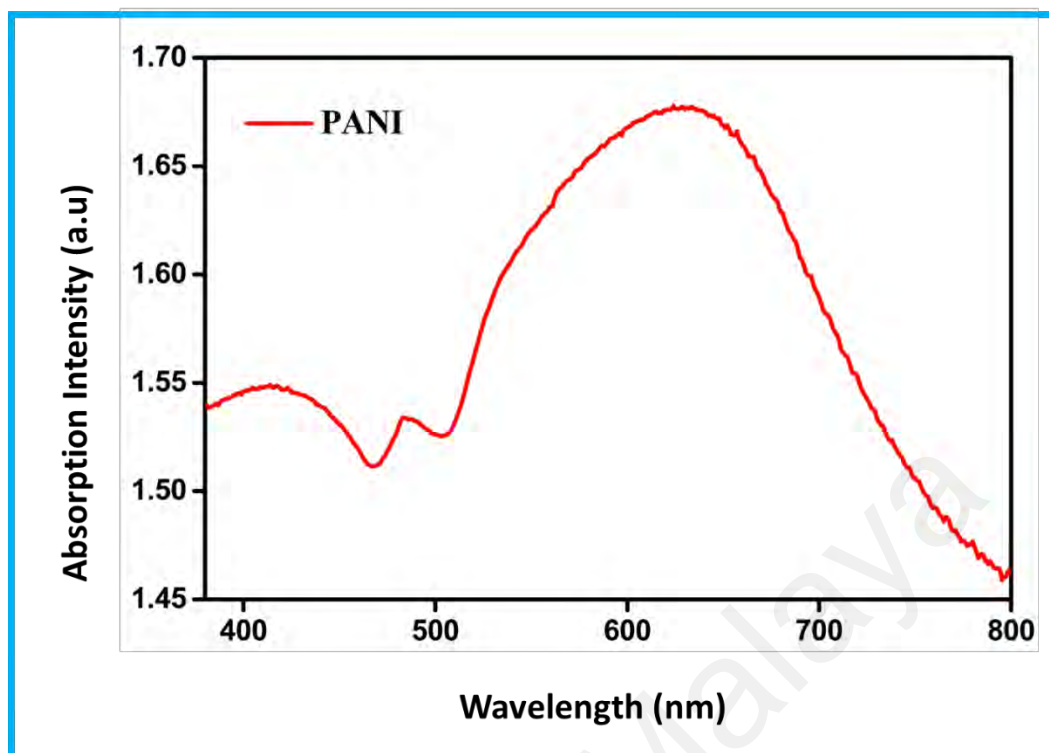


Figure 4.14: UV-vis spectrum of PANI nanotubes

4.2.5 Cyclic Voltammetry

The cyclic voltammogram (CV) curve of synthesized material was examined in 0.1 M potassium ferricyanide analyte as an electrolyte; well resolve oxidation-reduction peaks were for bare ITO, PANI-3 and Pt counter electrode as shown in Figure 4.15. The catalytic performance of different counter electrode was investigated in a potential range of -0.2 to 0.8 V (Versus Ag/AgCl as reference counter electrode) using scan rate of 10 mV.s⁻¹. For efficient device performance, reduction of electrolyte is key factor, and here we will discuss only about oxidation/reduction peaks. Catalytic conversion rate of oxidation/ reduction is directly related to peak current density. For evaluating the electro catalytic activity of the electrodes, the peak current density and peak to peak separation (E_{pp}) are the vital parameters. The bare ITO show well-resolved oxidation and reduction peak value for current 0.798 mA and 0.893 mA at potential values of 0.113V and 0.231V respectively. The redox peak for synthesized PANI-3 counter electrode was also resolved

and well patterned with peak current values of 1.084 mA and 1.240 mA at 0.237 V and 0.118 V respectively.

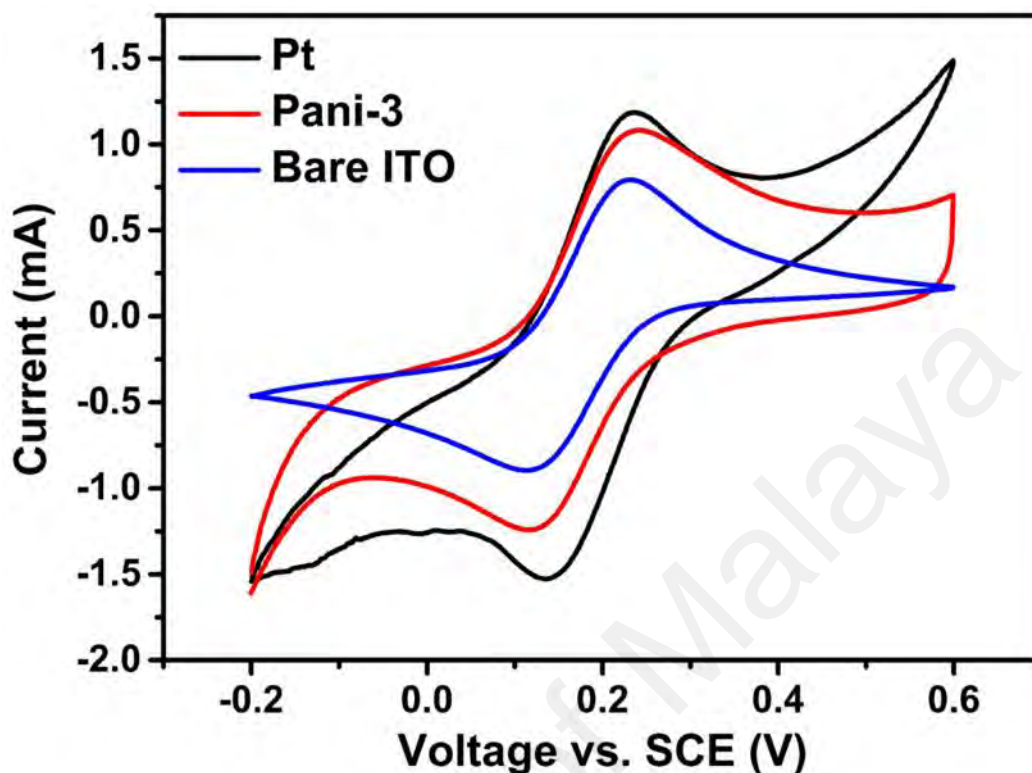


Figure 4.15 Cyclic voltammetry of Pt, PANI-3 and bare ITO counter electrode at a scan rate of 50 mV/s

4.2.6 Electrochemical Impedance Spectroscopy EIS

To study the detail for interference of electron between the electrode and electrolyte, recombination of charges, the electrochemical performance of fabricated counter electrodes was investigated EIS with same protocols discussed in previous section 4.1.7. When PANI nano particle were entailed with electrolyte, the electrons started to diffuse due to the reduction of electrolyte, hence resulting in the reduction of dye. The diameter of semicircle along X-axis in figure 4.15, represents the charge transfer resistance (RCT) which coincide the transfer of charges occurs at the interference of electrode and electrolyte (G. T. Yue, Li, Li, & Chen, 2016). It is observed that bare ITO shows high charge transfer resistance (Rct) value $600\Omega\text{cm}^2$ toward the interference of electron. The conducting substrate coating with synthesized material PANI-3 exhibits the charge

transfer resistance value of $120 \Omega\text{cm}^2$ which is less than that of bare ITO. The commercially available Pt counter electrode show meager value toward the flow of electron. i.e. $20 \Omega\text{cm}^2$.

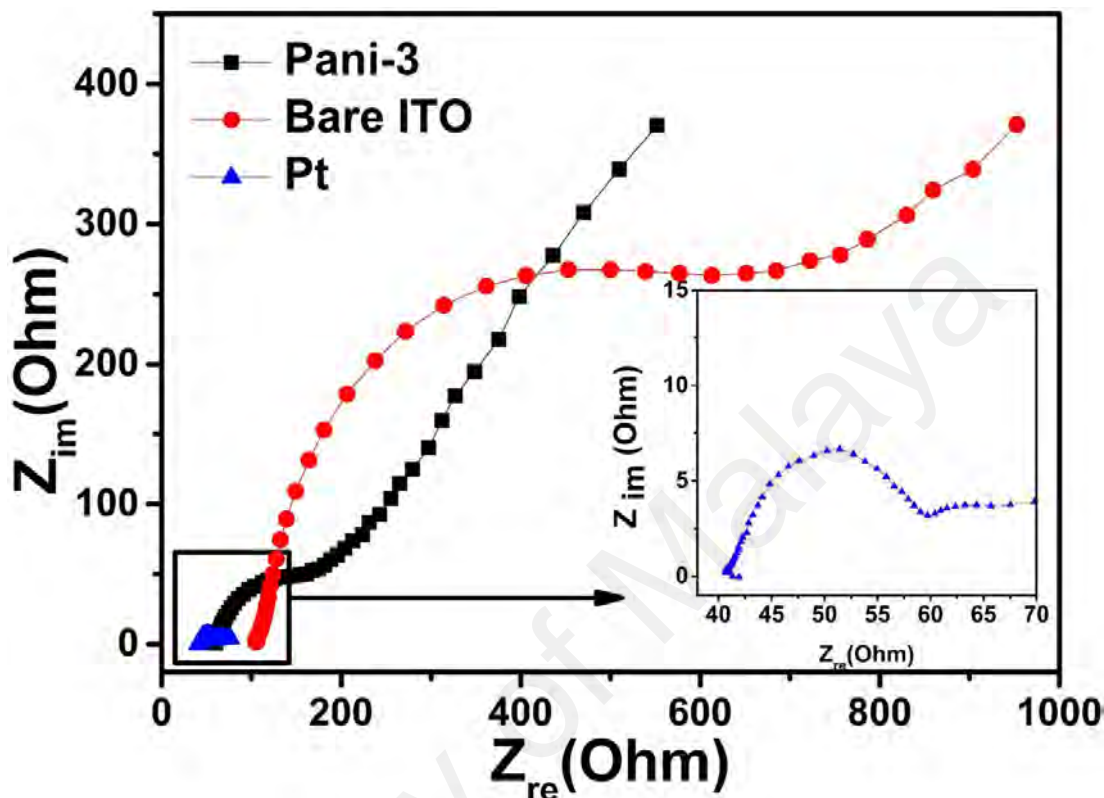


Figure 4.16: Electrochemical impedance spectroscopy of bare ITO, PANI-3 and Pt counter electrodes

4.2.7 Photovoltaic Performance Analysis

The photoelectrical behaviour of PANI under standard test conditions (Cell temperature 25°C , AM 1.5, illumination with a light intensity of $100 \text{ mW}/\text{cm}^2$) shows that with the increase in a weight concentration of PANI, the fill factor, and performance of PANI counter electrode was enhanced. With high weight concentration, the surface area of PANI increases and the FF also increases with the decrease of charge transfer resistance (R_{CT}). PANI with different weight concentration exhibit the J_{sc} values of $1.779 \text{ mA}/\text{cm}^2$, $2.29 \text{ mA}/\text{cm}^2$, $2.92 \text{ mA}/\text{cm}^2$, and $5.48 \text{ mA}/\text{cm}^2$ for PANI-1, PANI-2, PANI-3 and Pt respectively. The current density-voltage ($J-V$) curves of DSSCs are illustrated in Figure 4.17.

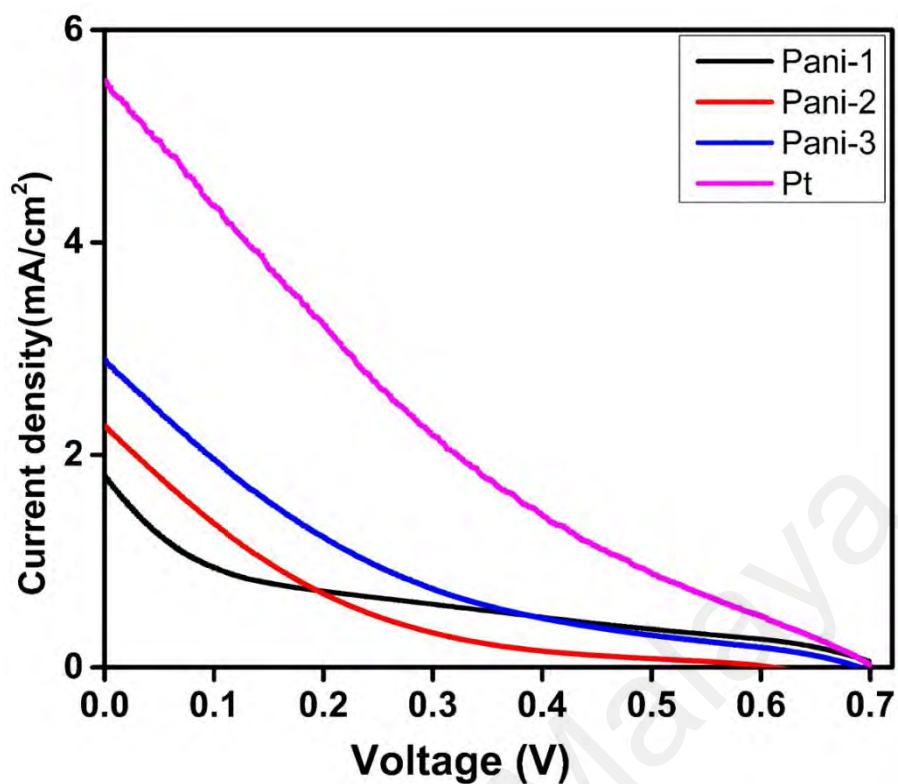


Figure 4.17: J-V curve of various concentration of PANI counter electrode Used for DSSC

Table 4.4: Illustrating the PV performance of PANI based counter electrode in Dye sensitized solar cell

| Sr. No | Counter Electrodes | J _{sc} (mA/cm ²) | V _{oc} (V) | FF | η (%) |
|--------|--------------------|---------------------------------------|---------------------|------|-------|
| 1. | PANI-1 | 1.76 | 0.691 | 0.13 | 0.15 |
| 2. | PANI-2 | 2.27 | 0.631 | 0.15 | 0.21 |
| 3. | PANI-3 | 2.93 | 0.686 | 0.35 | 0.71 |
| 4. | Pt | 5.51 | 0.689 | 0.42 | 1.57 |

CHAPTER 5: CONCLUSIONS, RECOMMENDATIONS AND FUTURE WORK

5.1 Conclusions

Solar cell devices are altering from experimental stage to commercialization. New techniques and fabrication methods were developed to improve the power conversion efficiency and to make DSSC cost effective. DSSCs exhibit high potential and attract the interest of scientist from last thirty years due to cost effectiveness highly efficiency and easy fabrication methods. Certain elements including photoanode, counter electrode, sensitizing dye and electrolyte effects the PV performance of DSSCs. Each component has its own significance but among all others, CE plays a vital role as it receives electron from an external circuit and send these electrons towards the electrolyte for redox reactions. These electrons are then transfer towards the dye, where the regeneration of dye electron occurs. All these components significantly affect the overall performance of DSSC.

Numerous materials containing metals sulfides and oxide of metals, conducting polymers, and carbonaceous materials with different structural morphology and chemical composition have been explored and studied by researchers as CE in DSSCs. Although few materials showed high efficiency and electrochemical response but still are not as good as Pt based CE in terms of low charge transfer resistance, photo catalytic activity, and stability. The electrocatalytic response and PV characteristics as mentioned in literature review directs that in conducting polymer material PANI, PPy and PEDOT showed high catalytic performance and stability. Furthermore, different metal oxide and sulfides also exhibit high electrocatalytic properties, and high surface area which help in the efficient flow of electron with low resistance value. We examined that conducting polymers in composite with any other material exhibit remarkable properties which

favors the high PV performance of DSSC. Hence, there are few key points which need to be considered regarding material which can improve PV performance and of DSSC, such as: (i) Different structure of metal oxides, (ii) carbon-based nanocomposite materials and (iii) exploration of conducting polymer-based nanocomposite materials.

In present work, PPy-SrTiO₃ nanocomposite was successfully synthesized by the chemical oxidative polymerization method with interesting electrocatalytic properties. FESEM, FTIR, XRD analysis confirmed the uniform distribution of SrTiO₃ nanocubes in the polymer matrix of PPy, hence resulting in uniform composite formation. The nanostructured composition of PPy-SrTiO₃ provides a high surface area which helps in fast mass transportation of electron to an electrolyte and allow PPy- SrTiO₃ (50%) counter electrode to enhance the reduction of triiodide to iodide. Under standard condition the DSSC assembled with fabricated PPy- SrTiO₃-50% CE exhibited high photo conversion efficiency of 2.52% under illumination of 100 mW cm⁻² compare able with the efficiency of Pt-based counter electrode i.e. (2.17%). This work suggests PPy- SrTiO₃-50% CE exhibits remarkable potential as a highly efficient and economical counter electrode for dye-sensitized solar cell.

Furthermore, it was found that polyaniline (PANI) due to its peculiar properties also showed great potency as CE in DSSC. It is well known that Pt, as an expensive metal, exhibit high photoelectric response by dint of its high conductivity and is an electroactive material. Thereupon, commercially available Pt counter electrode showed higher efficiency as compared to the fabricated counter electrode (PANI). It was also examined that PANI-3 CE exhibited well-define oxidation and reduction peaks indicating high electrocatalytic response towards the reduction of electrolyte. According to the obtained results it is concluded that unaided PANI-3 CE exhibit high catalytic activity and low charge transfer resistance as compare to other fabricated counter electrodes. The catalytic

properties and PV performance of PANI can be improve by doping it with metal, metal oxide and carbon bases materials.

5.2 Recommendations

DSSC is an environmentally friendly, easy to fabricate, and economical technology which can be used as in several applications. For commercial use of DSSC, the PV performance of several components of DSSC need to be improve. The material preparation methods such as in-situ/ oxidative polymerization, hydrothermal, chemical processing, electrodeposition, and chemical bath method are impressive, cost effective and environmental friendly method exploited for the synthesis of metal based, composite based martials as carbonaceous and conducting polymer based counter electrode for DSSC. The thickness of coated film effects the efficiency of flow of electron, for the efficient flow of electrons the thickness of coated film should be in between 30 nm to 80 nm. Doctor Blade method is frequently used technique for the deposition of counter electrode materials on conducting substrate, but as a manual method it is very difficult to optimize the thickness of coating accurately for every time. Hence to optimize the thickness of coating and better performance of C.E, it is to be suggested exploring other approaches like screen printing EPD and spin coating should be considered as best method. Due to high stability carbonaceous materials showed electrochemical response, low charge transfer resistance, and high electrocatalytic response in conducting polymers is due to high conductivity of polymers. It was observed that the composite materials exhibit high stability and electrocatalytic response and high PV performance as compare to unaided materials. Hence, it is suggested that the consideration of composite of carbonaceous materials, conducting polymer-based materials and metal oxides as counter electrode will help to fabricate low cost and highly efficient CE for DSSC.

5.3 Future Work

The current work is mainly focused on low cost counter electrode to replace Pt based CE in DSSC. As it was found that with the addition of metal oxide the performance of conducting polymer was enhanced. The optimized concentration of PANI will be used in composition with different concentrations of SrTiO_3 . The integration of oxides of tungsten and molybdenum in composition with PPy and PANI will also be investigated further as counter electrode in DSSC. Furthermore, metal oxides in composition with carbonaceous materials including activated carbon, carbon nanotubes (CNT), and graphene (GO, rGO) will also investigated to enhance the efficiency counter electrodes in DSSC.

University of Malaysia

REFERENCES

- Aegerter, M. A., & Mennig, M. (2013). *Sol-gel technologies for glass producers and users*: Springer Science & Business Media.
- Ahmad, K., Mohammad, A., & Mobin, S. M. (2017). Hydrothermally grown α -MnO₂ nanorods as highly efficient low cost counter-electrode material for dye-sensitized solar cells and electrochemical sensing applications. *Electrochimica Acta*, 252, 549-557.
- Ahmad, M., Pandey, A., & Rahim, N. (2018). *Effect of Germanium on the TiO₂ Photoanode for Dye Sensitized Solar Cell Applications. A Potential Sintering Aid*. Paper presented at the IOP Conference Series: Materials Science and Engineering.
- Ahmad, M. S., Pandey, A., & Rahim, N. A. (2018). Effect of Nanodiamonds on the Optoelectronic Properties of TiO₂ Photoanode in Dye-Sensitized Solar Cell. *Arabian Journal for Science and Engineering*, 43(7), 3515-3519.
- Ahmad, S., Dell'Orto, E., Yum, J.-H., Kessler, F., Nazeeruddin, M. K., & Grätzel, M. (2012). Towards flexibility: metal free plastic cathodes for dye sensitized solar cells. *Chemical Communications*, 48(78), 9714-9716.
- Ahmad, W., Chu, L., Al-bahrani, M. R., Yang, Z., Wang, S., Li, L., & Gao, Y. (2015). Formation of short three dimensional porous assemblies of super hydrophobic acetylene black intertwined by copper oxide nanorods for a robust counter electrode of DSSCs. *RSC Advances*, 5(45), 35635-35642.
- Ahmadi, S., Asim, N., Alghoul, M., Hammadi, F., Saeedfar, K., Ludin, N. A., Sopian, K. (2014). The role of physical techniques on the preparation of photoanodes for dye sensitized solar cells. *International Journal of Photoenergy*, 2014.
- Ahmed, U., Rahim, N. A., Shahabuddin, S., Alizadeh, M., & Pandey, A. (2018). Influence of concentration of polyaniline (PANI) as counter electrode in dye sensitized solar cell.
- Aitola, K., Borghei, M., Kaskela, A., Kemppainen, E., Nasibulin, A. G., Kauppinen, E. I., Halme, J. (2012). Flexible metal-free counter electrode for dye solar cells based on conductive polymer and carbon nanotubes. *Journal of Electroanalytical Chemistry*, 683, 70-74.
- Al-Bahrani, M. R., Ahmad, W., Mehnane, H. F., Chen, Y., Cheng, Z., & Gao, Y. (2015). Enhanced electrocatalytic activity by RGO/MWCNTs/NiO counter electrode for dye-sensitized solar cells. *Nano-Micro Letters*, 7(3), 298-306.

- Anothumakkool, B., Agrawal, I., Bhange, S. N., Soni, R., Game, O., Ogale, S. B., & Kurungot, S. (2015). Pt-and TCO-free flexible cathode for DSSC from highly conducting and flexible PEDOT paper prepared via in situ interfacial polymerization. *ACS applied materials & interfaces*, 8(1), 553-562.
- Aparna, S., Elakhya, N., Gopal, G., Rajesh, P., & Ramasamy, P. (2017). Influence of polyaniline in polyaniline-tin oxide nanocomposite as counter electrode for dye sensitized solar cells. *Optik-International Journal for Light and Electron Optics*.
- Badawy, W. A. (2015). A review on solar cells from Si-single crystals to porous materials and quantum dots. *Journal of advanced research*, 6(2), 123-132.
- Bagnall, D. M., & Boreland, M. (2008). Photovoltaic technologies. *Energy Policy*, 36(12), 4390-4396.
- Bahramian, A., & Vashae, D. (2015). In-situ fabricated transparent conducting nanofiber-shape polyaniline/coral-like TiO₂ thin film: Application in bifacial dye-sensitized solar cells. *Solar Energy Materials and Solar Cells*, 143, 284-295.
- Bai, Y., Mora-Sero, I., De Angelis, F., Bisquert, J., & Wang, P. (2014). Titanium dioxide nanomaterials for photovoltaic applications. *Chemical reviews*, 114(19), 10095-10130.
- Balamurugan, J., Thanh, T. D., Kim, N. H., & Lee, J. H. (2016). Nitrogen-doped graphene nanosheets with FeN core-shell nanoparticles as high-performance counter electrode materials for dye-sensitized solar cells. *Advanced Materials Interfaces*, 3(1), 1500348.
- Bandara, T., Dissanayake, M., Jayasundara, W., Albinsson, I., & Mellander, B.-E. (2012). Efficiency enhancement in dye sensitized solar cells using gel polymer electrolytes based on a tetrahexylammonium iodide and MgI₂ binary iodide system. *Physical Chemistry Chemical Physics*, 14(24), 8620-8627.
- Banerjee, A., Upadhyay, K. K., Bhatnagar, S., Tathavadekar, M., Bansode, U., Agarkar, S., & Ogale, S. B. (2014). Nickel cobalt sulfide nanoneedle array as an effective alternative to Pt as a counter electrode in dye sensitized solar cells. *Rsc Advances*, 4(16), 8289-8294.
- Barua, P., Tawney, L., & Weischer, L. (2012). Delivering on the clean energy economy: The role of policy in developing successful domestic solar and wind industries. *World Resources Institute Working Paper*. *World Resources Institute*. Retrieved from http://pdf.wri.org/delivering_clean_energy_economy.pdf.
- Baxter, J. B. (2012). Commercialization of dye sensitized solar cells: Present status and future research needs to improve efficiency, stability, and manufacturing. *Journal*

of Vacuum Science & Technology A: Vacuum, Surfaces, and Films, 30(2), 020801.

Bella, F., Galliano, S., Falco, M., Viscardi, G., Barolo, C., Grätzel, M., & Gerbaldi, C. (2016). Unveiling iodine-based electrolytes chemistry in aqueous dye-sensitized solar cells. *Chemical Science*, 7(8), 4880-4890.

Bella, F., Galliano, S., Falco, M., Viscardi, G., Barolo, C., Grätzel, M., & Gerbaldi, C. (2017). Approaching truly sustainable solar cells by the use of water and cellulose derivatives. *Green Chemistry*, 19(4), 1043-1051.

Bella, F., Galliano, S., Gerbaldi, C., & Viscardi, G. (2016). Cobalt-based electrolytes for dye-sensitized solar cells: recent advances towards stable devices. *Energies*, 9(5), 384.

Bockris, J. (2013). *Electrochemistry of cleaner environments*: Springer Science & Business Media.

Bu, C., Liu, Y., Yu, Z., You, S., Huang, N., Liang, L., & Zhao, X.-Z. (2013). Highly transparent carbon counter electrode prepared via an in situ carbonization method for bifacial dye-sensitized solar cells. *ACS applied materials & interfaces*, 5(15), 7432-7438.

Bu, C., Tai, Q., Liu, Y., Guo, S., & Zhao, X. J. J. o. P. S. (2013). A transparent and stable polypyrrole counter electrode for dye-sensitized solar cell. *221*, 78-83.

Cheah, K., Forsyth, M., & Truong, V.-T. J. S. m. (1998). Ordering and stability in conducting polypyrrole. *94(2)*, 215-219.

Chen, J., Li, K., Luo, Y., Guo, X., Li, D., Deng, M., Meng, Q. (2009). A flexible carbon counter electrode for dye-sensitized solar cells. *Carbon*, 47(11), 2704-2708.

Chen, X., Tang, Q., He, B., Lin, L., & Yu, L. (2014). Platinum-Free Binary Co-Ni Alloy Counter Electrodes for Efficient Dye-Sensitized Solar Cells. *Angewandte Chemie International Edition*, 53(40), 10799-10803.

Cheng, L., Hou, Y., Zhang, B., Yang, S., Guo, J. W., Wu, L., & Yang, H. G. (2013). Hydrogen-treated commercial WO₃ as an efficient electrocatalyst for triiodide reduction in dye-sensitized solar cells. *Chemical Communications*, 49(53), 5945-5947.

Chiang, C.-H., & Wu, C.-G. (2013). High-efficient dye-sensitized solar cell based on highly conducting and thermally stable PEDOT: PSS/glass counter electrode. *Organic Electronics*, 14(7), 1769-1776.

- Choi, H., Kim, H., Hwang, S., Choi, W., & Jeon, M. (2011). Dye-sensitized solar cells using graphene-based carbon nano composite as counter electrode. *Solar Energy Materials and Solar Cells*, 95(1), 323-325.
- Chong, M. Y., Numan, A., Liew, C. W., Ramesh, K., & Ramesh, S. (2017). Comparison of the performance of copper oxide and yttrium oxide nanoparticle based hydroxylethyl cellulose electrolytes for supercapacitors. *Journal of Applied Polymer Science*, 134(13).
- Chopra, K., Paulson, P., & Dutta, V. (2004). Thin-film solar cells: an overview. *Progress in Photovoltaics: Research and Applications*, 12(2-3), 69-92.
- Chu, S., & Majumdar, A. (2012). Opportunities and challenges for a sustainable energy future. *nature*, 488(7411), 294.
- Cogal, S., Ela, S. E., Cogal, G. C., Micusik, M., Omastova, M., & Oksuz, A. U. J. P. C. (2018). Plasma-enhanced modification of multiwalled carbon nanotube with conducting polymers for dye sensitized solar cells. 39(3), 668-674.
- Conibeer, G. (2007). Third-generation photovoltaics. *Materials today*, 10(11), 42-50.
- Costa, R. D., Lodermeier, F., Casillas, R., & Guldi, D. M. (2014). Recent advances in multifunctional nanocarbons used in dye-sensitized solar cells. *Energy & Environmental Science*, 7(4), 1281-1296.
- Dai, X., Li, A., Wu, F., & Xie, A. (2016). Solid-state synthesis of a conducting polythiophene as efficient Pt-free thin film counter electrode for dye-sensitized solar cells. *Materials Letters*, 174, 91-94.
- Das, S., Sudhagar, P., Nagarajan, S., Ito, E., Lee, S. Y., Kang, Y. S., & Choi, W. (2012). Synthesis of graphene-CoS electro-catalytic electrodes for dye sensitized solar cells. *Carbon*, 50(13), 4815-4821.
- Dickerson, J. H., & Boccaccini, A. R. (2011). *Electrophoretic deposition of nanomaterials*: Springer.
- Du, F., Yang, Q., Qin, T., & Li, G. (2017). Morphology-controlled growth of NiCo₂O₄ ternary oxides and their application in dye-sensitized solar cells as counter electrodes. *Solar Energy*, 146, 125-130.
- Duraisamy, N., Numan, A., Fatin, S. O., Ramesh, K., & Ramesh, S. (2016). Facile sonochemical synthesis of nanostructured NiO with different particle sizes and its electrochemical properties for supercapacitor application. *Journal of colloid and interface science*, 471, 136-144.

- Edmonds, J., & Reilly, J. (1983). A long-term global energy-economic model of carbon dioxide release from fossil fuel use. *Energy Economics*, 5(2), 74-88.
- Fakharuddin, A., Jose, R., Brown, T. M., Fabregat-Santiago, F., & Bisquert, J. (2014). A perspective on the production of dye-sensitized solar modules. *Energy & Environmental Science*, 7(12), 3952-3981.
- Faraday, M. (1834). VI. Experimental researches in electricity.—Sixth series. *Philosophical Transactions of the Royal Society of London*, 124, 77-122.
- Feihl, S., & Costa, R. (2012). S. Pock, C. Schmidt, J. Schönamsgruber, S. Backes, A. Hirsch and DM Guldi. *RSC Adv*, 2, 11495-11503.
- Ghasemi, S., Hosseini, S. R., & Kazemi, Z. (2017). Electrochemical deposition of Pt-Ni on reduced graphene oxide as counter electrode material for dye-sensitized solar cell. *Journal of Photochemistry and Photobiology A: Chemistry*, 348, 263-268.
- Gong, H. H., Hong, S. B., & Hong, S. C. (2014). Dispersion controlled platinum/multi-walled carbon nanotube hybrid for counter electrodes of dye-sensitized solar cells. *Macromolecular Research*, 22(4), 397-404.
- Grätzel, M. (2001). Photoelectrochemical cells. *nature*, 414(6861), 338.
- Grätzel, M. (2003). Dye-sensitized solar cells. *Journal of Photochemistry and Photobiology C: Photochemistry Reviews*, 4(2), 145-153.
- Green, M. (2004). Recent developments in photovoltaics. *Solar Energy*, 76(1-3), 3-8.
- Green, M. A. (1990). *Photovoltaics: coming of age*. Paper presented at the Photovoltaic Specialists Conference, 1990., Conference Record of the Twenty First IEEE.
- Green, M. A. (2001). Third generation photovoltaics: Ultra-high conversion efficiency at low cost. *Progress in Photovoltaics: Research and Applications*, 9(2), 123-135.
- Green, M. A. (2007). Thin-film solar cells: review of materials, technologies and commercial status. *Journal of Materials Science: Materials in Electronics*, 18(1), 15-19.
- Green, M. A., Emery, K., Hishikawa, Y., Warta, W., & Dunlop, E. D. (2015). Solar cell efficiency tables (Version 45). *Progress in Photovoltaics: Research and Applications*, 23(1), 1-9.

- Green, M. A., Hishikawa, Y., Dunlop, E. D., Levi, D. H., Hohl-Ebinger, J., & Ho-Baillie, A. W. Y. (2018). Solar cell efficiency tables (version 51). *Progress in Photovoltaics: Research and Applications*, 26(1), 3-12. doi:10.1002/pip.2978
- Gu, X., Yang, Y., Hu, Y., Hu, M., Huang, J., & Wang, C. J. J. o. M. C. A. (2015). Facile fabrication of graphene–polypyrrole–Mn composites as high-performance electrodes for capacitive deionization. 3(11), 5866-5874.
- Guo, M., Yao, Y., Zhao, F., Wang, S., Wang, D., Yin, S., Xiao, J. (2017). An In₂S₃@conductive carbon composite with superior electrocatalytic activity for dye-sensitized solar cells. *Journal of Photochemistry and Photobiology A: Chemistry*, 332, 87-91.
- Hagfeldt, A., Boschloo, G., Sun, L., Kloo, L., & Pettersson, H. (2010). Dye-sensitized solar cells. *Chemical reviews*, 110(11), 6595-6663.
- Halme, J. (2002). Dye-sensitized nanostructured and organic photovoltaic cells: technical review and preliminary tests. *Department of Engineering Physics and Mathematics*, 115.
- Hashmi, G., Miettunen, K., Peltola, T., Halme, J., Asghar, I., Aitola, K., . . . Lund, P. (2011). Review of materials and manufacturing options for large area flexible dye solar cells. *Renewable and Sustainable Energy Reviews*, 15(8), 3717-3732.
- He, J., Lee, L. T. L., Yang, S., Li, Q., Xiao, X., & Chen, T. (2014). Printable highly catalytic Pt-and TCO-Free counter electrode for dye-sensitized solar cells. *ACS applied materials & interfaces*, 6(4), 2224-2229.
- He, J., Pringle, J. M., & Cheng, Y.-B. (2014). Titanium carbide and titanium nitride-based nanocomposites as efficient catalysts for the Co²⁺/Co³⁺ redox couple in dye-sensitized solar cells. *The Journal of Physical Chemistry C*, 118(30), 16818-16824.
- He, Q., Qian, T., Zai, J., Qiao, Q., Huang, S., Li, Y., & Wang, M. (2015). Efficient Ag₈GeS₆ counter electrode prepared from nanocrystal ink for dye-sensitized solar cells. *Journal of Materials Chemistry A*, 3(40), 20359-20365.
- Herzog, H., & Golomb, D. (2004). Carbon capture and storage from fossil fuel use. *Encyclopedia of energy*, 1(6562), 277-287.
- Hou, W., Xiao, Y., Han, G., Fu, D., & Wu, R. (2016). Serrated, flexible and ultrathin polyaniline nanoribbons: An efficient counter electrode for the dye-sensitized solar cell. *Journal of Power Sources*, 322, 155-162.

- Hou, W., Xiao, Y., Han, G., & Zhou, H. (2016). Electro-polymerization of polypyrrole/multi-wall carbon nanotube counter electrodes for use in platinum-free dye-sensitized solar cells. *Electrochimica Acta*, *190*, 720-728.
- Hou, Y., Chen, Z. P., Wang, D., Zhang, B., Yang, S., Wang, H. F., . . . Yang, H. G. (2014). Highly Electrocatalytic Activity of RuO₂ Nanocrystals for Triiodide Reduction in Dye-Sensitized Solar Cells. *Small*, *10*(3), 484-492.
- Hou, Y., Wang, D., Yang, X. H., Fang, W. Q., Zhang, B., Wang, H. F., Yang, H. G. (2013). Rational screening low-cost counter electrodes for dye-sensitized solar cells. *Nature communications*, *4*, 1583.
- Huang, M., Yang, H., Wu, J., Lin, J., Lan, Z., Li, P., Jiang, Q. (2007). Preparation of a novel polymer gel electrolyte based on N-methyl-quinoline iodide and its application in quasi-solid-state dye-sensitized solar cell. *Journal of sol-gel science and technology*, *42*(1), 65-70.
- Huang, S.-T., Lee, W. W., Chang, J.-L., Huang, W.-S., Chou, S.-Y., & Chen, C.-C. J. J. o. t. T. I. o. C. E. (2014). Hydrothermal synthesis of SrTiO₃ nanocubes: Characterization, photocatalytic activities, and degradation pathway. *45*(4), 1927-1936.
- Huang, S., Yang, Z., Zhang, L., He, R., Chen, T., Cai, Z., Zhu, X. (2012). A novel fabrication of a well distributed and aligned carbon nanotube film electrode for dye-sensitized solar cells. *Journal of Materials Chemistry*, *22*(33), 16833-16838.
- Huang, X., Shen, P., Zhao, B., Feng, X., Jiang, S., Chen, H., Cells, S. (2010). Stainless steel mesh-based flexible quasi-solid dye-sensitized solar cells. *94*(6), 1005-1010.
- Huo, J., Wu, J., Zheng, M., Tu, Y., & Lan, Z. (2015). High performance sponge-like cobalt sulfide/reduced graphene oxide hybrid counter electrode for dye-sensitized solar cells. *Journal of Power Sources*, *293*, 570-576.
- Huo, J., Wu, J., Zheng, M., Tu, Y., & Lan, Z. (2016). A transparent cobalt sulfide/reduced graphene oxide nanostructure counter electrode for high efficient dye-sensitized solar cells. *Electrochimica Acta*, *187*, 210-217.
- Jang, J. S., Ham, D. J., Ramasamy, E., Lee, J., & Lee, J. S. (2010). Platinum-free tungsten carbides as an efficient counter electrode for dye sensitized solar cells. *Chemical Communications*, *46*(45), 8600-8602.
- Jena, A., Mohanty, S. P., Kumar, P., Naduvath, J., Gondane, V., Lekha, P., Bhargava, P. (2012). Dye sensitized solar cells: a review. *Transactions of the Indian Ceramic Society*, *71*(1), 1-16.

- Jeon, S. S., Kim, C., Ko, J., & Im, S. S. (2011). Spherical polypyrrole nanoparticles as a highly efficient counter electrode for dye-sensitized solar cells. *Journal of Materials Chemistry*, 21(22), 8146-8151.
- Jha, P., Veerender, P., Koiry, S., Sridevi, C., Chabbi, P., Samanta, S., Gadkari, S. (2017). *Freestanding polypyrrole films as counter electrode for low cost dye sensitized solar cells*. Paper presented at the AIP Conference Proceedings.
- Jia, J., Wu, J., Dong, J., & Lin, J. (2015). Cobalt telluride/reduced graphene oxide using as high performance counter electrode for dye-sensitized solar cells. *Electrochimica Acta*, 185, 184-189.
- Johansson, T. B., Reddy, A. K., Kelly, H., Williams, R. H., & Burnham, L. (1993). *Renewable energy: sources for fuels and electricity*: Island press.
- Kakiage, K., Aoyama, Y., Yano, T., Otsuka, T., Kyomen, T., Unno, M., & Hanaya, M. (2014). An achievement of over 12 percent efficiency in an organic dye-sensitized solar cell. *Chemical Communications*, 50(48), 6379-6381.
- Kang, E., Neoh, K., & Tan, K. (1998). Polyaniline: a polymer with many interesting intrinsic redox states. *Progress in Polymer Science*, 23(2), 277-324.
- Kay, A., & Grätzel, M. (1996). Low cost photovoltaic modules based on dye sensitized nanocrystalline titanium dioxide and carbon powder. *Solar Energy Materials and Solar Cells*, 44(1), 99-117.
- Kelly, C. A., & Meyer, G. J. (2001). Excited state processes at sensitized nanocrystalline thin film semiconductor interfaces. *Coordination Chemistry Reviews*, 211(1), 295-315.
- Kim, B.-K., & White, L. (2012). Who Drives the PV Industry? The Road to a Sustainable Industry. *Journal of Nanoelectronics and Optoelectronics*, 7(5), 454-459.
- Kim, H., Choi, H., Hwang, S., Kim, Y., & Jeon, M. (2012). Fabrication and characterization of carbon-based counter electrodes prepared by electrophoretic deposition for dye-sensitized solar cells. *Nanoscale research letters*, 7(1), 53.
- Kim, K. S., Song, H., Nam, S. H., Kim, S. M., Jeong, H., Kim, W. B., & Jung, G. Y. (2012). Fabrication of an Efficient Light-Scattering Functionalized Photoanode Using Periodically Aligned ZnO Hemisphere Crystals for Dye-Sensitized Solar Cells. *Advanced Materials*, 24(6), 792-798.

- Kim, S.-J., Ko, H.-S., Jeong, G.-H., Park, K.-H., Yun, J.-J., & Han, E.-M. (2014). Fabrication and characterization of reduced graphene oxide counter electrode for dye-sensitized solar cells. *Molecular Crystals and Liquid Crystals*, 598(1), 1-5.
- Ko, A.-R., Oh, J.-K., Lee, Y.-W., Han, S.-B., & Park, K.-W. (2011). Characterizations of tungsten carbide as a non-Pt counter electrode in dye-sensitized solar cells. *Materials Letters*, 65(14), 2220-2223.
- Kouhnavard, M., Ludin, N. A., Ghaffari, B. V., Ikeda, S., Sopian, K., & Miyake, M. (2016). Hydrophilic carbon/TiO₂ colloid composite: a potential counter electrode for dye-sensitized solar cells. *Journal of Applied Electrochemistry*, 46(2), 259-266.
- Kouhnavard, M., Ludin, N. A., Ghaffari, B. V., Sopian, K., & Ikeda, S. (2015). Carbonaceous Materials and Their Advances as a Counter Electrode in Dye-Sensitized Solar Cells: Challenges and Prospects. *ChemSusChem*, 8(9), 1510-1533.
- Krebs, F. C., Gevorgyan, S. A., Gholamkhash, B., Holdcroft, S., Schlenker, C., Thompson, M. E., Cells, S. (2009). A round robin study of flexible large-area roll-to-roll processed polymer solar cell modules. 93(11), 1968-1977.
- Kuliček, J., Gemeiner, P., Omastová, M., & Mičušík, M. J. C. P. (2018). Preparation of polypyrrole/multi-walled carbon nanotube hybrids by electropolymerization combined with a coating method for counter electrodes in dye-sensitized solar cells. 1-17.
- Lan, Z., Que, L., Wu, W., & Wu, J. (2016). High-performance Pt-NiO nanosheet-based counter electrodes for dye-sensitized solar cells. *Journal of Solid State Electrochemistry*, 20(3), 759-766.
- Lan, Z., Wu, J., Lin, J., & Huang, M. (2012). Morphology controllable fabrication of Pt counter electrodes for highly efficient dye-sensitized solar cells. *Journal of Materials Chemistry*, 22(9), 3948-3954.
- Lau, S. C., Lim, H. N., Ravoof, T., Yaacob, M. H., Grant, D. M., MacKenzie, R. C. I., . . . Huang, N. M. (2017). A three-electrode integrated photo-supercapacitor utilizing graphene-based intermediate bifunctional electrode. *Electrochimica Acta*, 238, 178-184. doi:10.1016/j.electacta.2017.04.003
- Lee, B., He, J., Chang, R. P., & Kanatzidis, M. G. (2012). All-solid-state dye-sensitized solar cells with high efficiency. *nature*, 485(7399), 486.

- Lee, C.-P., Lai, K.-Y., Lin, C.-A., Li, C.-T., Ho, K.-C., Wu, C.-I., He, J.-H. (2017). A paper-based electrode using a graphene dot/PEDOT: PSS composite for flexible solar cells. *Nano Energy*, 36, 260-267.
- Lee, K.-M., Chiu, W.-H., Wei, H.-Y., Hu, C.-W., Suryanarayanan, V., Hsieh, W.-F., & Ho, K.-C. (2010). Effects of mesoscopic poly (3, 4-ethylenedioxythiophene) films as counter electrodes for dye-sensitized solar cells. *Thin Solid Films*, 518(6), 1716-1721.
- Lee, W. J., Ramasamy, E., Lee, D. Y., & Song, J. S. (2008). Performance variation of carbon counter electrode based dye-sensitized solar cell. *Solar Energy Materials and Solar Cells*, 92(7), 814-818.
- Li, C.-T., Lee, C.-P., Li, Y.-Y., Yeh, M.-H., & Ho, K.-C. (2013). A composite film of TiS₂/PEDOT: PSS as the electrocatalyst for the counter electrode in dye-sensitized solar cells. *Journal of Materials Chemistry A*, 1(47), 14888-14896.
- Li, C.-T., Tsai, Y.-L., & Ho, K.-C. (2016). Earth Abundant Silicon Composites as the Electrocatalytic Counter Electrodes for Dye-Sensitized Solar Cells. *ACS applied materials & interfaces*, 8(11), 7037-7046.
- Li, G. r., Wang, F., Jiang, Q. w., Gao, X. p., & Shen, P. w. (2010). Carbon Nanotubes with Titanium Nitride as a Low-Cost Counter-Electrode Material for Dye-Sensitized Solar Cells. *Angewandte Chemie International Edition*, 49(21), 3653-3656.
- Li, H., Xiao, Y., Han, G., & Hou, W. (2017). Honeycomb-like poly (3, 4-ethylenedioxythiophene) as an effective and transparent counter electrode in bifacial dye-sensitized solar cells. *Journal of Power Sources*, 342, 709-716.
- Li, H., Xiao, Y., Han, G., & Li, M. (2017). Honeycomb-like polypyrrole/multi-wall carbon nanotube films as an effective counter electrode in bifacial dye-sensitized solar cells. *Journal of Materials Science*, 52(14), 8421-8431.
- Li, P., Cai, H., Tang, Q., He, B., & Lin, L. (2014). Counter electrodes from binary ruthenium selenide alloys for dye-sensitized solar cells. *Journal of Power Sources*, 271, 108-113.
- Li, Q., Wu, J., Tang, Q., Hao, S., Xiao, Y., Lin, J., & Huang, M. J. M. R. I. (2010). Low cost method to obtain counter electrode for dye sensitised solar cells. *14*(5), 410-413.
- Li, Q., Wu, J., Tang, Q., Lan, Z., Li, P., Lin, J., & Fan, L. (2008a). Application of microporous polyaniline counter electrode for dye-sensitized solar cells. *Electrochemistry Communications*, 10(9), 1299-1302.

- Li, Q., Wu, J., Tang, Q., Lan, Z., Li, P., Lin, J., & Fan, L. J. E. C. (2008b). Application of microporous polyaniline counter electrode for dye-sensitized solar cells. *10*(9), 1299-1302.
- Li, R., Tang, Q., Yu, L., Yan, X., Zhang, Z., & Yang, P. (2016). Counter electrodes from conducting polymer intercalated graphene for dye-sensitized solar cells. *Journal of Power Sources*, *309*, 231-237.
- Li, Y., Wang, H., Feng, Q., Zhou, G., & Wang, Z.-S. (2013). Reduced graphene oxide-TaON composite as a high-performance counter electrode for Co (bpy) $33+/2+$ -mediated dye-sensitized solar cells. *ACS applied materials & interfaces*, *5*(16), 8217-8224.
- Li, Z., Gong, F., Zhou, G., & Wang, Z.-S. (2013). NiS₂/reduced graphene oxide nanocomposites for efficient dye-sensitized solar cells. *The Journal of Physical Chemistry C*, *117*(13), 6561-6566.
- Li, Z., Xu, J., Chen, L., Zhang, R., Yang, X., & Xia, J. (2017). Influence of Sheet Resistance Effect on Poly (3, 4-ethylenedioxythiophene) Counter Electrode for Dye-Sensitized Solar Cell. *Electrochimica Acta*, *242*, 219-226.
- Liang, L., Chen, G., & Guo, C.-Y. J. M. C. F. (2017). Polypyrrole nanostructures and their thermoelectric performance. *1*(2), 380-386.
- Liang, X., Wen, Z., Liu, Y., Wang, X., Zhang, H., Wu, M., & Huang, L. J. S. S. I. (2011). Preparation and characterization of sulfur-polypyrrole composites with controlled morphology as high capacity cathode for lithium batteries. *192*(1), 347-350.
- Lim, S. P., Pandikumar, A., Lim, Y. S., Huang, N. M., & Lim, H. N. J. S. r. (2014). In-situ electrochemically deposited polypyrrole nanoparticles incorporated reduced graphene oxide as an efficient counter electrode for platinum-free dye-sensitized solar cells. *4*, 5305.
- Lin, C.-H., Tsai, C.-H., Tseng, F.-G., Ma, C.-C. M., Wu, H.-C., & Hsieh, C.-K. (2017). Three-dimensional vertically aligned hybrid nanoarchitecture of two-dimensional molybdenum disulfide nanosheets anchored on directly grown one-dimensional carbon nanotubes for use as a counter electrode in dye-sensitized solar cells. *Journal of Alloys and Compounds*, *692*, 941-949.
- Lin, X., Wu, M., Wang, Y., Hagfeldt, A., & Ma, T. (2011). Novel counter electrode catalysts of niobium oxides supersede Pt for dye-sensitized solar cells. *Chemical Communications*, *47*(41), 11489-11491.

- Liu, J., Tang, Q., He, B., & Yu, L. (2015). Cost-effective bifacial dye-sensitized solar cells with transparent iron selenide counter electrodes. An avenue of enhancing rear-side electricity generation capability. *Journal of Power Sources*, 275, 288-293.
- Longo, C., & De Paoli, M.-A. (2003). Dye-sensitized solar cells: a successful combination of materials. *Journal of the Brazilian Chemical Society*, 14(6), 898-901.
- Lukaszkoicz, K., Szindler, M., Drygała, A., Dobrzański, L. A., & Prokopowicz, M. P., Pasternak, I., . . . Domański, M. (2017). Graphene-based layers deposited onto flexible substrates: Used in dye-sensitized solar cells as counter electrodes. *Applied Surface Science*, 424, 157-163.
- Luo, Y., Cheng, R., Shen, J., Chen, X., Lu, Z., Chen, Y., Huang, S. (2014). Plasma-modified SnO₂: F substrate for efficient cobalt selenide counter in dye sensitized solar cell. *RSC Advances*, 4(85), 44896-44901.
- Luo, Y., Shen, J., Cheng, R., Chen, X., Chen, Y., Sun, Z., & Huang, S. (2015). Facile synthesis of mixed-phase cobalt sulfide counter electrodes for efficient dye sensitized solar cells. *Journal of Materials Science: Materials in Electronics*, 26(1), 42-48.
- Ma, J., Qingfeng, S., Fengbao, Z., & Mingxing, W. (2017). Improvement on the catalytic activity of the flexible PEDOT counter electrode in dye-sensitized solar cells. *Materials Research Bulletin*.
- Maiaugree, W., Pimparue, P., Jarernboon, W., Pimanpang, S., Amornkitbamrung, V., & Swatsitang, E. (2017). NiS (NPs)-PEDOT-PSS composite counter electrode for a high efficiency dye sensitized solar cell. *Materials Science and Engineering: B*, 220, 66-72.
- Masuda, H., & Fukuda, K. (1995). Ordered metal nanohole arrays made by a two-step replication of honeycomb structures of anodic alumina. *science*, 268(5216), 1466-1468.
- Mehmood, U. (2017). Efficient and economical dye-sensitized solar cells based on graphene/TiO₂ nanocomposite as a photoanode and graphene as a Pt-free catalyst for counter electrode. *Organic Electronics*, 42, 187-193.
- Memon, A. A., Arbab, A. A., Sahito, I. A., Sun, K. C., Mengal, N., & Jeong, S. H. (2017). Synthesis of highly photo-catalytic and electro-catalytic active textile structured carbon electrode and its application in DSSCs. *Solar Energy*, 150, 521-531.

- Mengal, N., Arbab, A. A., Memon, A. A., Sahito, I. A., & Jeong, S. H. (2017). A promising hybrid graphite counter electrode doped with fumed silica nano-spacers for efficient quasi-solid state dye sensitized solar cells. *Electrochimica Acta*.
- Meyer, G. J. (1997). Efficient light-to-electrical energy conversion: nanocrystalline TiO₂ films modified with inorganic sensitizers. In: ACS Publications.
- Miao, X., Pan, K., Pan, Q., Zhou, W., Wang, L., Liao, Y., Wang, G. (2013). Highly crystalline graphene/carbon black composite counter electrodes with controllable content: Synthesis, characterization and application in dye-sensitized solar cells. *Electrochimica Acta*, 96, 155-163.
- Morey, G. W., & Niggli, P. (1913). The hydrothermal formation of silicates, a review. *Journal of the American Chemical Society*, 35(9), 1086-1130.
- Mozaffari, S., & Nateghi, M. R. (2014). Effects of multi anchoring groups of catecholamine polymer dyes on the electrical characteristics of metal free dye-sensitized solar cells: a comparison study. *Solar Energy*, 106, 63-71.
- Mozaffari, S., Nateghi, M. R., & Zarandi, M. B. (2017). An overview of the Challenges in the commercialization of dye sensitized solar cells. *Renewable and Sustainable Energy Reviews*, 71, 675-686.
- Murakami, T. N., Ito, S., Wang, Q., Nazeeruddin, M. K., Bessho, T., Cesar, I., Péchy, P. (2006). Highly efficient dye-sensitized solar cells based on carbon black counter electrodes. *Journal of the Electrochemical Society*, 153(12), A2255-A2261.
- Muthuraaman, B., Ganesan, S., Paul, B. J., Maruthamuthu, P., & Suthanthiraraj, S. A. (2011). Studies on isomeric effects of 2-and 4-Mercapto pyridine as dopants in polymer electrolyte in dye-sensitized solar cells. *Electrochimica Acta*, 56(15), 5405-5409.
- Muthusamy, S., Charles, J., Renganathan, B., & Sastikumar, D. J. J. o. m. s. (2018). In situ growth of Prussian blue nanocubes on polypyrrole nanoparticles: facile synthesis, characterization and their application as fiber optic gas sensor. 53(22), 15401-15417.
- Muto, T., Ikegami, M., & Miyasaka, T. (2010). Polythiophene-based mesoporous counter electrodes for plastic dye-sensitized solar cells. *Journal of the Electrochemical Society*, 157(8), B1195-B1200.
- Mutta, G. R., Popuri, S. R., Vasundhara, M., Maciejczyk, M., Racu, A. V., Banica, R., . . . Bennett, N. S. (2016). Facile hydrothermal synthesis of economically viable VO₂ (M1) counter electrode for dye sensitized solar cells. *Materials Research Bulletin*, 83, 135-140.

- Nadiah, N., Omar, F. S., Numan, A., Mahipal, Y., Ramesh, S., & Ramesh, K. (2017). Influence of acrylic acid on ethylene carbonate/dimethyl carbonate based liquid electrolyte and its supercapacitor application. *International Journal of Hydrogen Energy*, 42(52), 30683-30690.
- Nakashima, K., Kera, M., Fujii, I., & Wada, S. J. C. I. (2013). A new approach for the preparation of SrTiO₃ nanocubes. 39(3), 3231-3234.
- Nazeeruddin, M. K., De Angelis, F., Fantacci, S., Selloni, A., Viscardi, G., Liska, P., . . . Grätzel, M. (2005). Combined experimental and DFT-TDDFT computational study of photoelectrochemical cell ruthenium sensitizers. *Journal of the American Chemical Society*, 127(48), 16835-16847.
- Niu, H., Qin, S., Mao, X., Zhang, S., Wang, R., Wan, L., Miao, S. (2014). Axle-sleeve structured MWCNTs/polyaniline composite film as cost-effective counter-electrodes for high efficient dye-sensitized solar cells. *Electrochimica Acta*, 121, 285-293.
- Numan, A., Duraisamy, N., Omar, F. S., Gopi, D., Ramesh, K., & Ramesh, S. (2017). Sonochemical synthesis of nanostructured nickel hydroxide as an electrode material for improved electrochemical energy storage application. *Progress in Natural Science: Materials International*, 27(4), 416-423.
- Numan, A., Duraisamy, N., Omar, F. S., Mahipal, Y., Ramesh, K., & Ramesh, S. (2016). Enhanced electrochemical performance of cobalt oxide nanocube intercalated reduced graphene oxide for supercapacitor application. *RSC Advances*, 6(41), 34894-34902.
- Numan, A., Shahid, M. M., Omar, F. S., Rafique, S., Bashir, S., Ramesh, K., & Ramesh, S. (2017). Binary nanocomposite based on Co₃O₄ nanocubes and multiwalled carbon nanotubes as an ultrasensitive platform for amperometric determination of dopamine. *Microchimica Acta*, 184(8), 2739-2748.
- O'Brian, N., Grübler, A., Nakicenovic, N., Obersteiner, M., Riahi, K., Schrattenholzer, L., & Toth, F. (2003). Planning for future energy resources. *Science*, 300(5619), 581-584.
- Omar, F. S., Numan, A., Duraisamy, N., Bashir, S., Ramesh, K., & Ramesh, S. (2016). Ultrahigh capacitance of amorphous nickel phosphate for asymmetric supercapacitor applications. *RSC Advances*, 6(80), 76298-76306.
- Omar, F. S., Numan, A., Duraisamy, N., Bashir, S., Ramesh, K., & Ramesh, S. (2017). A promising binary nanocomposite of zinc cobaltite intercalated with polyaniline for supercapacitor and hydrazine sensor. *Journal of Alloys and Compounds*, 716, 96-105.

- Omar, F. S., Numan, A., Duraisamy, N., Ramly, M. M., Ramesh, K., & Ramesh, S. (2017). Binary composite of polyaniline/copper cobaltite for high performance asymmetric supercapacitor application. *Electrochimica Acta*, 227, 41-48.
- Pan, J., Wang, L., Jimmy, C. Y., Liu, G., & Cheng, H.-M. (2014). A nonstoichiometric SnO_{2-δ} nanocrystal-based counter electrode for remarkably improving the performance of dye-sensitized solar cells. *Chemical Communications*, 50(53), 7020-7023.
- Pandey, A., Ahmad, M. S., Alizadeh, M., & Rahim, N. A. (2018). Improved electron density through hetero-junction binary sensitized TiO₂/CdTe/D719 system as photoanode for dye sensitized solar cell. *Physica E: Low-dimensional Systems and Nanostructures*, 101, 139-143.
- Pandikumar, A., Lim, S.-P., Jayabal, S., Huang, N. M., Lim, H. N., & Ramaraj, R. (2016). Titania@ gold plasmonic nanoarchitectures: An ideal photoanode for dye-sensitized solar cells. *Renewable and Sustainable Energy Reviews*, 60, 408-420.
- Panwar, N., Kaushik, S., & Kothari, S. (2011). Role of renewable energy sources in environmental protection: a review. *Renewable and Sustainable Energy Reviews*, 15(3), 1513-1524.
- Park, B.-w., Pazoki, M., Aitola, K., Jeong, S., Johansson, E. M., Hagfeldt, A., & Boschloo, G. (2014). Understanding interfacial charge transfer between metallic PEDOT counter electrodes and a cobalt redox shuttle in dye-sensitized solar cells. *ACS applied materials & interfaces*, 6(3), 2074-2079.
- Park, S.-H., Jung, H.-R., Kim, B.-K., & Lee, W.-J. (2012). MWCNT/mesoporous carbon nanofibers composites prepared by electrospinning and silica template as counter electrodes for dye-sensitized solar cells. *Journal of Photochemistry and Photobiology A: Chemistry*, 246, 45-49.
- Park, S. H., Cho, Y.-H., Choi, M., Choi, H., Kang, J. S., Um, J. H., Sung, Y.-E. (2014). Nickel-nitride-coated nickel foam as a counter electrode for dye-sensitized solar cells. *Surface and Coatings Technology*, 259, 560-569.
- Patil, S. A., Kim, E.-K., Shrestha, N. K., Chang, J., Lee, J. K., & Han, S.-H. (2015). Formation of semimetallic cobalt telluride nanotube film via anion exchange tellurization strategy in aqueous solution for electrocatalytic applications. *ACS applied materials & interfaces*, 7(46), 25914-25922.
- Peng, S., Tian, L., Liang, J., Mhaisalkar, S. G., & Ramakrishna, S. (2011). Polypyrrole nanorod networks/carbon nanoparticles composite counter electrodes for high-efficiency dye-sensitized solar cells. *ACS applied materials & interfaces*, 4(1), 397-404.

- Pierson, H. O. (1999). *Handbook of chemical vapor deposition: principles, technology and applications*: William Andrew.
- Polman, A., Knight, M., Garnett, E. C., Ehrler, B., & Sinke, W. C. (2016). Photovoltaic materials: Present efficiencies and future challenges. *Science*, 352(6283), aad4424.
- PVPS, I. (2017). Snapshot of Global Photovoltaic Markets. *Report IEA PVPS T1-31*.
- Qian, X., Li, H., Shao, L., Jiang, X., & Hou, L. (2016). Morphology-tuned synthesis of nickel cobalt selenides as highly efficient Pt-free counter electrode catalysts for dye-sensitized solar cells. *ACS applied materials & interfaces*, 8(43), 29486-29495.
- Rafique, S., Abdullah, S. M., Shahid, M. M., Ansari, M. O., & Sulaiman, K. (2017). Significantly improved photovoltaic performance in polymer bulk heterojunction solar cells with graphene oxide/PEDOT: PSS double decked hole transport layer. *Scientific reports*, 7, 39555.
- Raj, C. C., & Prasanth, R. (2016). A critical review of recent developments in nanomaterials for photoelectrodes in dye sensitized solar cells. *Journal of Power Sources*, 317, 120-132.
- Ravve, A. (2013). *Principles of polymer chemistry*: Springer Science & Business Media.
- Ren, N., & Tang, Y. (2005). Template-induced assembly of hierarchically ordered zeolite materials. *Petrochemical Technology*, 34(5), 405-411.
- Sayama, K., Sugihara, H., & Arakawa, H. (1998). Photoelectrochemical properties of a porous Nb₂O₅ electrode sensitized by a ruthenium dye. *Chemistry of Materials*, 10(12), 3825-3832.
- Sebastián, D., Baglio, V., Girolamo, M., Moliner, R., Lázaro, M., & Aricò, A. (2014). Carbon nanofiber-based counter electrodes for low cost dye-sensitized solar cells. *Journal of Power Sources*, 250, 242-249.
- Seo, H.-K., Song, M., Ameen, S., Akhtar, M. S., & Shin, H. S. (2013). New counter electrode of hot filament chemical vapor deposited graphene thin film for dye sensitized solar cell. *Chemical engineering journal*, 222, 464-471.
- Shahabuddin, S., Muhamad Sarih, N., Mohamad, S., & Joon Ching, J. J. P. (2016). SrTiO₃ nanocube-doped polyaniline nanocomposites with enhanced photocatalytic degradation of methylene blue under visible light. 8(2), 27.

- Shahabuddin, S., Sarih, N. M., Afzal Kamboh, M., Rashidi Nodeh, H., & Mohamad, S. J. P. (2016). Synthesis of polyaniline-coated graphene oxide@ SrTiO₃ nanocube nanocomposites for enhanced removal of carcinogenic dyes from aqueous solution. *8*(9), 305.
- Shahid, M. M., Rameshkumar, P., Basirun, W. J., Juan, J. C., & Huang, N. M. (2017). Cobalt oxide nanocubes interleaved reduced graphene oxide as an efficient electrocatalyst for oxygen reduction reaction in alkaline medium. *Electrochimica Acta*, *237*, 61-68.
- Shahid, M. M., Rameshkumar, P., & Huang, N. M. (2015). Morphology dependent electrocatalytic properties of hydrothermally synthesized cobalt oxide nanostructures. *Ceramics International*, *41*(10), 13210-13217.
- Shih, Y.-C., Lin, H.-L., & Lin, K.-F. (2017). Electropolymerized polyaniline/graphene nanoplatelet/multi-walled carbon nanotube composites as counter electrodes for high performance dye-sensitized solar cells. *Journal of Electroanalytical Chemistry*, *794*, 112-119.
- Song, D., Li, M., Li, Y., Zhao, X., Jiang, B., & Jiang, Y. (2014). Highly transparent and efficient counter electrode using SiO₂/PEDOT–PSS composite for bifacial dye-sensitized solar cells. *ACS applied materials & interfaces*, *6*(10), 7126-7132.
- Su'ait, M. S., Rahman, M. Y. A., & Ahmad, A. (2015). Review on polymer electrolyte in dye-sensitized solar cells (DSSCs). *Solar Energy*, *115*, 452-470.
- Sudhagar, P., Nagarajan, S., Lee, Y.-G., Song, D., Son, T., Cho, W., . . . Kang, Y. S. (2011). Synergistic catalytic effect of a composite (CoS/PEDOT: PSS) counter electrode on triiodide reduction in dye-sensitized solar cells. *ACS applied materials & interfaces*, *3*(6), 1838-1843.
- Sun, H., Luo, Y., Zhang, Y., Li, D., Yu, Z., Li, K., & Meng, Q. (2010). In situ preparation of a flexible polyaniline/carbon composite counter electrode and its application in dye-sensitized solar cells. *The Journal of Physical Chemistry C*, *114*(26), 11673-11679.
- Sun, P., Huang, T., Chen, Z., Tian, L., Huang, H., Huang, N., Sun, X. (2017). Solution Processed Ni_xS_y Films: Composition, Morphology and Crystallinity Tuning via Ni/S-Ratio-Control and Application in Dye-Sensitized Solar Cells. *Electrochimica Acta*, *246*, 285-293.
- Syed, S. (2016). Polyaniline based nanocomposites as adsorbents and photocatalysts in the removal of organic dyes/Syed Shahabuddin. University of Malaya,

- Tang, B., Hu, G., Gao, H., & Shi, Z. (2013). Three-dimensional graphene network assisted high performance dye sensitized solar cells. *Journal of Power Sources*, 234, 60-68.
- Tang, Q., Duan, J., Duan, Y., He, B., & Yu, L. (2015). Recent advances in alloy counter electrodes for dye-sensitized solar cells. A critical review. *Electrochimica Acta*, 178, 886-899.
- Tang, Z., Wu, J., Zheng, M., Huo, J., & Lan, Z. (2013). A microporous platinum counter electrode used in dye-sensitized solar cells. *Nano Energy*, 2(5), 622-627.
- Taş, R., Gülen, M., Can, M., & Sönmezoğlu, S. (2016). Effects of solvent and copper-doping on polyaniline conducting polymer and its application as a counter electrode for efficient and cost-effective dye-sensitized solar cells. *Synthetic Metals*, 212, 75-83.
- Theerthagiri, J., Senthil, A. R., Madhavan, J., & Maiyalagan, T. (2015). Recent Progress in Non-Platinum Counter Electrode Materials for Dye-Sensitized Solar Cells. *ChemElectroChem*, 2(7), 928-945.
- Trancik, J. E., Barton, S. C., & Hone, J. (2008). Transparent and catalytic carbon nanotube films. *Nano letters*, 8(4), 982-987.
- Tsai, C.-H., Fei, P.-H., Lin, C.-M., & Shiu, S.-L. (2018). CuO and CuO/Graphene Nanostructured Thin Films as Counter Electrodes for Pt-Free Dye-Sensitized Solar Cells. *Coatings*, 8(1), 21.
- Tsai, C.-H., Huang, W.-C., Hsu, Y.-C., Shih, C.-J., Teng, I.-J., & Yu, Y.-H. (2016). Poly (o-methoxyaniline) doped with an organic acid as cost-efficient counter electrodes for dye-sensitized solar cells. *Electrochimica Acta*, 213, 791-801.
- Veerappan, G., Bojan, K., & Rhee, S.-W. (2011). Sub-micrometer-sized graphite as a conducting and catalytic counter electrode for dye-sensitized solar cells. *ACS applied materials & interfaces*, 3(3), 857-862.
- Veerappan, G., Bojan, K., & Rhee, S.-W. (2012). Amorphous carbon as a flexible counter electrode for low cost and efficient dye sensitized solar cell. *Renewable Energy*, 41, 383-388.
- Wan, J., Fang, G., Yin, H., Liu, X., Liu, D., Zhao, M., Tang, Z. (2014). Pt-Ni Alloy nanoparticles as superior counter electrodes for dye-sensitized solar cells: Experimental and theoretical understanding. *Advanced Materials*, 26(48), 8101-8106.

- Wang, G., Dong, W., Yan, C., Hou, S., & Zhang, W. J. M. L. (2018). Facile synthesis of hierarchical nanostructured polypyrrole and its application in the counter electrode of dye-sensitized solar cells. *214*, 158-161.
- Wang, G., Kuang, S., Wang, D., & Zhuo, S. (2013). Nitrogen-doped mesoporous carbon as low-cost counter electrode for high-efficiency dye-sensitized solar cells. *Electrochimica Acta*, *113*, 346-353.
- Wang, G. Q., Dong, W. N., Ma, P., Yan, C., Zhang, W., & Liu, J. Q. (2018). Interconnected nitrogen and sulfur co-doped graphene-like porous carbon nanosheets with high electrocatalytic activity as counter electrodes for dye-sensitized and quantum dot-sensitized solar cells. *Electrochimica Acta*, *290*, 273-281. doi:10.1016/j.electacta.2018.09.063
- Wang, H., Sun, K., Tao, F., Stacchiola, D. J., & Hu, Y. H. (2013). 3D Honeycomb-Like Structured Graphene and Its High Efficiency as a Counter-Electrode Catalyst for Dye-Sensitized Solar Cells. *Angewandte Chemie*, *125*(35), 9380-9384.
- Wang, H., Wei, W., & Hu, Y. H. (2013). Efficient ZnO-based counter electrodes for dye-sensitized solar cells. *Journal of Materials Chemistry A*, *1*(22), 6622-6628.
- Wang, L., Liu, H., Konik, R. M., Misewich, J. A., & Wong, S. S. (2013). Carbon nanotube-based heterostructures for solar energy applications. *Chemical Society Reviews*, *42*(20), 8134-8156.
- Wang, L., Shi, Y., Wang, Y., Zhang, H., Zhou, H., Wei, Y., Ma, T. (2014). Composite catalyst of rosin carbon/Fe₃O₄: highly efficient counter electrode for dye-sensitized solar cells. *Chemical Communications*, *50*(14), 1701-1703.
- Wang, L., Shi, Y., Zhang, H., Bai, X., Wang, Y., & Ma, T. (2014). Iron oxide nanostructures as highly efficient heterogeneous catalysts for mesoscopic photovoltaics. *Journal of Materials Chemistry A*, *2*(37), 15279-15283.
- Wang, P., Zakeeruddin, S. M., Comte, P., Exnar, I., & Grätzel, M. (2003). Gelation of ionic liquid-based electrolytes with silica nanoparticles for quasi-solid-state dye-sensitized solar cells. *Journal of the American Chemical Society*, *125*(5), 1166-1167.
- Wang, Y., Zhao, C., Wu, M., Liu, W., & Ma, T. (2013). Highly efficient and low cost Pt-based binary and ternary composite catalysts as counter electrode for dye-sensitized solar cells. *Electrochimica Acta*, *105*, 671-676.
- Wei, Y.-S., Jin, Q.-Q., & Ren, T.-Z. (2011). Expanded graphite/pencil-lead as counter electrode for dye-sensitized solar cells. *Solid-State Electronics*, *63*(1), 76-82.

- Weinberg, S. (2003). *The discovery of subatomic particles revised edition*: Cambridge University Press.
- Wu, J., Lan, Z., Lin, J., Huang, M., Huang, Y., Fan, L., & Luo, G. (2015). Electrolytes in dye-sensitized solar cells. *Chemical reviews*, *115*(5), 2136-2173.
- Wu, J., Li, Q., Fan, L., Lan, Z., Li, P., Lin, J., & Hao, S. (2008a). High-performance polypyrrole nanoparticles counter electrode for dye-sensitized solar cells. *Journal of Power Sources*, *181*(1), 172-176.
- Wu, J., Li, Q., Fan, L., Lan, Z., Li, P., Lin, J., & Hao, S. J. J. o. P. S. (2008b). High-performance polypyrrole nanoparticles counter electrode for dye-sensitized solar cells. *181*(1), 172-176.
- Wu, J., Li, Y., Tang, Q., Yue, G., Lin, J., Huang, M., & Meng, L. (2014). Bifacial dye-sensitized solar cells: A strategy to enhance overall efficiency based on transparent polyaniline electrode. *Scientific reports*, *4*, 4028.
- Wu, M., Guo, H., Lin, Y.-n., Wu, K., Ma, T., & Hagfeldt, A. (2014). Synthesis of highly effective vanadium nitride (VN) peas as a counter electrode catalyst in dye-sensitized solar cells. *The Journal of Physical Chemistry C*, *118*(24), 12625-12631.
- Wu, M., Lin, X., Guo, W., Wang, Y., Chu, L., Ma, T., & Wu, K. (2013). Great improvement of catalytic activity of oxide counter electrodes fabricated in N₂ atmosphere for dye-sensitized solar cells. *Chemical Communications*, *49*(11), 1058-1060.
- Wu, M., Lin, X., Hagfeldt, A., & Ma, T. (2011a). Low-cost molybdenum carbide and tungsten carbide counter electrodes for dye-sensitized solar cells. *Angewandte Chemie*, *123*(15), 3582-3586.
- Wu, M., Lin, X., Hagfeldt, A., & Ma, T. (2011b). A novel catalyst of WO₂ nanorod for the counter electrode of dye-sensitized solar cells. *Chemical Communications*, *47*(15), 4535-4537.
- Wu, M., Lin, X., Wang, T., Qiu, J., & Ma, T. (2011). Low-cost dye-sensitized solar cell based on nine kinds of carbon counter electrodes. *Energy & Environmental Science*, *4*(6), 2308-2315.
- Wu, M., Lin, X., Wang, Y., Wang, L., Guo, W., Qi, D., . . . Ma, T. (2012). Economical Pt-free catalysts for counter electrodes of dye-sensitized solar cells. *Journal of the American Chemical Society*, *134*(7), 3419-3428.

- Xiao, Y., & Han, G. (2015). Efficient hydrothermal-processed platinum–nickel bimetallic nano-catalysts for use in dye-sensitized solar cells. *Journal of Power Sources*, 294, 8-15.
- Xiao, Y., & Han, G. (2016). High performance platinum nanofibers with interconnecting structure using in dye-sensitized solar cells. *Organic Electronics*, 37, 239-244.
- Xiao, Y., Han, G., Li, Y., Li, M., & Chang, Y. (2014). High performance of Pt-free dye-sensitized solar cells based on two-step electropolymerized polyaniline counter electrodes. *Journal of Materials Chemistry A*, 2(10), 3452-3460.
- Xiao, Y., Wu, J., Lin, J.-Y., Yue, G., Lin, J., Huang, M., Fan, L. (2013). A dual function of high performance counter-electrode for stable quasi-solid-state dye-sensitized solar cells. *Journal of Power Sources*, 241, 373-378.
- Xiao, Y., Wu, J., Yue, G., Lin, J., Huang, M., Fan, L., & Lan, Z. (2012). The surface treatment of Ti meshes for use in large-area flexible dye-sensitized solar cells. *Journal of Power Sources*, 208, 197-202.
- Xiao, Y., Wu, J., Yue, G., Lin, J., Huang, M., Lan, Z., & Fan, L. (2012). Electrodeposition of high performance PEDOT/Ti counter electrodes on Ti meshes for large-area flexible dye-sensitized solar cells. *Electrochimica Acta*, 85, 432-437.
- Xie, Y., Kocafe, D., Chen, C., & Kocafe, Y. (2016). Review of research on template methods in preparation of nanomaterials. *Journal of Nanomaterials*, 2016, 11.
- Xu, H., Zhang, C., Wang, Z., Pang, S., Zhou, X., Zhang, Z., & Cui, G. (2014). Nitrogen-doped carbon and iron carbide nanocomposites as cost-effective counter electrodes of dye-sensitized solar cells. *Journal of Materials Chemistry A*, 2(13), 4676-4681.
- Xu, H., Zhang, X., Zhang, C., Liu, Z., Zhou, X., Pang, S., Zhang, L. (2012). Nanostructured titanium nitride/PEDOT: PSS composite films as counter electrodes of dye-sensitized solar cells. *ACS applied materials & interfaces*, 4(2), 1087-1092.
- Xu, S.-j., Luo, Y.-f., Zhong, W., & Xiao, Z.-h. (2013). An efficient dye-sensitized solar cell using surfactant-modified mesoporous carbon film as a counter electrode. *New Carbon Materials*, 28(4), 254-260.
- Xu, S., Liu, C., & Wiezorek, J. (2018). 20 renewable biowastes derived carbon materials as green counter electrodes for dye-sensitized solar cells. *Materials Chemistry and Physics*, 204, 294-304.

- Xu, S., Luo, Y., & Zhong, W. (2011). Investigation of catalytic activity of glassy carbon with controlled crystallinity for counter electrode in dye-sensitized solar cells. *Solar Energy*, 85(11), 2826-2832.
- Yamaguchi, M., Takamoto, T., Araki, K., & Ekins-Daukes, N. J. S. E. (2005). Multi-junction III–V solar cells: current status and future potential. 79(1), 78-85.
- Yamaguchi, M., Takamoto, T., Araki, K. J. S. e. m., & cells, s. (2006). Super high-efficiency multi-junction and concentrator solar cells. 90(18-19), 3068-3077.
- Yeh, M. H., Lin, L. Y., Chang, L. Y., Leu, Y. A., Cheng, W. Y., Lin, J. J., & Ho, K. C. (2014). Dye-Sensitized Solar Cells with Reduced Graphene Oxide as the Counter Electrode Prepared by a Green Photothermal Reduction Process. *ChemPhysChem*, 15(6), 1175-1181.
- Yin, X., Wu, F., Fu, N., Han, J., Chen, D., Xu, P., . . . Lin, Y. (2013). Facile synthesis of poly (3, 4-ethylenedioxythiophene) film via solid-state polymerization as high-performance Pt-free counter electrodes for plastic dye-sensitized solar cells. *ACS applied materials & interfaces*, 5(17), 8423-8429.
- Yu, S., You, J. S., Yang, I. S., Kang, P., Rawal, S. B., Do Sung, S., & Lee, W. I. (2016). Tailoring of nanoporous TiO₂ spheres with 100–200 nm sizes for efficient dye-sensitized solar cells. *Journal of Power Sources*, 325, 7-14.
- Yue, G., Wang, L., Zhang, X. a., Wu, J., Jiang, Q., Zhang, W., Lin, J. (2014). Fabrication of high performance multi-walled carbon nanotubes/polypyrrole counter electrode for dye-sensitized solar cells. *Energy*, 67, 460-467.
- Yue, G., Wu, J., Xiao, Y., Lin, J., Huang, M., Fan, L., & Yao, Y. (2013). A dye-sensitized solar cell based on PEDOT: PSS counter electrode. *Chinese Science Bulletin*, 58(4-5), 559-566.
- Yue, G., Wu, J., Xiao, Y., Lin, J., Huang, M., & Lan, Z. (2012). Application of poly (3, 4-ethylenedioxythiophene): polystyrenesulfonate/polypyrrole counter electrode for dye-sensitized solar cells. *The Journal of Physical Chemistry C*, 116(34), 18057-18063.
- Yue, G. T., Li, P., Li, F. M., & Chen, C. (2016). Nickel sulfide counter electrode modified with polypyrrole nanoparticles to enhance catalytic ability for flexible dye-sensitized solar cells. *Rsc Advances*, 6(66), 61278-61283. doi:10.1039/c6ra10585h
- Yun, S., Wang, L., Guo, W., & Ma, T. (2012). Non-Pt counter electrode catalysts using tantalum oxide for low-cost dye-sensitized solar cells. *Electrochemistry Communications*, 24, 69-73.

- Zhai, P., Wei, T. C., Chang, Y. H., Huang, Y. T., Yeh, W. T., Su, H., & Feng, S. P. (2014). High Electrocatalytic and Wettable Nitrogen-Doped Microwave-Exfoliated Graphene Nanosheets as Counter Electrode for Dye-Sensitized Solar Cells. *Small*, *10*(16), 3347-3353.
- Zhang, D., Li, X., Li, H., Chen, S., Sun, Z., Yin, X., & Huang, S. (2011). Graphene-based counter electrode for dye-sensitized solar cells. *Carbon*, *49*(15), 5382-5388.
- Zhang, S., Dong, G.-Y., Lin, B., Qu, J., Yuan, N.-Y., Ding, J.-N., & Gu, Z. (2016). Performance enhancement of aqueous dye-sensitized solar cells via introduction of a quasi-solid-state electrolyte with an inverse opal structure. *Solar Energy*, *127*, 19-27.
- Zhang, X., Chen, X., Zhang, K., Pang, S., Zhou, X., Xu, H., Zhang, C. (2013). Transition-metal nitride nanoparticles embedded in N-doped reduced graphene oxide: superior synergistic electrocatalytic materials for the counter electrodes of dye-sensitized solar cells. *Journal of Materials Chemistry A*, *1*(10), 3340-3346.
- Zheng, X., Deng, J., Wang, N., Deng, D., Zhang, W. H., Bao, X., & Li, C. (2014). Podlike N-Doped Carbon Nanotubes Encapsulating FeNi Alloy Nanoparticles: High-Performance Counter Electrode Materials for Dye-Sensitized Solar Cells. *Angewandte Chemie International Edition*, *53*(27), 7023-7027.
- Zhong, J., Peng, Y., Zhou, M., Zhao, J., Liang, S., Wang, H., & Cheng, Y.-B. (2014). Facile synthesis of nanoporous TiC-SiC-C composites as a novel counter-electrode for dye sensitized solar cells. *Microporous and Mesoporous Materials*, *190*, 309-315.
- Zhou, H., Shi, Y., Dong, Q., Wang, Y., Zhu, C., Wang, L., . . . Ma, T. (2014). Interlaced W₁₈O₄₉ nanofibers as a superior catalyst for the counter electrode of highly efficient dye-sensitized solar cells. *Journal of Materials Chemistry A*, *2*(12), 4347-4354.
- Zhou, H., Shi, Y., Wang, L., Zhang, H., Zhao, C., Hagfeldt, A., & Ma, T. (2013). Notable catalytic activity of oxygen-vacancy-rich WO_{2.72} nanorod bundles as counter electrodes for dye-sensitized solar cells. *Chemical Communications*, *49*(69), 7626-7628.
- Zhou, H., Yin, J., Nie, Z., Yang, Z., Li, D., Wang, J., . . . Ma, T. (2016). Earth-abundant and nano-micro composite catalysts of Fe₃O₄@ reduced graphene oxide for green and economical mesoscopic photovoltaic devices with high efficiencies up to 9%. *Journal of Materials Chemistry A*, *4*(1), 67-73.
- Zhu, Y., Gao, C., Han, Q., Wang, Z., Wang, Y., Zheng, H., & Wu, M. (2017). Large-scale high-efficiency dye-sensitized solar cells based on a Pt/carbon spheres

composite catalyst as a flexible counter electrode. *Journal of Catalysis*, 346, 62-69.

University of Malaya